Artificial and natural photosensitizers in Photodynamic Therapy: Expanded porphycene conjugates and hypericin

Cormac Elías Hally Garcia

DOCTORAL THESIS

Title	**Artificial and natural photosensitizers in Photodynamic Therapy: Expanded porphycene conjugates and hypericin**
Presented by	**Cormac Elías Hally Garcia**
Centre	**IQS School of Engineering**
Department	**Analytical and Applied Chemistry**
Directed by	**Prof. Dr. Santi Nonell Marrugat** **Prof. Dr. Cristiano Viappiani**

UNIVERSITÀ DI PARMA

UNIVERSITA' DEGLI STUDI DI PARMA

DOTTORATO DI RICERCA IN
FISICA

CICLO XXXIII

in CO-TUTELA con
UNIVERSITAT RAMON LLULL

ARTIFICIAL AND NATURAL PHOTOSENSITIZERS IN PHOTODYNAMIC THERAPY: EXPANDED PORPHYCENE CONJUGATES AND HYPERICIN

Coordinatore:
Chiar.mo Prof. Stefano Carretta

Tutore:
Chiar.mo Prof. Cristiano Viappiani
Chiar.mo Prof. Santi Nonell Marrugat

Dottorando: Cormac Elías Hally Garcia

Anni 2017/2020

A la meva família,

Al Pol,

Agraïments

Primerament voldria agrair al Dr. Santi Nonell, a Barcelona, i al Dr. Cristiano Viappiani, a Parma, per acompanyar-me en el llarg camí que és una tesi doctoral. Segurament en una tesi doctoral un sap com hi entra, però poques vegades sap com en sortirà. Al final és la ciència que va marcant el pas i el camí a seguir. Gràcies per totes les explicacions en el laboratori, les discussions sobre ciència, els viatges i congressos i en definitiva, el dia a dia d'un doctorat en co-tutela.

Vull donar un sentit agraïment a la Dra. Montserrat Agut pel suport microbiològic de la tesi, però sobretot totes les estones compartides i de suport durant aquests anys.

Als FotoQs actuals, Mireia, Elena, Jaume pels riures i drames al laboratori i escapades fora de IQS. Als FotoQs "vells", que em van introduir a la Fotoquímica, Oriol, Bea, Joaquim, Roger i Íngrid ja tots doctors. Als FotoQs itinerants, Miguel Ángel i Matias. Als companys de sala, Eli, Raul i Ángel. I finalment al incombustible Òscar del lab de microbiologia.

A tutti i amici di Parma, specialmente a Stefania. Anche a Chiara, Eleonora, Ludovica, Lucrezia, Andrea, Anjali, Víctor e Michele.

A la família pel suport durant tots els anys al Químic

I al Pol, que tot i estar a distància, ha estat allà sempre de forma incondicional.

Senza tutti voi questa tesi non sarebbe stata possibile!

Finalment vull agrair als Fons Socials Europeus i a la Secretaria d'Universitats i Recerca del Departament d'Empresa i Coneixement de la Generalitat de Catalunya per els ajuts de contractació que m'han permès realitzar aquesta tesi (2017 FI_B00617, 2018 FI_B1 00174 i 2019 FI_B2 00167), així com també al finançament del Ministerio de Asuntos Económicos y Transformación Digital (MINECO; CTQ2016-78454-C2-1-R) i a IQS School of Engineering.

Abstract

This thesis reports the study of antimicrobial and antineoplastic applications of novel 2-aminothiazolo porphycene conjugates and Hypericin in Photodynamic therapy (PDT), while aiming to understand their mechanism of action.

The conjugation of 9-isothiocyanate-2,7,12,17-methoxyethylporphycene to two hydrophilic entities, gentamicin as an antibiotic and triphenylphosphonium as a lipophilic cation, rendered amphiphilic compounds with high biological activity against microorganisms and HeLa cells. The conjugates presented dual aromatic systems, highly absorbing in the deep red with high singlet oxygen yields. Their fluorescence, despite being dim, was still exploited in applications such as confocal microscopy and even stimulated emission depletion super-resolution microscopy (STED). The Gentamicin conjugate was able to inactivate *S. aureus*, *E. coli* and *C. albicans* in the submicromolar range, but lacking the intended selectivity since it also inactivates cancer cells. The conjugate endowed with the Triphenylphosphonium cation presented less activity against microorganisms than the previous conjugate, but higher for cancer PDT due to the partial subcellular localization guidance towards mitochondria.

Hypericin, on the other hand, is a powerful and well-known naturally occurring photosensitizer which is costly to both purify from a plant extract or chemically synthesized. In this regard, a non-purified lyophilized hydroalcoholic *H. perforatum* extract was compared with pure hypericin, observing how its photophysical properties are not quenched by other compounds in the extract and that its antimicrobial activity against *S. aureus* was preserved.

Continuing with Hypericin, retinoic acid was incorporated into the previously reported β-lactoglobulin-Hypericin complex in order to test its antimicrobial *in vitro* potential. Despite being a singlet oxygen quencher, this addition did not affect the Hypericin's performance against *S. aureus*, proving its potential as a double payload vehicle when treating *acne vulgaris*: Hypericin to treat infections and the retinoid to calm inflammation.

Astratto

Questa tesi riguarda lo studio di applicazioni antimicrobiche e antineoplastiche di nuovi coniugati di 2-aminotiazoloporficeno e dell'Ipericina nella terapia fotodinamica (TFD), con l'obiettivo di comprendere il loro meccanismo d'azione.

La coniugazione del 9-isotiocianato-2,7,12,17-metossietilporficeno in due entitá idrofiliche, con gentamicina come antibiotico e trifenilfosfonio come catione lipofilo, ha reso composti anfifilici con elevata attività biologica contro i microrganismi e le cellule HeLa. I coniugati presentavano sistemi aromatici doppi, altamente assorbenti nel rosso lontano con una alta resa di ossigeno singoletto. La loro fluorescenza, nonostante fosse debole, è stata tuttavia utilizzata in applicazioni come la Microscopia Confocale e persino nella Microscopia di svuotamento dell'emissione stimolata (STED). Il coniugato di gentamicina è stato in grado di inattivare *S. aureus*, *E. coli* e *C. albicans* nell'intervallo di concentrazioni del submicromolare, ma si è rivelato carente nella selettività voluta poiché inattiva anche le cellule tumorali. Il coniugato fornito del catione trifenilfosfonio presentava minor attività contro i microrganismi rispetto al coniugato precedente, ma un'attivitá maggiore contro il cancro a causa del parziale indirizzamento con localizzazione subcellulare nei i mitocondri.

L'ipericina, d'altra parte, è un ben noto fotosensibilizzatore naturale e potente, costoso sia se ottenuto per purificazione da un estratto di piante, sia se sintetizzato chimicamente. A questo proposito, un estratto liofilizzato idroalcolico di *H. perforatum* non purificato è stato confrontato con l'ipericina pura, osservando come le sue proprietà fotofisiche non siano soppresse da altri composti nell'estratto e come sia preservata la sua attività antimicrobica contro *S. aureus*.

Continuando con l'ipericina, l'acido retinoico è stato incorporato nel complesso β-lattoglobulina-ipericina precedentemente riportato per esaminare il suo potenziale antimicrobico *in vitro*. Nonostante sia un soppressore di ossigeno singoletto, questa aggiunta non ha avuto impatto sull'efficacia dell'ipericina contro *S. aureus*, dimostrando il suo potenziale come doppio agente nella cura dell'*acne vulgaris*: l'ipericina per le infezioni e l'acido retinoico per calmare l'infiammazione.

Resum

Aquesta tesi presenta l'estudi d'aplicacions antimicrobianes i antineoplàstiques de conjugats 2-aminotiazoloporificè i d'hipericina en teràpia fotodinàmica (TFD), tot intentant entendre el mecanisme d'acció.

La conjugació de 9-isotiocianat-2,7,12,17-metoxietilporficè a dues entitats hidrofíliques, l'antibiòtic gentamicina i el catió lipofílic trifenilfosfoni, formen compostos amfifílics amb gran activitat biològica contra microorganismes i cèl·lules HeLa. La conjugació presenta un sistema aromàtic dual, amb gran absorció al vermell i amb alts rendiments d'oxigen singlet. La seva fluorescència, tot i ser tènue, ha estat utilitzada en aplicacions com la microscòpia confocal i fins i tot en microscòpia de super-resolució d'emissió estimulada (STED). El conjugat amb Gentamicina és capaç d'inactivar *S. aureus*, *E. coli* i *C. albicans* en el rang submicromolar, però sense la selectivitat buscada doncs també inactiva cèl·lules canceroses. El conjugat amb el catió Trifenilfosfoni presenta una menor activitat en microorganismes que el conjugat anterior, però més elevat en càncer degut a una localització subcel·lular parcialment dirigida cap a mitocondris.

La Hipericina, per altra banda, és un conegut i potent fotosensibilitzador natural que és costós d'obtenir tant purificant un extracte de planta com la seva síntesi química. En aquest sentit, s'ha comparat un extracte hidroalcòholic liofilitzat de *H. perforatum* sense purificar amb hipericina pura, observant com les seves propietats fotofísiques no es veuen mitigades per altres productes en l'extracte i com la seva activitat contra *S. aureus* és preservada.

Seguint amb la Hipericina, àcid retinoic ha estat incorporat al complex b-lactoglobulina-Hipericina prèviament descrit per avaluar el seu potencial en assajos antimicrobians *in vitro*. Tot i ser un mitigador d'oxigen singlet, aquesta adició no afecta al rendiment de la Hipericina contra *S. aureus*, demostrant així el potencial del complex per alliberar dos fàrmacs simultàniament en tractar *acne vulgaris*: la hipericina per tractar infeccions i l'àcid retinoic per calmar la inflamació.

Resumen

Esta tesis presenta el estudio de aplicaciones antimicrobianas y antineoplásticas de conjugados 2-aminotiazoloporficenos e Hipericina en terapia fotodinámica, procurando entender su mecanismo de acción.

La conjugación de 9-isotiocianato-2,7,12,17-metoxietilporficeno con dos entidades hidrofílicas, el antibiótico gentamicina y el catión lipofílico trifenilfosfonio, forma compuestos anfifílicos con gran actividad biológica contra microorganismos y células HeLa. Los conjugados presentan un sistema aromático dual, gran absorción en el rojo y altos rendimientos de oxígeno singlete. Su fluorescencia, pese a ser débil, ha sido usada en aplicaciones como la microscopía confocal e incluso en microscopía de super-resolución de emisión estimulada (STED). El conjugado de Gentamicina es capaz de inactivar *S. aureus*, *E. coli* y *C. albicans* en el rango submicromolar, pero sin la selectividad buscada ya que también inactiva células cancerígenas. El conjugado de trifenilfosfonio presenta menos actividad que el conjugado anterior en microorganismos, pero mayor en cáncer debido a una sublocalización celular parcialmente dirigida hacia mitocondrias.

La Hipericina, por otro lado, es un conocido y potente fotosensibilizador natural que es costoso de obtener ya sea purificando extractos naturales de plantes o mediante síntesis. En este aspecto, se ha comparado un extracto hidroalcohólico liofilizado sin purificar de *H. perforatum* con Hipericina pura, observando como las propiedades fotofísicas no se ven mitigadas debido a la presencia de otros compuestos en el extracto y preservando su actividad contra *S. aureus*.

Siguiendo con Hipericina, ácido retinoico ha sido añadido al complejo β-lactoglobulina-hipericina previamente descrito para probar su potencial actividad antimicrobiana *in vitro*. Pese a ser un mitigador de oxígeno singlete, la adición de ácido retinoico no afecta al rendimiento de la Hipericina contra *S. aureus*, demostrando el potencial del complejo para liberar dos fármacos simultáneamente para tractar *acne vulgaris*: la hipericina para tratar la infección y el ácido retinoico para calmar la inflamación.

Table of Contents

To everything there is a season,
and a time to every purpose under the heaven:

A time to be born, and a time to die;
a time to plant, and a time to pluck up that which is planted;

A time to kill, and a time to heal;
a time to break down, and a time to build up;

A time to weep, and a time to laugh;
a time to mourn, and a time to dance;

A time to cast away stones, and a time to gather stones together;
a time to embrace, and a time to refrain from embracing;

A time to get, and a time to lose;
a time to keep, and a time to cast away;

A time to rend, and a time to sew;
a time to keep silence, and a time to speak;

A time to love, and a time to hate;
a time of war, and a time of peace.

The Ecclesiastes 3:1-8

CHAPTER 1

Introduction

This chapter will talk about current health issues concerning drug-resistant microbial infections and cancer, and how Photodynamic Therapy is called to be an added treatment to those already existing in the clinics. Photodynamic Therapy is discussed from a molecular basis, specially focusing on the photosensitizer's mechanism of action, while discussing their current limitations and possible solutions to improve the outcome of a treatment.

"Knowledge is high in the head, but the salmon of wisdom swims deep"

— Neil Gunn, An Bradán Feasa

1.1 Unwanted Cell Proliferation - A Health Matter

One of life's goals is perpetuation. This is achieved through maintenance of the organism or by reproduction of itself, and to this end, all life-forms have endeavoured to extend and improve their living conditions, to which people are not an exception. Regarding human health, unguents and ointments have been used for thousands of years to help a wound to heal or to relieve pain, evolving exponentially until what we refer to nowadays as "modern medicine".

Infections and cancer have been (and still are) two of the major death causes in the world, accounting for approximately 30% of all deaths for 2016.[1] These two afflictions share both uncontrolled and unwanted cell proliferation. Pathogenic bacteria parasitize their host by growing and living off an organism until it perishes due to organ failure or due to septic shock, while cancer is an abnormal growth of "own-cells" which can extend to other organs and usually ends in organ collapse.[2,3]

Focusing on infections, a major milestone in the history of medicine was the discovery of penicillin by Alexander Fleming in 1928,[4] inaugurating the antibiotics era. Until then, infections were one of the greatest causes of death, tuberculosis being one of the main pathogens killing millions over centuries.[5] Antibiotics did not only treat infections that one could contract on a day-to-day basis, but also enabled the performance of many surgical interventions that before would not even have been considered due to the high risk of infection it entailed.

After this spur, during the 20th century, many different families of antibiotics were developed such as other β-lactam, sulphonamides, aminoglycosides, tetracyclines, glycopeptides, rifamycins, quinolones, etc.[5] These families of antibiotics were discovered mainly as toxins liberated by fungi to the environment to inhibit bacterial growth. This great development was derived initially from the apparition of resistant strains to the known antibiotics, but also due to the evolutionary stress bacteria were placed under because of the abuse and misuse of these

drugs. Antibiotic cocktails are now used in order to surpass the acquired resistance by affecting different targets simultaneously.[6]

Microbial infections (including bacterial, fungal, viral and protozoal pathogens) caused close to 8.5 million deaths worldwide in 2016, of which 700,000 have been attributed to drug-resistant infections.[1] This latter figure could rapidly increase in the upcoming years for, in a worse-case scenario, up to 10 million people could die annually due to antibiotic resistance infections if action is not is taken.[7] These predictions also include illness caused by other microorganisms such as fungi, virus and protozoa which are not treated with antibiotics.

No new antibiotic families with the necessary chemical and physical properties have been discovered since the beginning of the 2000s,[8,9] and in light of the uprising resistance to traditional antibiotics, several alternatives have begun to be exploited:[10]

- Bacteriocins: Bactericidal peptides produced by bacteria, which actuate primarily at the cell envelope or affecting gene and protein expression. They are analogous to antibiotics produced by fungi and moulds.[11–15]
- Bacteriophages: which consists in the use of viruses that infect bacteria and use the host's machinery to replicate.[16,17]
- Lysins: Membrane lysing proteins generated by bacteriophages which disrupt the cell envelope.[18]
- Photodynamic Therapy (PDT): Visible light-mediated treatment with a photosensitive drug which oxidizes the whole cell non-specifically. [19,20]

Out of all these possible alternatives, this thesis will mainly focus on the latter, antimicrobial photodynamic therapy (aPDT), as well as some anticancer studies.

1.2 Another Bright Implement for the Toolbox

Civilization has used light for medicinal purposes for millennia, even when back in Ancient Egypt vitiligo was treated by applying certain plant extracts on the affected skin patch and let actuate under the sun.[21]

Light can be used as a treatment alone or in combination with other agents so, depending on the elements which intervene and the mechanism of action, light therapies can be divided into three groups: phototherapy, photochemotherapy and photodynamic therapy (PDT).

Rapidly, phototherapy is based on the beneficial effects of light alone, without any extra drug. Psoriasis and neonatal jaundice are two examples of afflictions treated only with light, using ultraviolet and B and A light respectively (UVB and UVA). In the first case, UVB downregulates protein expression of the immune system cells responsible for psoriasis, while neonatal jaundice is cured by photo-oxidising the excess bilirubin, which is later excreted.[21] Photochemotherapy is an evolved form of phototherapy in which a light-sensitive drug uses the absorbed light to react with cellular components. The most prominent case is the treatment of psoriasis with psoralens (PUVA), which dimerises with DNA once it absorbs UVA light.[21] Similarly, psoralens are used to perform *extracorporeal photopheresis*, which has per goal to sterilize blood. After administering the drug, blood is circulated outside of the body through a UV light and it is then reintroduced into the vascular system.[22]

The last group in which light therapies are classified is PDT, which differs from the other treatments in the fact that three individually non-toxic elements must come together simultaneously in order to induce its effect: a phototoxic drug named photosensitizer (PS), non-ionizing light (typically visible or near IR) and molecular oxygen (O_2).[23–26] The combination of these elements generate reactive oxygen intermediates (ROI) which are the final "active ingredients" which actuate on cells by enhancing their oxidative stress and, therefore, causing irreversible damage to vital cell components.

PDT has been clinically approved for cancer and antimicrobial applications, having per goal to inactivate only the desired cells. In addition, in contrast with the systemic administration of chemotherapy or antibiotics, the required combined action of three different elements make it a very localized therapy since the three components must meet in time and space, thus, causing fewer side-effects on the patient. Furthermore, administration of the photosensitizer and illumination can be separated in time, assuring a proper accumulation in the targeted area.

The first reported study on photodynamic therapy was reported in Germany by medical student Oskar Raab in 1900.[27] *Paramecium caudatum* dyed with acridine orange died when left under sunlight, whilst those kept in the dark did not.[20] Soon after, professor von Tappeiner and professor Jesionek developed this field further when experimenting in tumoral cells, opening the field to anticancer photodynamic therapy, while discovering also the necessity of combining light, oxygen and a dye in order to observe these effects.[20]

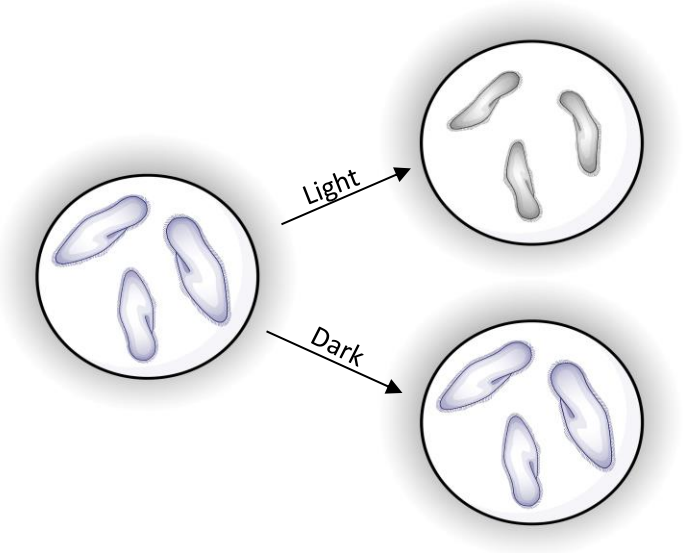

Figure 1. Photodynamic inactivation of Paramecium caudatum comparing light treated and non-light cells.

A final light induced treatment is photothermal therapy, which is in fact similar to PDT. This treatment looks for cell inactivation through heat release by photosensitizers. Instead of the photosensitizer relaxing to its original state forming ROI, it liberates heat.[28,29]

1.3 Photodynamic Therapy Mechanism of Action

The therapeutic action in PDT is performed by oxygen, a paramagnetic molecule due to being a "biradical with two electrons occupying separate π^* orbitals with parallel spins".[30] This stable electronic triplet configuration in the ground state ($^3O_2$) is the reason behind the non-spontaneous combustion of organic compounds in the presence of molecular oxygen at room temperature. Organic molecules typically have a closed-shell electronic structure (having all electrons paired) in a singlet spin multiplicity (^{1}RH), which makes reaction with triplet oxygen non-spin compatible. The Wigner Spin rules help understand this quantum prohibition, making combustion with oxygen from the triplet difficult, while being favoured from the excited singlet oxygen state ($^1O_2$) (Scheme 1).[31]

$$^1RH + \ ^3O_2 \rightarrow \ ^1RO_2H$$ ✗

$$^1RH + \ ^1O_2 \rightarrow \ ^1RO_2H$$ ✓

Scheme 1. Quantum prohibited and favoured combustion of organic matter depending on the molecular spin of oxygen.

Therefore, the role of PDT is to catalyse the oxidation of organic compounds with oxygen. The reaction velocity between oxygen and the organic substrate is enhanced, while the photosensitizer returns to its original state ready to begin the cycle once again. In comparison with regular drugs which require an uptake of many active molecules, each photosensitizer taken in by a cell has, in average, an approximate turnover of 10^6-10^7 per second,[32] indicating that only one photosensitising molecule is able to generate millions of therapeutic agents. Having said this, the photodegradation (or photobleaching) of the drug is practically unavoidable and the little diffusion of the ROI generated reduces the overall outcome.

Mechanistically speaking, the photophysical processes which take place once light is absorbed by a molecule are represented in the Jablonski diagram (Figure 2). If light irradiated on the molecule matches an electronic transition in the proper orientation, an electron will be

promoted to a higher energy state ($^1S_0 \rightarrow {}^1S_n^*$) conserving its spin angular momentum. The molecule will return then to its initial less-energetic state by different pathways.

An electron in an S_n electronic state will rapidly transition to the S_1 level (in the picosecond time scale) releasing its excess energy as heat through Internal Conversion (IC) into vibrational energy. Once in the S_1 state, the electron can spontaneously follow various pathways when returning to the ground state. It can continue to lose energy has heat (IC), it can fluorescence (F) emitting photons with energy equivalent to the energy loss, or it can undergo Intersystem Crossing (ISC), in which a quantumly forbidden spin change takes place, forming an excited Triplet state ($^3T_n^*$). This triplet state is lower in energy and longer-lived than its singlet counterpart (Hund's Rule).[33] Typically, a singlet excited state lives in the nanosecond range while a triplet usually lives from the micro- to millisecond range. From this triplet state, the molecule can undergo back-intersystem crossing to a singlet spin orientation (liberating then its excess energy as heat and returning to the ground state) or releasing its energy phosphorescing (P).

In addition to these spontaneous phenomena, stimulated emission (SE) can be induced by having external radiation interact with the excited singlet state. If the wavelength of the external radiation matches an energy gap towards the ground state, the excited electron will emit light of the same wavelength and in phase as the external beam, and therefore releasing energy and returning to the ground state.[34]

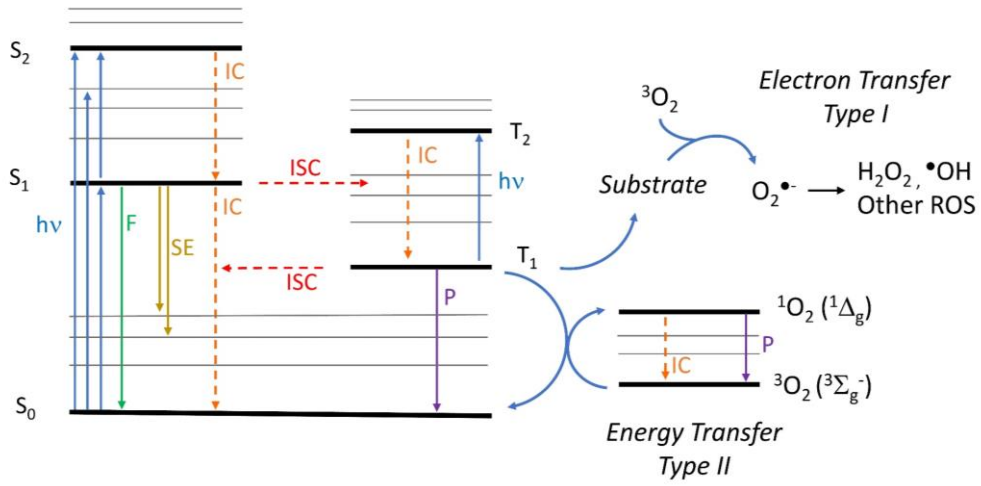

Figure 2. Jablonski diagram presenting the main photophysical and photochemical processes which takes place once a molecule absorbs light. Colour blue presents absorption processes (h ν), orange internal conversion (IC), green fluorescence emission (F), yellow stimulated emission (SE), red intersystem crossing (ISC) and purple phosphorescence (P). On the right side of the panel, there are two mechanisms of interaction between an excited triplet and molecular oxygen.

All these mentioned phenomena can be grouped as "photophysical processes" since they take place inside the same molecule and the ground state is finally recovered so it can begin the cycle again.

The right side of Figure 2 depicts the photochemical processes which can take place once the excited photosensitizer interacts with molecular oxygen.

Type I corresponds to an electron or hydrogen transfer process mediated by the substrate. Oxygen is the final acceptor of this electron, restoring the photosensitizer in its ground state and leaving a cationic radical on the substrate. The acceptance of an electron by molecular oxygen forms superoxide radical anion ($O_2^{\bullet-}$), which then can continue to accept electrons generating hydrogen peroxide (H_2O_2), hydroxyl radical ($OH^{\bullet}$), and finally the completely reduced water. Scheme 2 presents the stepwise reduction reactions of molecular oxygen to water and the reduction potential of each reaction at pH 7.[30,35] All these reduction steps take electrons from the substrate, damaging cellular components.

$$O_2 + e^- \rightarrow O_2^{\bullet -} \quad E^{\circ'} = -0.16\,V$$

$$O_2^{\bullet -} + e^- + 2H^+ \rightarrow H_2O_2 \quad E^{\circ'} = 0.94\,V$$

$$H_2O_2 + e^- + H^+ \rightarrow OH^{\bullet} + H_2O \quad E^{\circ'} = 0.38\,V$$

$$OH^{\bullet} + e^- + H^+ \rightarrow H_2O \quad E^{\circ'} = 2.33\,V$$

$$O_2 + 4e^- + 4H^+ \rightarrow 2\,H_2O \quad E^{\circ'} = 0.82\,V$$

Scheme 2. Stepwise reduction of molecular oxygen to water indicating the redox potential for each reaction at pH 7.[35]

Regarding Type II, an energy transfer takes place from the photosensitizer to molecular oxygen, yielding singlet oxygen ($^1\Delta_g$ or $^1O_2$).[33]

Singlet oxygen is the lowest excited state of molecular oxygen, lying 94.3 kJ·mol^{-1} above the ground state. It is highly reactive with electron rich groups in comparison to its ground state due to the different spin stemming from the distribution of the outer electrons. $^1O_2$ cannot be formed efficiently by exciting directly an electron to a higher state due to spin incompatibility, and therefore it must be generated indirectly. Even though the photochemical pathway already described is one of the most efficient ways to generate $^1O_2$, other "dark" chemical processes such as the decomposition of peroxides, ozonides and the formation from other reactive oxygen species can also be used.[36–38]

Once generated, this oxygen metastable state returns to its ground state mostly by non-radiative processes, while a small fraction decays radiatively, emitting phosphorescence at 1275 nm (Figure 3; A). Its lifetime presents a great dependency on the environment due to the electronic-vibrational coupling with C-H and O-H bonds of the solvent, resulting in a very short lifetime of $^1O_2$ in physiological environments.[39,40] Following the trend (and in the absence of quenchers), $^1O_2$ lives 3.3 μs in aqueous environments (Figure 3; B), 66 μs in D_2O, and even up to 73 ms in carbon tetrachloride.[33]

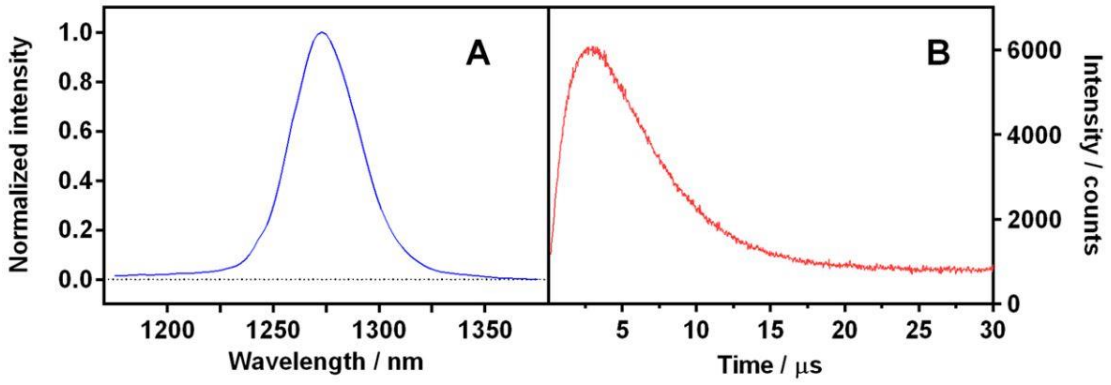

Figure 3. Singlet oxygen phosphorescent emission spectra (A) and transient decay of singlet oxygen in water (B). Sourced from reference.[41]

$^1O_2$ can be detected either directly taking advantage of its phosphorescent emission or by indirect methods. Emission at 1275 nm is very characteristic, but also very weak, and therefore the sensitivity of detection systems must be enhanced by using amplifiers and cooling systems to reduce electrical noise.[41] Different types of probes which detect $^1O_2$ indirectly have been developed which are based on changes in absorption (like diphenylanthracene)[42] or in fluorescence (such as the commercially available Singlet Oxygen Sensor Green).[39,43,44]

$^1O_2$ easily performs [2+2] cycloadditions with double bonds, which are present in many biomolecules such as polyunsaturated fatty acids and cholesterol,[45,46] nucleic acids, such as guanine,[47] and amino acids such as methionine, cysteine, tryptophan, tyrosine and histidine.[48] The other ROI formed are also electron deficient and will oxidize those electron rich compounds.

This random and generalized oxidation of different biomolecules and organelles inside the cell is of utmost importance since it is the key factor by which treated cells find it much harder to develop resistance in comparison to traditional antibiotics or chemotherapeutic agents.[49]

Having said this, PDT-treated cells can eventually develop resistance to treatment by similar mechanisms to those of conventional drug or radio-resistance which mainly entail changes in the bioavailability of the PS and the detoxification of the generated oxygen species.[49] Overexpression of p-glycoprotein, a broad-range efflux transmembrane protein that can modify

greatly the uptake of a photosensitizer, and the overexpression of glutathione as a ROI scavenger can seriously hinder the treatment.[50]

1.4 Light Sources

As previously mentioned, the chosen wavelength to illuminate the targeted cells for PDT is typically in the visible and near-infrared region of the spectra. More energetic lights, namely the harmful UV, X-ray and gamma rays, are not used for this application because they induce irreversible damage on DNA and generate free radicals on the illuminated area (regardless of the photosensitizer), and therefore cannot be used. Lower energy radiations (infrared and microwave) cannot be used for this approach since water begins to absorb light at 1300 nm and, furthermore, wavelengths longer than 850 nm cannot efficiently transfer a minimum energy from a photosensitizer to generate $^1O_2$. Even though the LUMO-HOMO energy gap of oxygen is found at 1275 nm (94 kJ·mol^{-1}), energy transfer is not 100% efficient and therefore shorter wavelengths above 850 nm must be used.[51]

Another very important aspect regarding light sources is the location of the treatment area. Previous of course to the absorption of light by the PS is its delivery to the desired location. The dosimetry which will take place will not be the same if the lesion to treat is on the skin or inside the organism. In this regard, light scattering phenomena and absorption of light by other molecules present in the body are the main factors which must be considered.

Rayleigh scattering phenomena occurs when radiation penetrates a non-transparent area (in this case the body), changing light direction in a wavelength dependant manner. Blue light is scattered more than red light, where the first can penetrate only 1 millimetre of skin while the far-red can undergo up to 1 centimetre.[52,53] This complex field of study uses mostly simulations to predict and optimize light dosimetry, such as the Monte Carlo approach.[53,54]

Living organisms are full of coloured molecules, to which porphyrins and melanin are two of the most abundant elements. Porphyrins absorb light mainly in the blue region of the spectra, while

melanin presents an absorption tail beyond 600 nm. All these aspects brought together coined the concept "optical window" (Figure 4), in which light in this region of the spectrum presents maximum tissue penetration.[53] In this region of the spectra light is less-absorbed by intrinsic chromophores of the body, is less dispersed, water does not yet absorb and tissues present less autofluorescence.[55]

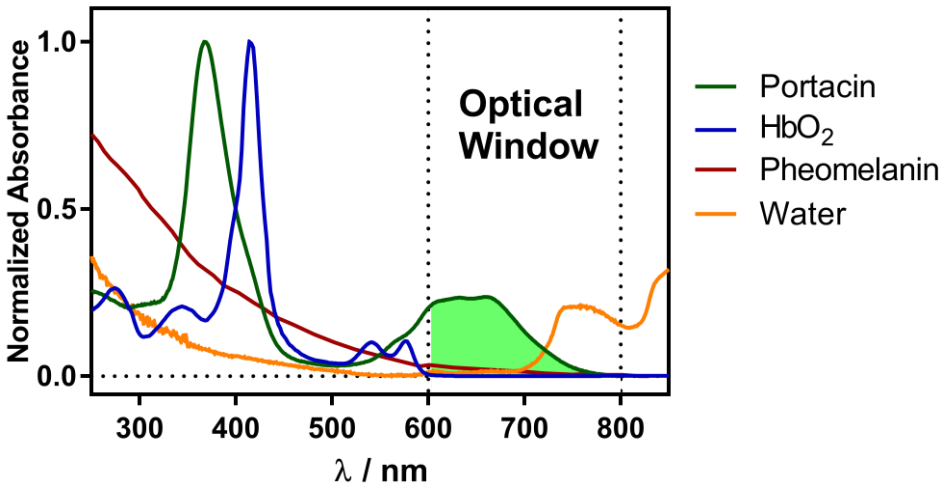

Figure 4. Optical window in tissue representing the normalized absorption spectra in PBS of Portacin, oxygenated haemoglobin, pheomelanin and water.

Light may penetrate up to some centimetres, but not more. Skin, oral and other areas of easy access (stomach, bladder, lungs…) can benefit from direct application, but light delivery to more hidden parts of the body is a challenge for clinical applications of PDT. Despite this initial drawback, nowadays light can be efficiently delivered practically everywhere in the body with minor invasive techniques by means of catheters and endoscopies.[56,57]

1.5 Types of Photosensitizers

Many different types of photosensitizers have been described during the years, and in fact, any light absorbing molecule with a reasonable intersystem crossing yield could be a candidate as photosensitizer. Photosensitizers are usually organic molecules with notable π-electron systems which enable their light absorption in the visible range of the spectrum. Nowadays, one can find photosensitizers with maximum absorption at practically any wavelength.

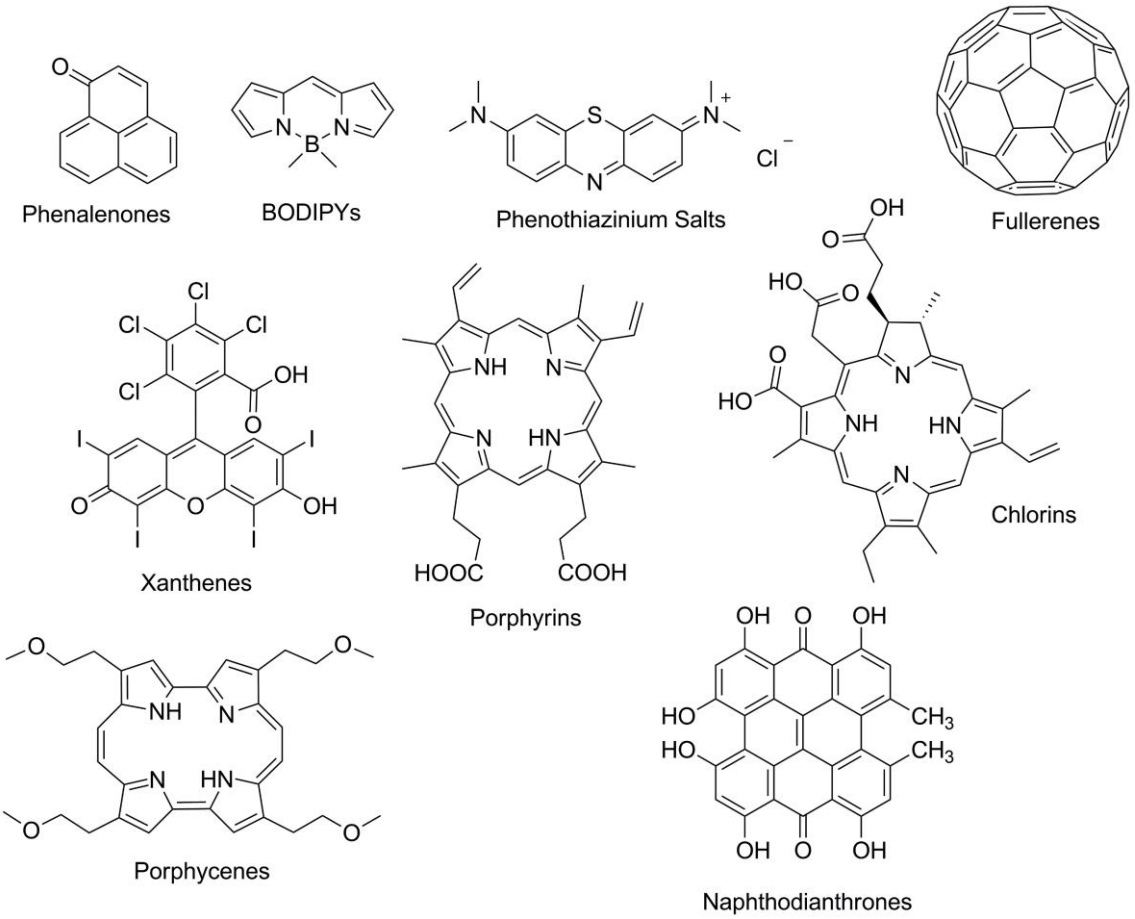

Figure 5. Molecular structures of different of photosensitizing families.

Photosensitizers are developed to perform in medical centres as efficiently as possible, and therefore, some optimal properties must be met. An ideal photosensitizer must be a chemically pure and well-defined compound, soluble in physiological media, non-toxic but greatly phototoxic, with high singlet oxygen quantum yield (Φ_Δ), absorb in the red region of the spectrum (600-800 nm) for deeper penetration, photostable (so it can perform during long periods of time), be selective to the target cells and have fast clearance time to reduce side effects.[58] Most photosensitizers excel in some properties and are deficient in others, and therefore a compromised scenario between these features must be met.

Furthermore, if the photosensitizer would also have a high fluorescence quantum yield (Φ_F), the drug would also be a diagnostic reporter on the location of the malady, becoming therefore a *theranostic* drug.[57] Theranostics (or theragnostics) is a term which began to be used at the

beginning of the 2000's to describe materials capable of diagnosing an affliction (localizing and imaging) and at the same time treating from the one single entity.[59,60]

Many PSs are based on tetrapyrroles, and therefore these photoactive drugs may be classified as tetrapyrrolic and non-tetrapyrrolic.

Tetrapyrrolic PSs

This family of compounds is probably the largest group of photosensitizers, whose fundamental structures are based on 4 pyrrole rings link together. These molecules are found ubiquitously across nature, playing essential roles in life such as photosynthesis and oxygen transport in blood.

Porphyrins are the simplest type of tetrapyrroles, in which the pyrrole rings are linked symmetrically together by means of methine bridges generating an 18π electronic system. The derivatization of the α and β positions of the rings lead to a vast variety of natural and synthetical products. Porphyrins can also be found chelated, keeping a metallic ion within its core.[61] They present an intense absorption band in the ultraviolet-blue range named Soret and other minor absorption bands in the 500-600 nm called Q-bands, whilst also being fluorescent in the red.

Not surprisingly, hematoporphyrin was the first photosensitizer to be used in clinical trials during the 60's after the observation of fluorescent red light occurring from tumours with accumulation of this drug.[62] Since then, hematoporphyrin has been derivatized and purified, leading to Photofrin®, the first PDT treatment to be approved by the American Federal Drug Administration (FDA) in 1995 to treat different types of cancers.[63] Still within the family of porphyrins, 5-aminolevulinic acid (ALA; Levulan®) was approved also by the FDA in 1999 for treatment of actinic keratosis. Administration of ALA on the region of interest leads to an overaccumulation of protoporphyrin IX (PpIX) in the heme biosynthesis pathway due to low activity of ferrochelatase enzyme in non-healthy tissue.[60,64,65] Unlike the poor photochemistry of heme, the lack of the central iron ion endows PpIX with a high Φ_Δ, and even though it presents a low

fluorescent quantum yield (Φ_F), it is used as a theranostic agent. Its fluorescence reveals its location and the ROI generation leads to inactivation.[66]

Despite approvals by the FDA, hematoporphyrin and Photofrin® present some disadvantages such as the low absorptivity in the red where the optical window is found, little solubility in physiological media, lack of selectivity towards the targeted cells and may not be pure (in the case of Photofrin®).

Considering these downsides, second-generation photosensitizers were developed, in which their absorption in the red is enhanced and are chemically pure.[67] The many modifications consisted mainly in introducing asymmetry into the tetrapyrrole ring, resulting in a bathochromic shift and in an increase in the molar absorptivity of the Q-bands.[68,69] For example, the reduction of 1 or 2 double bonds of the porphyrin ring yields the chlorin and bacteriochlorin families respectively, in which meta-tetra(hydroxyphenyl)chlorin (m-THPC; Foscan®) and Chlorin e6 (Radachlorin®; Ce6) are approved photosensitizers for head and neck cancer and skin cancer respectively.[70,71]

Other ways of introducing asymmetry are skeletal rearrangements of the bonds linking the pyrrole cycles (isomers) and the addition of aromatic cycles on the pyrroles, resulting in an expansion of possibilities entailing red absorbing photosensitizers, such as benzoporphyrins, porphycenes or corroles, to mention a few.[72] A latter important tetrapyrrolic family used in photodynamic therapy are phthalocyanines (Pc) and naphthalocyanines.[73,74] Despite usually being symmetric, they have a rather low absorption in the blue, but great absorption coefficients in the Q bands which make them good candidates for PDT. For example, Photosens® is mixture of chloroaluminium sulfonate phthalocyanines approved in Russia for cancer treatments in 2001.[70]

The broad aromatic system that confers the photophysical properties to tetrapyrroles is a drawback when solubility in physiological media is concerned. Different strategies are adopted

in order to improve their activity in these environments, since aggregated they are usually photochemically inactive. Derivatizing photosensitizers with bulky substituents, introducing net charges and conjugation to other water-soluble entities are approaches pursued to enhance solubility.[75,76] Other strategies involve using nanoparticles, proteins and liposomes to act as drug deliverers.[3,77]

Non-tetrapyrrolic

Many different types of photosensitizing molecules fall in this classification, both organic and inorganic, natural and synthetic. Some examples are aromatic ketones (such as phenalenones[78–80] and perylenequinones[81–83]), flavins,[84–86] psoralens,[87] curcumin,[88] coumarins,[89] fluorinated BODIPYs,[90] phenothiazinium salts (such as methylene blue[91] and toluidine blue[92,93]), xanthenes such as Rose Bengal (RB)[94] and even inorganic structures such as titanium dioxide,[95] fullerenes[96] and nanotubes.[97]

Even though the potential of PDT has been vastly proven, only methylene blue, toluidine blue and curcumin have yet received approval by the FDA to be used as antimicrobial disinfectants of, mainly, oral infections.[20]

1.6 Selectivity, Drug Delivery and Targeting Strategies

The goal of PDT is to eliminate either microbial cells or cancer cells while sparing the healthy ones. The use of antibiotics cause little side-effects on patients since most of these drugs present selective action to bacteria thanks to the physiological differences between eukaryotic and prokaryotic cells, such as the cellular wall,[98] the size of ribosomes[99] and several crucial enzymes. Following this same idea, chemotherapy causes terrible side effects due to similarity between a cancerous cell and a healthy one and not being able to completely differentiate them.

Despite needing three elements together, PDT is still not as selective as antibiotics are. Some treatments deliver the photosensitizer systemically and end up presenting severe prolonged skin sensitivity.[67,100]

Some photosensitizers present intrinsic selectivity, such as ALA, which accumulates in tumoral cells due to the high demand on nutrients and extended vascularization, but it is not a frequent asset.[60] Therefore some form of selectivity enhancement is required, which usually involves vehicles and/or targeting elements.

Nanoparticles (NPs) are being used normally in clinics, which benefit from the delivery of high payloads, the biocompatibilization of hydrophobic drugs in physiological media and the possibility of constructing large nanoplatforms with several active elements. Most photosensitizers are aromatic organic molecules, so the use of nanoparticles can prevent aggregation, maintain their photophysical properties intact and avoid their premature photobleaching.[101]

NPs can be mainly classified into two groups: biodegradable and non-biodegradable. Biodegradable nanoparticles such as micelles, liposomes,[102,103] proteins,[104] polymeric (such as poly-lactic-co- glycolic acid or polyacrylamide)[105,106] present great versatility and are finally cleaved and degraded by enzymes, clearing them from the organism. Non-biodegradable NPs such as those made of noble metals (gold and silver),[107] inorganic oxides (silica,[108] titanium and zinc) and quantum dots are also appealing but present the major downside of not being degradable by the body, and as a result the FDA has delayed their approvals in clinics.[77]

An added benefit of using NPs is the enhanced permeation effect (EPR), by which cancer cells present higher uptakes of NPs than healthy cells, actuating as passive tumour targeting (Figure 6).[109] EPR is based on the structural deficiencies in endothelial cells during neovascularization processes during solid-tumour development.[110,111]

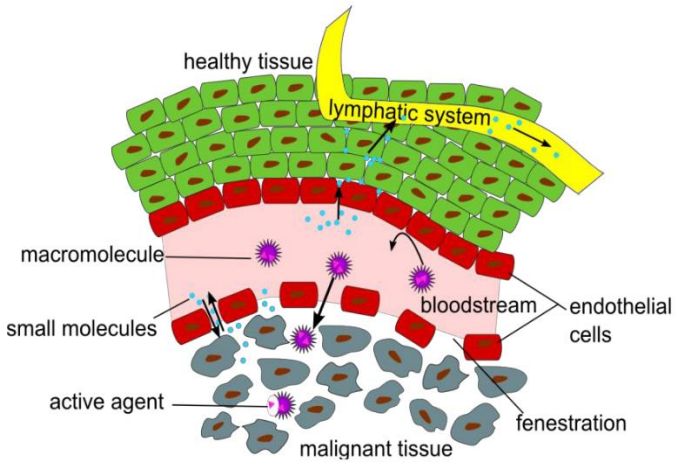

Figure 6. Schematic representation of the Enhanced Permeation and Retention effect. Sourced from reference[109].

Despite this basal selectivity level, it is usually still not enough to achieve an adequate selectivity and, therefore, active targeting elements must be introduced. Third-generation PSs are being developed to overcome this issue, in which these targeting elements can either be linked directly to the PS or can be used indirectly by means of a NP.[112]

The conjugation of photosensitizers, and nanoparticles, to different types of biomolecules can enhance the specificity of PDT, targeting the desired cells.[112–115] Antibodies[116,117] and its fragments,[118–120] peptides,[121,122] folate molecules,[123,124] mannose sugars,[108,125,126] lectins,[127] aptamers,[128,129] etc, present specific recognition to overexpressed surface elements of the target cells, and therefore, enhance the PS uptake and improve the outcome of the therapy. The size of these targeting elements and how these are linked to the PS will determine its efficacy. Large and small targeting agents have different pharmacokinetic and clearance profiles, varying time lapses from injection, illumination and elimination from the body after the treatment.[130,131] This promising approach must be exploited with care since it presents a potential inconvenient, by which the covalent binding of the photosensitizer to a large entity (as for example an antibody) may impede the drug reaching its optimal subcellular localization and reduce its efficacy photoinactivating the cell.[132]

1.7 Antimicrobial PDT (aPDT)

After cancer, the photoinactivation of microorganisms is one of the main applications of photodynamic therapy. There are several advantages to aPDT in comparison with regular antibiotics since treatments are usually short and limited in space and time, it activates the immune system and causes multitarget damage to cells simultaneously.[58,133] Many studies have published excellent preclinical results, but these are not as efficient in biofilms and *in vivo* tests.[134]

The random oxidation of biomolecules caused by ROI within cells (and viruses) make it a broad spectrum treatment since it can inactivate bacteria, fungi, protozoa and even viruses.[20,135] Even though PDT was discovered in 1900, the discovery of penicillin in 1928 left antimicrobial PDT applications aside due to the simplicity of antibiotic administration in comparison to having to add light to an uptaken PS on the region of interest. During the golden antibiotic era (50's-60's),[8] these medicines were regarded as "the solution" to any sort of infection, until nowadays, when proliferation of multidrug resistant microorganisms have risen to alarming levels. Furthermore, these acquired resistances, if expressed from a plasmid, can be disseminated throughout the whole bacterial cohort by horizontal gene transfer.[5] There are different types resistance mechanisms which stem from a genetical modification of the microorganism:[136]

- Efflux of the antibiotic from the cell via a collection of membrane-associated pumping proteins.[137,138]
- Modification of the antibiotic target through mutation of key binding elements. This mechanism has little probability of happening since modifications on key features, such as ribosomes, usually make the organism non-viable.
- Via synthesis of modifying enzymes that selectively target and cancel antibiotic activity. These enzymatic strategies may actuate by hydrolysis, such as the cleavage of vulnerable bonds such as β-lactamases on penicillins and cephalosporins, or by group transfer enzymes which covalently modify the antibiotic which results in structural

alterations that impairs its binding and therefore, reducing its activity. Other examples of modifying enzymes are acyltransferases and phosphotransferases.

aPDT became popular once again during the 90's and since then many studies have developed a large variety of photosensitizers and investigated its mechanism of uptake and action, hoping to overcome antibiotic resistance by multitargeting with ROI.

In this regard, the bacterial wall has a primordial influence on aPDT, since Gram-positive bacteria have a greater susceptibility to PDT than Gram-negative ones.[20,139,140] Down to a physiological level, they share an inner lipid bilayer membrane similar to that of eukaryotic cells, but mainly differ in the absence or presence of an outer also lipid bilayer membrane. Gram-positive bacteria do not have an outer membrane, but a large layer of peptidoglycan between 30 and 100 nm thick, leaving the periplasmic space between the glycan and the inner membrane. This layer built from N-acetyl glucosamine-N-acetyl muramic acid and cross-linked by pentapeptides helps maintain the osmotic pressure of the cell and protect the bacteria from external agents.[141,142] In addition to the peptidoglycan, lipoteichoic acids and wall teichoic acids complete the composition of the Gram-positive bacterial wall.

Gram-negative bacteria also present a peptidoglycan membrane in its wall, but much thinner, only a few nanometres thick, forming also the periplasm.[142] The outer membrane envelopes the peptidoglycan with a phospholipid bilayer, made of two leaflets. The inner leaflet is similar to that of the inner membrane, while the outer leaflet presents proteins and polysaccharides which extend out into the aqueous environment. These lipopolysaccharides (LPS) complexes are strongly negatively charged and regulate the movement of molecules across into the cytoplasm. The charge difference in the external part of the bacteria explains why anionic and neutrally charged PS only affect Gram-positive bacteria, and why the introduction of positive charges are beneficial to inactivate Gram-negative ones.[91] Figure 7 presents the structural elements of a Gram positive (left) and Gram negative (right) bacterial wall.

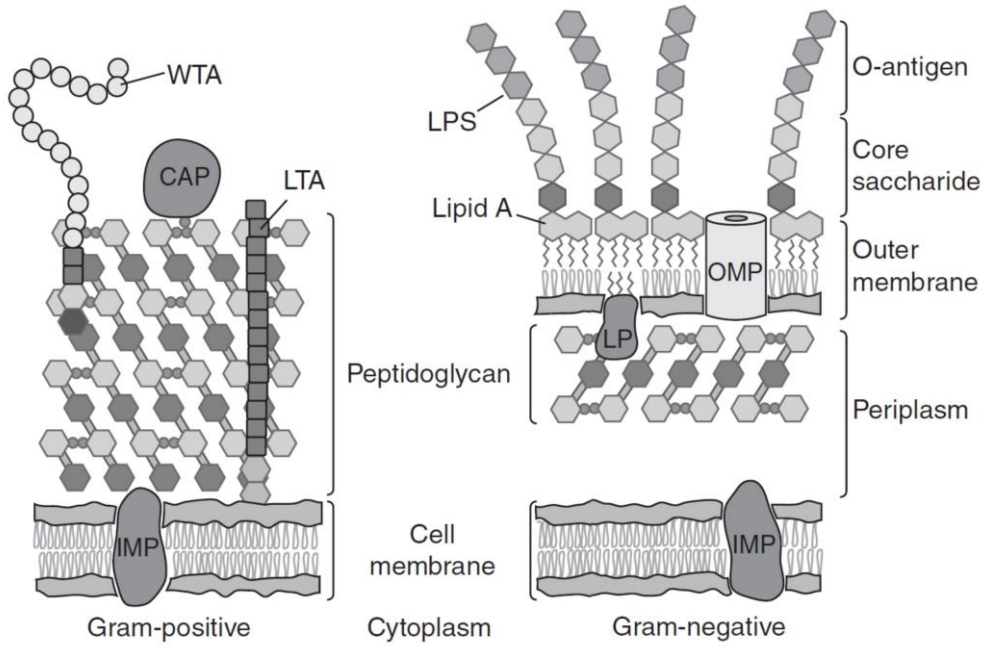

Figure 7. Bacterial wall structures of Gram positive (left) and Gram negative (right) bacteria. Figure adapted from reference[142].

Microorganisms have two modes of growth: planktonic and biofilm depending on the environmental conditions they find. Planktonic growth takes place when microorganisms grow as a suspension in solution, while a biofilm is a cell aggregate attached to a surface. Even though in nature most bacteria and fungi grow as biofilms most antimicrobial assays are performed in planktonic growth since they are more reproducible and simpler to perform.[143]

A biofilm is a complex aggregation of microorganisms that live in a self-produced matrix of hydrated extracellular polymeric substances (EPS) that form their environment. The EPS is formed by polysaccharides, proteins and nucleic acids. It provides bacteria with mechanical stability and protection against desiccation, antibiotics, host immune defences, among others. The biofilm cells are adhered to the surface forming part of a cohesive and three-dimensional polymer network that interconnects (through quorum sensing molecules) and immobilizes biofilm cells.[144] One of the most important characteristics is that biofilms enable microorganisms to regulate the expression of certain genes, allowing them to adapt to changing conditions. The most remarkable phenotypical property is its increased resistance towards antimicrobial agents.

Some factors considered to be responsible for this increased resistance are the restricted penetration of antimicrobials, expression of gene resistance and decreased growth rate.[145]

The localization of photosensitizers in bacterial cells is a difficult issue to study due to the size of bacteria, which are far smaller than eukaryotic cells. Being only up to a few micrometres in size, electron microscopy has had (and still has) an important role in understanding the molecular structure and cellular functioning from a mechanical point of view, but has the disadvantage of not being able to work with live cells. Super-resolution optical microscopy techniques are nowadays aiming to image live-cell physiology below the visible light diffraction limit, which would enable further understanding of the microbiologic cosmos. The discovery of optimal subcellular locations within bacteria would greatly aid in optimizing aPDT as a clinical treatment.

For a number of years now, combination therapies of antibiotics and photosensitizers to treat microbial infections has become a steadily growing field. This approach is analogous to administrating a cocktail of drugs which has per goal to target different cellular components simultaneously.[6,146] Up until now it has proven to generate a synergistic effect in the outcome of the treatment, meaning that combined present higher biological activity than by simply adding the effects of the individual components.[134,147]

As a few examples on combination therapy in planktonic systems, in 2014 Almeida and co-workers tested 5,10,15,20-tetrakis(1-methyl-4-pyridinio)porphyrin tetra(p-toluenesulfonate) in combination with ampicillin or chloramphenicol proving an enhanced combination effect,[148] Ronqui and co-workers evaluated the combination of methylene blue and ciprofloxacin against *S. aureus* and *E. coli*[149] and recently in 2017 and 2018 Pérez-Laguna tried rose bengal with gentamycin, mupirocin and linezolid.[94,150] Reports in biofilms are also present, such as produced by Barra in 2015 combining 5-aminolevulinic acid with gentamicin[151] and again Perez-Laguna in 2018 with gentamicin and rose bengal as photosensitizer.[150] Finally, some *in vivo* assays have been performed all using 5-ALA as photosensitizing precursor, such as reported by Xu[146] and

Sun[152], treating acne by combining with minocycline and general skin infections with several different antibiotics respectively.

Fungi are another type of microorganism which has generated interest by PDT. Even though most fungi are harmless and have fundamental roles in organic matter decomposition, in symbiosis with algae and are used by people to produce wine and cheese, some few fungi can take advantage of immunosuppressed patients. Infections on the dermis, on other soft tissues and even in blood are related to fungi are not rare. In fact, *Candida* spp. is the third-most lethal fungi concerning infections related to catheters.[153]

Being eukaryotic cells as they are, fungi possess an external cell wall made of chitin, β-glucan and mannoproteins which is not present in animal cells. This structural difference is harnessed to selectively treat fungal infections by targeting the formation of the cell wall. As bacteria, fungi can also become resistant to classical antifungal approaches, and PDT can potentially be used as an alternative.[154] Some studies have reported that the external wall in fungi is less permeable than the wall of Gram-positive bacteria, but more than Gram-negative ones.[155]

1.8 Antineoplastic PDT

Cancer is, in fact, the major application for photodynamic therapy nowadays having many treatments already being used in hospitals.[70] This disease is still one of the major death causes in the world, and it is currently being tackled through different approaches: chemotherapy, immunotherapy, radiotherapy and surgical resection. Different treatment combinations are followed depending on the patient, type, location and size of the tumour.

In the exact same way as microorganisms, cancer cells can develop resistance to treatment after consecutive sessions. Furthermore, since cancer cells are indeed far more alike its own healthy cells than in an infection, the body cannot tolerate such treatments for prolonged periods of time due to its severe side effects.[156]

In this regard, PDT becomes another treatment option in addition to the already existing ones. PDT has a double effect on the cancer, on one hand tackling cancer cells directly, while on the other it also damages the vasculature around them, precluding cells their source of nutrients. Furthermore, in sharp contrast with other anticancer treatments, PDT activates the immune system which is fundamental when trying to help the organism to eliminate the malady and also in order to avoid opportunistic pathogens.[155,157]

Photosensitizers for cancer treatments need different characteristics in comparison with antibacterial photosensitizers. Animal cells do not have an intense charge differential on either side of the plasmatic membrane, and therefore neutral or slightly charged PS have better outcomes than heavily charged PSs. Most of the clinically approved PSs for cancer are neutrally charged.[70] Skin cancer aside, these are internal and therefore red-absorbing photosensitizers are desired to make the most of the optical window.[158]

In cancer, the adequate subcellular localization is a very important factor to consider which has been studied extensively by fluorescence microscopy (without the need of super-resolution techniques).[26,58,159] The localization of the oxidation damage in different parts of the cell result in different cell death pathways, namely, apoptosis, necrosis and autophagy (Figure 8).[3,51,160,161] The dominant specific pathway depends on many parameters such as PS concentration, localization and light dose.[161,162]

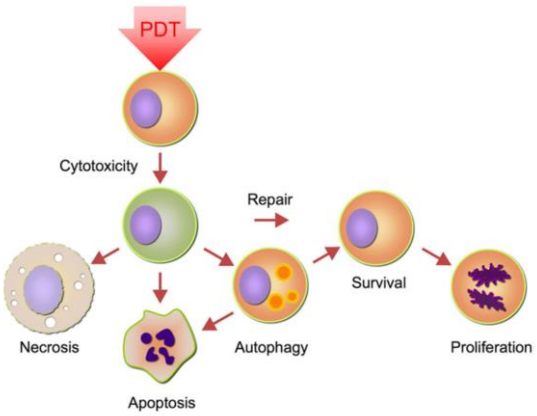

Figure 8. Cell death pathways. Sourced from reference[161].

The photosensitizers can enter the cell through various pathways, being endocytosis one of the most typical ones due to the size and polarity of the drugs. The endosome then formed must be broken so the PS can proceed to inactivate from its optimal subcellular localization, since this entrapment can hinder the outcome of the treatment. In fact, in 1999 *photochemical internalization* was described by Berg and co-workers in order to harness the formation of endosomes during uptake to ensure delivery to the cytosol.[163]

Treatments combining traditional anticancer procedures and PDT are currently being extensively studied. Furthermore, some treatments take advantage of the fluorescence of photosensitizers to guide resection, while finishing off the remaining less-visible cancer cells by illuminating the affected area.[164]

1.9 Objectives

The purpose of this thesis is to study the biological action and the photophysical properties of novel synthetic 2-aminothiazoloporphycenes and of the naturally occurring Hypericin in physiological environments. This goal is further detailed in the following specific objectives:

- Study of the photophysical properties and photoinactivation outcome of *gentamicin*, *triphenylphosphonium* and *butyl*- 2-aminothiazoloporphycene conjugates against model microorganisms and HeLa cells. Elucidation of the mechanism of action of the aforementioned photosensitizers using spectroscopic and microscopic techniques.

- Comparison of the photophysical properties and biological activity of Hypericin against *S. aureus* from a chemically pure source and from a non-purified hydrophilic natural extract of *Hypericum perforatum*.

- Evaluation of the biological impact of incorporating Retinoic Acid to the β-lactoglobulin-Hypericin construct against *S. aureus* for potential *acne vulgaris* treatments.

CHAPTER 2

General Techniques and Methods

This chapter describes the common procedures and methods that have been used throughout this thesis, most specifically, about the photophysical and microbiological techniques used.

2.1 General

All spectroscopic measurements were performed using 1 cm path quartz cuvettes (Hellma) at room temperature, unless differently stated. All solvents used were Spectrosol grade and water Milli-Q grade (Millipore Bedford, Massachusetts system, resistivity of 18 MΩ cm). Phosphate buffer saline was prepared by dissolving NaCl (137 mM), KCl (2.7 mM), Na_2HPO_4 (10 mM) and KH_2PO_4 (1.8 mM) in Milli-Q water and adjusting pH to 7.4.

2.2 Steady-state optical techniques

Absorption spectra were recorded on a UV-Vis double beam Cary 6000i spectrophotometer (Agilent Technologies, Santa Clara, CA).

Fluorescence spectra were recorded on a Fluoromax-4 spectrofluorometer (Horiba Jobin-Yvon, Edison, NJ).

The fluorescence quantum yield (Φ_F) of a compound is defined as the ratio between the number of photons emitted and the photons absorbed (Equation 1).

$$\Phi_F = \frac{Emitted\ Photons}{Absorbed\ Photons} \qquad Eq.1$$

The absorption fraction of photons ($f(\lambda)$) can be calculated as follows (Equation 2). P_o is the incident radiant power, P the transmitted radiant power.

$$A = log\left(\frac{P_o}{P}\right);\ f(\lambda) = 1 - \ 10^{-A(\lambda)} \qquad Eq.2$$

Φ_F can be calculated by comparing the number of absorbed and emitted photons of the sample with a reference compound (Equation 3). The slope of each compound is obtained by plotting the integrated fluorescence against the absorbed photons. "X" stands for sample and "R" for reference. The refractive index (n) of the solvent must also be taken into account. Tetraphenyl porphyrin dissolved in toluene was used as reference.[165]

$$\Phi_{F(X)} = \Phi_{F(R)} \cdot \frac{Slope_X}{Slope_R} \cdot \frac{{n^2}_X}{{n^2}_R} \qquad Eq.3$$

2.3 Time-resolved optical techniques

2.3.1 Time Correlated Single Photon Counting

Time-resolved fluorescence decays were measured using a Fluotime 200 time-correlated fluorescence lifetime spectrophotometer (PicoQuant GmbH, Berlin, Germany), equipped with a red sensitive photomultiplier. Excitation was achieved by means of picosecond diode lasers (500 nm or a 596 nm as stated) working at 10 MHz repetition rate. The counting frequency was always below 1%. Fluorescence lifetimes were analysed using PicoQuant FluoFit 4.6.6 data analysis software deconvoluting the signal from the Instrument Response Function (IRF).

2.3.2 Time-resolved NIR emission (TRNIR)

TRNIR allows the determination of phosphorescence decays in the near-infrared using a photomultiplier as detector (H9170-45 Hamamatsu Photonic, Japan). The laser used to excite the sample was a pulsed Nd:YAG (FTSS355-Q, Crystal Laser, Berlin, Germany) emitting at 355 nm. The laser worked at 10 kHz repetitions when measuring in PBS, while in organic solvents and heavy water the laser repetition was lowered to 1 kHz.

TRNIR requires of interference filters to select the desired wavelength. $^1O_2$ emits light at 1275 nm as phosphorescence, whilst the triplet state of porphycene emits at 1110 nm. Other filters such as 1220 nm and 1325 nm can also be used if the emission spectra of the ^{3}PS interfered with $^1O_2$. Contributions of $^1O_2$ emission at those wavelengths are minimum.

Data was analysed with PicoQuant FluoFit 4.6.6 data analysis software.

$^1O_2$ decays were fitted using a biexponential decay model (Equation 4), being τ_Δ and τ_T the lifetimes of singlet oxygen and the triplet state of the photosensitizer and $S_{1275}(0)$ the amplitude of the signal at time zero.

$$S_{1275}(t) = S_{1275}(0) \times \frac{\tau_\Delta}{\tau_\Delta - \tau_T} \times \left(e^{-t/\tau_\Delta} - e^{-t/\tau_T}\right) \qquad Eq.4$$

The singlet oxygen quantum yield (Φ_Δ) of a compound is defined as the ratio between the number of singlet oxygen molecules formed and the photons absorbed by the photosensitizer at the excitation wavelength.

Φ_Δ can be calculated by comparing the singlet oxygen production of the sample with a reference compound (Equation 5). The slope obtained when plotting $S_{1275}(0)$ at different concentrations of the compound against the absorption fraction (Equation 2) is then used to compare with a reference compound. Phenalenone (PN) was used as reference in organic solvents[166], while phenalenone-2-sulfonic acid (PNS) was chosen when working in aqueous environments.[167]

$$\Phi_{\Delta(X)} = \Phi_{\Delta(R)} \cdot \frac{Slope_X}{Slope_R} \qquad Eq.5$$

2.3.3 Nanosecond Laser flash photolysis

Laser Flash Photolysis is a time resolved technique which is able to study the excited states of molecules. Its principle is based on the use of an intense pulsed laser which creates a population of excited states in a sample. At a 90° angle, a spectrophotometer beam is constantly irradiating the sample, which is able to detect the changes in absorbance between the ground and excited states, and since the pulse of the laser is synchronized with the detector, time resolved measurements can be performed.

Transient absorption spectra were monitored by nanosecond laser flash photolysis using a Q-switched Nd:YAG Laser (Surelite I-10, Continuum) with right-angle geometry and analysing the beam produced by a Xe lamp (PTI, 75 W) in combination with a dual-grating monochromator (mod. 101, PTI) coupled to a UV–Vis radiation detector (PTI 710). The signal was fed to a Lecroy WaveSurfer 454 oscilloscope for digitizing and averaging (typically 10 shots) and finally transferred to a PC for data storage and analysis.

2.4 Microbial strains, culture conditions and photodynamic inactivation assays

The microorganisms studied were *Staphylococcus aureus, Escherichia coli* and *Candida albicans* as a Gram-positive, Gram-negative and yeast models respectively. Each section specifies the particular strain used in each case.

Antimicrobial Photodynamic Inactivation Protocol

Bacterial cells were grown overnight in an orbital shaker at 37 °C ± 1 ˚C in Tryptic Soy Broth (TSB) medium. 150 μL were then suspended in fresh TSB and set to grow in exponential phase at 37 °C ± 1 ˚C to achieve approximately 10^8 colony forming units ($CFU \cdot mL^{-1}$). They were later centrifuged (5000 rpm, 10 min) and resuspended in phosphate buffer saline (PBS; pH = 7.4). This process was performed three times.

Candida albicans was grown overnight in an orbital shaker during 48 hours in liquid Sabouraud broth at 37 °C ± 1 ˚C. 150 μL were then suspended in fresh Sabouraud and set to grow in exponential phase at 37 °C ± 1 ˚C to achieve an approximate turbidity of 0.5 in the McFarland scale. *C. albicans* was then washed with PBS as previously mentioned to stop cellular growth.

The cells were incubated with the drug (delivered in dimethylsulfoxide (DMSO)) in the dark for 30 minutes (unless stated otherwise) under the same growth conditions. 300 μL placed in 96-well plates and irradiated from the top. Light sources are indicated specifically at each chapter.

In order to exclude any inactivation due to light or heating effects, controls without PS were performed, along with the evaluation of the toxicity of photosensitizers in the dark. After illumination, the bacteria were serially diluted and streaked on tryptic soy agar plates and incubated in the dark for 18 hours at 37 °C ± 1 ˚C, while the yeast were also serially diluted but streaked on Sabouraud dextrose agar and incubated in the dark during 48 hours at 37 °C ± 1 ˚C.

Three independent experiments were done for each photoinactivation treatment, which in turn were carried out in duplicate. The average and standard deviation (SD) values were calculated.

2.5 Light Sources

Three different light sources were used to perform the inactivation assays, both antimicrobial and antineoplastic. Their emission spectra can be found in Figure 9.

- Sorisa Photocare LED Light with two different light sources: green (521 ± 19 nm; 18 $mW \cdot cm^{-2}$) and red (635 ± 15 nm; 8 $mW \cdot cm^{-2}$).
- Red 670 nm Device® from Red Light Man (Hermes, Salford, United Kingdom) was used for deep red illumination (660 ± 10 nm; 62 $mW \cdot cm^{-2}$).

The irradiances of the lamps were regularly monitored with an Ophir AN/2 Laser Power Meter (Ophir Optronics Solutions Ltd, Har Hotzvim, Israel) to ensure the fluence delivered.

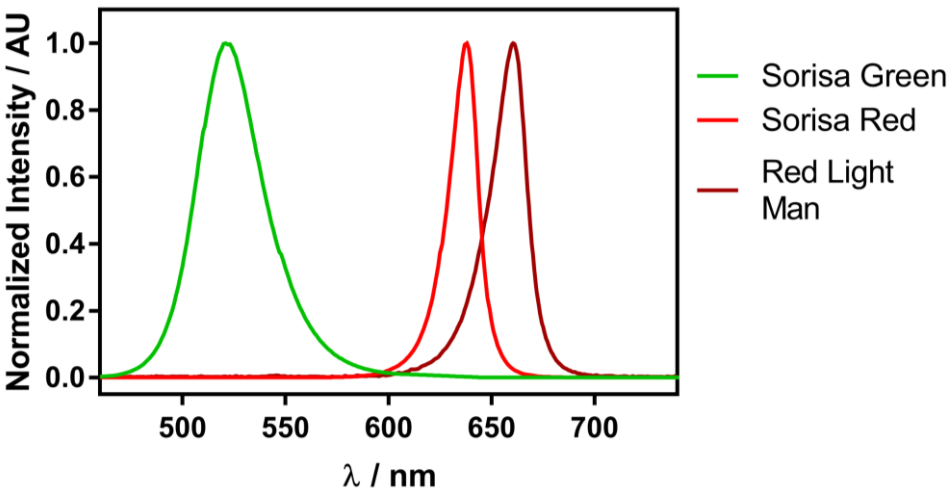

Figure 9. Emission spectra of Sorisa Photocare (green and red) and Red Light Man (dark red).

2.6 Quality Assurance

When performing any experimental measure, we are relying on the capability of the instrument and of the method used to faithfully reflect the desired phenomena. In this regard, the photophysical measures taken place during this thesis were performed under a controlled Good Manufacturing Practices (GMP) certified environment. GMP certifications are not common in research laboratories but are found ubiquitously in analysis and pharmaceutical facilities, having per goal to ensure that the procedures taking place within the system are reproducible and performed according to the quality standard defined.

Incorporating elements such as Standard Operating Procedures (SOPs) and scheduled maintenance programs for each instrument, controlled environmental conditions in the laboratory, restricted access of personal according to the individual induction training courses taken and a traceable documental system support the quality and reliability of the work and measurements performed.

This manner of working was initially not designed to be applied in research, and some may argue that GMPs and research are incompatible due to the loss of flexibility and bureaucracy it entails. But nonetheless, research can still benefit from adopting some of the features used in GMPs, adding value and security to the work performed in the laboratory.

CHAPTER 3

Amphiphilic Expanded Porphycenes: Red-absorbing, soluble and highly phototoxic

This chapter will verse on the use of 2-aminothiazoloporphycenes as a photosensitizers in antimicrobial and antineoplastic Photodynamic therapy, which is partially adapted from *I. Nieves, C. Hally, C. Viappiani, M. Agut and S. Nonell; A porphycene-gentamicin conjugate for enhanced photodynamic inactivation of bacteria, Bioorg. Chem., 2020, 97, 103661.*

Three different "expanded porphycenes" are studied, evaluating their photophysical properties, their biological activity against model Gram-positive, Gram-negative, yeast and HeLa cells, as well as deepening in the understanding of their mechanism of action using ultra-fast spectroscopic techniques and super-resolution microscopy.

"If you can't explain it to a six-year-old, you don't understand it yourself"

— Albert Einstein

3.1 Introduction

Porphycenes are synthetic aromatic 18π heteromacrocycles, isomers of porphyrins with enhanced optical properties, in which two 2,2'-bipyrrole systems are linked by ethylene bridges. They were firstly synthesized by Vogel in 1986 and since then many applications have been found such as in catalysis,[168] organic solar cells,[169–171] and material sciences.[172,173] They are between the most stable porphyrinoids,[174] which along with their high Φ_F and Φ_Δ, make these molecules excellent candidate photosensitizers for PDT and photodiagnosis applications.[175–178] Up until now, only one porphycene derivative (ATMPn) has been approved for medical use in Germany (1997) for psoriasis and non-melanoma skin cancer treatments.[67,70,179]

Figure 10 presents the structures and numbering of bare porphycene and porphyrin molecules, as well as the aromatic system in bold. In comparison with the symmetric square-like shape adopted in porphyrins, porphycenes' aromatic system adopts a rectangular shape which is responsible for its asymmetry, endowing it with its particular optical properties. Only regarding absorption, the Q bands can be up to an order of magnitude greater than those of porphyrins.[177]

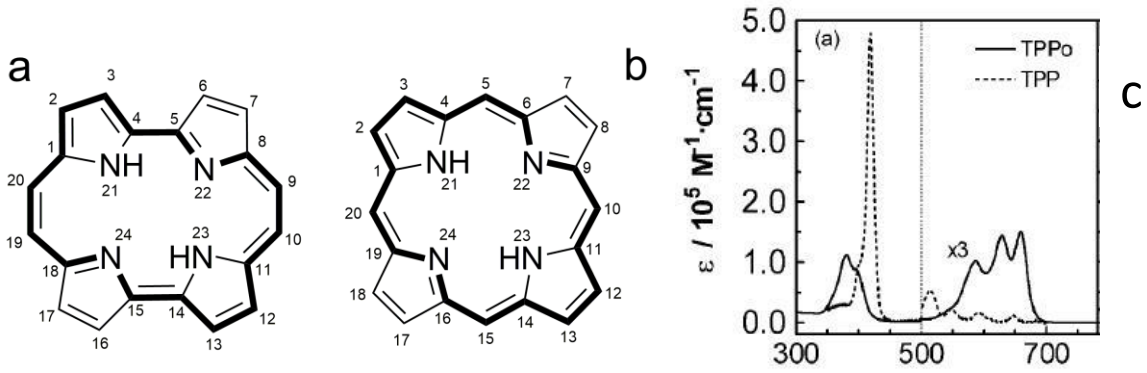

Figure 10.Porphycene (a), porphyrin (b) molecular structures and molar absorptivity comparison of tetraphenylporphyrin (TPP) and tetraphenylporphycene (TPPo) (c). Part c has been sourced from reference [180].

In a nutshell, porphycenes are synthesized via Ullmann coupling of 2 iodopyrroles, followed by decarboxylation of esters and formylation by Vilsmeier-Haack reaction. The final tetrapyrrole ring is achieved by a McMurry-type reductive coupling and spontaneous oxidation of the aromatic system (Figure 11).[173]

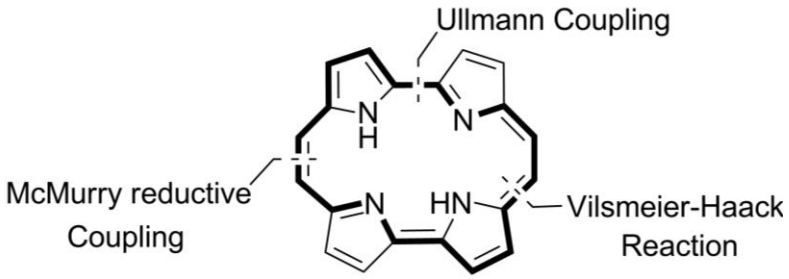

Figure 11. Main chemical reactions in the synthesis of porphycene.

Porphycenes are usually derivatized either in the β-β' positions of the pyrrole rings (carbons 2, 3, 6, 7, 12, 13, 16 and 17) or in the *meso* positions (carbons 9, 10, 19 and 20). The introduction of substituents in the β positions once the tetrapyrrole has been formed can be tedious, and therefore those moieties are usually included during the Knorr synthesis of pyrroles.[178] Different functional groups can be introduced into the *meso* position, mainly leading to *acyl* or *nitro* derivatives. These can then be modified yielding 9-hydroxyporphycene and 9-alkoxyporphycenes from the *acyl* derivative,[181] whilst the reduction of 9-nitroporphycene can generate 9-aminoporphycene and, subsequently, the respective amide derivatives and even 9-isothiocyanateporphycene.[182]

Porphycenes, being aromatic compounds as they are, are very insoluble in physiological media. Compounds with different substitutions in the β-position have been attempted in biological tests, such as with aryl, aliphatic and alkoxy moieties, being the latter which presented better fluorescence, photosensitizing properties and adequate solubility in biological media.[178] Other strategies to deliver these hydrophobic compounds have been the addition of Pluronic F-127[183], covalently binding porphycenes to poly-lysine polymer[184,185] and even using liposome formulations.[102,103,186] Further solubility in water of these PS was achieved by introducing positive charges in its molecular structure. Ragàs and Ruiz-González reported cationic-porphycene derivatives which introduced cationic pyridine and trialkylammonium moieties respectively.[187,188]

Recently, it is the 9-isothiocyanateporphycene derivative which has drawn special attention. In 2015, Planas and co-workers described an aromatic system expansion of the porphycene core from 18 π–electrons to 22 π-electrons after reacting spontaneously with an amine.[189,190] Mechanistically speaking, the isothiocyanate moiety readily reacts with an amine yielding a thiourea-porphycene derivative, followed by an intramolecular sulphur-to-ring charge transfer and by a final oxidation of the aromatic system, presumably by environmental oxygen. Figure 12 presents the reaction scheme of 9-isothiocyanate-2,7,12,17-tetrakis(methoxyethyl)porphycene (9-ITMPo) with a primary amine. The incorporation of this functional group enables click reactions with amines in a variety of contexts, being the conjugation to biomolecules (e.g. proteins and antibiotics) and nanoparticles in order to enhance porphycene solubility in physiological media one of the most attractive applications.[189]

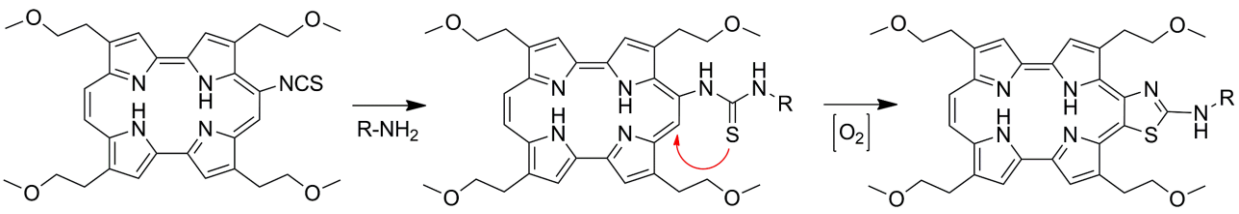

Figure 12. Cyclization reaction between 9-ITMPo and with a primary amine.

The cyclization entails an approximate 70 nm bathochromic shift of both absorption and fluorescence, giving birth to a near-infrared (NIR) theranostic agent thanks to its high fluorescent and singlet oxygen quantum yields. In PDT applications, this red shift is convenient since longer wavelengths are more penetrant in biological tissues. Expanded porphycenes have interesting photophysical features, since two different chromophores are present in the same molecular structure, corresponding to the 18π and 22π electronic systems. The polarity and acidity of the environment of the molecule will determine the ratio of either species (Figure 13).[190] In this regard, thiazoloporphycene derivatives may be used as pH and polarity probes.

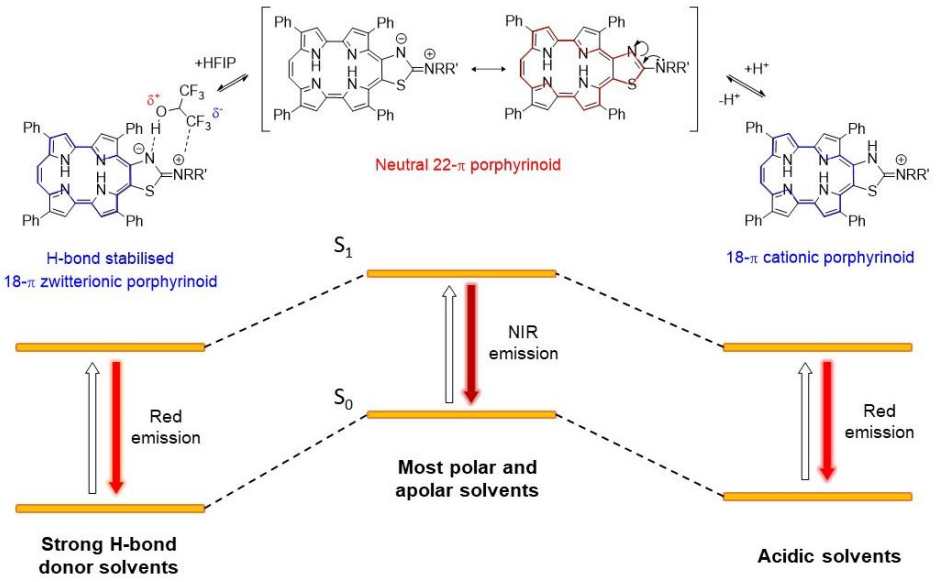

Figure 13. Acid and polarity effect on the 18π and 22π equilibrium. Figure sourced from reference [190].

Portacin: Conjugation between Porphycene and Gentamicin

Conjugation between apolar photosensitizers and hydrophilic entities render amphiphilic compounds, which is a property longed for when designing a photosensitizer. In this regard, aPDT combination therapies using antibiotics and photosensitizers can be brought a step further by covalently binding these two elements together. Very few antibiotic-photosensitizer conjugates have been reported so far. Some few examples are porphyrin derivatives linked to antimicrobial peptides[13,191,192], rose bengal bound to kanamycin and to penicillanic acid[193], a chlorin to vancomycin[194] and even a porphycene to apidaecin.[121]

One of the compounds described in this thesis is precisely a conjugate between the antibiotic Gentamicin and 2,7,12,17-tetrakis(methoxyethyl)porphycene (TMPo), yielding *2-gentamicin-thiazolo[4,5-c]2,7,12,17-tetrakis(methoxyethyl) porphycene* (Portacin; Figure 16-A).

Gentamicin is a BCS class 3,[195] well-established antibiotic that is in fact a mixture of several congeners, where C_1, C_{1a}, and C_2 are the three major components (Figure 14).[196]

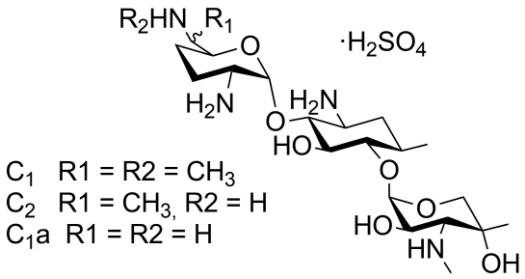

Figure 14. Gentamicin sulphate molecular structure, specifically of congeners C_1, C_2 and C_{1a}.

It selectively accumulates in bacterial cells,[197] being effective against Gram-negative bacteria and some Gram-positive microorganisms.[198] It is used to treat infections such as endocarditis, meningitis, pneumonia, septicaemia, brucellosis, endocarditis, respiratory tract infections, urinary tract infections, sepsis and even has even been used to treat intracellular infections (zoonosis). [199–201] However, many bacteria have developed resistance to this antibiotic[202] and there is still no selective method for combating this resistance nor the ototoxic and nephrotoxic side effects.[203]

Hereof, despite gentamicin having many distinct forms, we aimed to single couple the less hindered primary C6'-amino group of gentamicin's purpurosamine moiety with 9-ITMPo, in order to alter the pharmacokinetic properties of the antibiotic as little as possible. Since gentamicin contains many amino residues that will be protonated at physiological pH, conjugation of gentamicin to 9-ITMPo is expected to enhance the photoantimicrobial activity of TMPo due to an enhanced solubility in physiological media, as well as endowing it with selectivity towards bacteria due to the selective accumulation of gentamicin in bacteria than in eukaryotic cells.[197,204] On the other hand, conjugation may also lead to a reduction in the amount of gentamicin required for treating pathogenic bacterial infections, and therefore reducing the ototoxic and nephrotoxic effects this aminoglycoside presents.[203]

Porphonium: Conjugation between Porphycene and the Triphenylphosphonium lipophilic cation

Another functional group that can be exploited when willing to obtain amphiphilic photosensitizers are triphenylphosphonium cations (PPh_3^+). Triphenylphosphonium cations

have a delocalized charge distribution along the large hydrophobic area provided by the phenyl residues which results in weakened solvation enthalpy, allowing them to easily cross biological membranes,[205] and, furthermore, are accumulated in mitochondria due to the large electrochemical potential generated by the electron transport chain in this organelle.[206] MitoSox Red[207] (ThermoFisher, USA), MitoPerOx[208] (Abcam, UK) and MitoPY1[209] (Toronto Research Chemicals, Canada) are commercial examples of ROI probes that accumulate in mitochondria and contain a triphenylphosphonium group in their molecular structure (Figure 15).

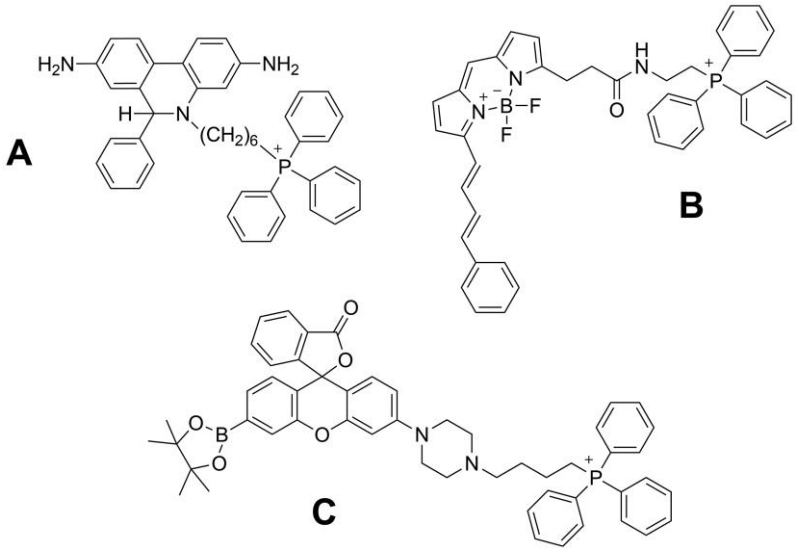

Figure 15. Molecular structure of mitochondria targeting fluorescent probes: MitoSoxRed (A), MitoPerOx (B) and MitoPY1 (C).

Mitochondria are very sensitive to oxidative stress, and therefore PDT has this organelle as a primary target to induce cell apoptosis.[210,211] Previous studies have already reported and proved the beneficial properties achieved by introducing a PPh_3^+ in antitumoral[159,212–214] and antimicrobial PDT.[79] 3-(aminopropyl)triphenylphosphonium was covalently bound to 9-ITMPo, yielding *2-(3-aminopropyl) triphenylphosphonium-thiazolo[4,5-c]2,7,12,17-tetrakis-(methoxyethyl) porphycene* (Porphonium; Figure 16-B). The expected accumulation of the photosensitizer in mitochondria will hopefully result in greater cancer cell inactivation.

Porbutyl: Conjugation between Butylamine and Porphycene

A final conjugate was prepared for control purpose by conjugating 9-ITMPo to butylamine, yielding 2-N-butylaminothiazolo[4,5-c]2,7,12,17-tetrakis(methoxyethyl)porphycene (Porbutyl; Figure 16-C). The analogous expanded porphycene obtained has only a butyl chain, in contrast with the amphiphilic targeting agents of the two previous conjugates described.

In this context, this chapter will discuss properties and features of the three photosensitizers resulting from reacting 9-isothiocyanate-2,7,12,17-tetrakis(methoxyethyl)porphycene (9-ITMPo) with the gentamicin sulphate (**Portacin**), with (3-aminopropy)triphenylphosphonium (**Porphonium**) and with butylamine (**Porbutyl**). More specifically, it will verse on their photophysical properties, their biological activity against model Gram-positive, Gram-negative, yeast and HeLa cells, as well as deepening in the understanding of their mechanism of action.

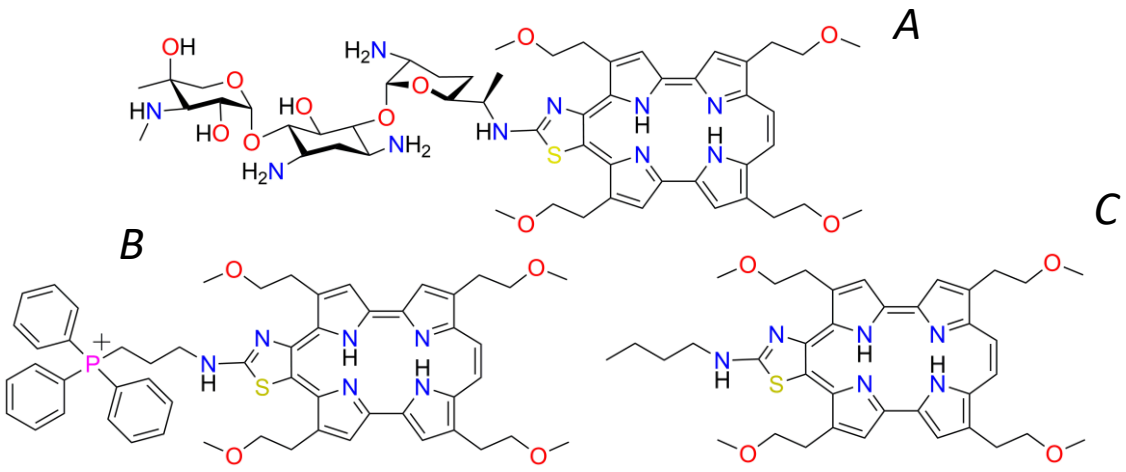

*Figure 16. A) 2-gentamicin-thiazolo[4,5-c]2,7,12,17-tetrakis(methoxyethyl)porphycene (**Portacin**).*
*B) 2-(3-aminopropyl) triphenylphosphonium-thiazolo[4,5-c]2,7,12,17-tetrakis-(methoxyethyl)porphycene (**Porphonium**).*
*C) 2-N-butylaminothiazolo[4,5-c]2,7,12,17-tetrakis(methoxyethyl)porphycene (**Porbutyl**).*

With the same purpose as for Portacin, a second antibiotic-photosensitizer conjugate was studied. Rose Bengal was conjugated to gentamicin and its photophysical properties and antimicrobial activity were compared to the photosensitizer alone (Figure 56).

3.2 Materials and Methods

3.2.1 Synthesis

All reagents were commercially acquired except for 3-aminopropyltriphenylphosphonium which was kindly provided by Dr. Marco Eugenio Vázquez from the Department of Organic Chemistry at the University of Santiago de Compostela. The synthesis of the three 2-aminothiazoloporphycene derivatives and of the Rose Bengal-Gentamicin conjugate was performed by Dr. Íngrid Nieves.

The synthesis of 9-ITMPo (and precursors), Portacin and Porbutyl are described in *Ingrid Nieves, Cormac Hally, Cristiano Viappiani, Montserrat Agut, and Santi Nonell in Bioorg. Chem., 2020, 97, 103661*.[215]

For Porphonium, a solution of 9-ITMPo (8 µmol), (3-aminopropyl)triphenylphosphonium iodide (42 µmol) and K_2CO_3 (42 µmol) in EtOH (1.5 mL) was stirred overnight at room temperature. The mixture was concentrated under reduced pressure and the resulting crude was purified by flash column chromatography ($CHCl_3$:MeOH; stepwise gradient from 0 to 10% of MeOH) to afford the green Porphonium in 60% (5 µmol).

For the Rose Bengal-Gentamicin conjugate, a solution of N-hydroxysuccinimide (120 µmol) in DMF (1 mL) was added to a mixture of Rose Bengal sodium salt (13 µmol) and N-(3-dimethylaminopropyl)-N'-ethylcarbodiimide hydrochloride (EDC·HCl, 130 µmol) in anhydrous DMF (2 mL). The resulting mixture was vigorously stirred at room temperature for 2h (the colour changing from pink to purple), which was then added dropwise to a solution of gentamicin (670 µmol) and K_2CO_3 (890 µmol) in DMF (9 mL). The mixture of reaction was stirred for 5 days until no conversion was observed by TLC. The purple mixture was concentrated under reduced pressure, and the resulting crude was purified by flash column chromatography on C18-RP silica-gel (glacial acetic acid:methanol; 5:95); stepwise gradient from 0 to 100% of MeOH) affording the desired Rose Bengal-gentamicin conjugate in 70% (9 µmol) yield.

3.2.2 Femtosecond Laser Flash Photolysis

Femtosecond spectroscopy was used to further understand the photophysical properties of these expanded porphycene conjugates.[216] This ultra-fast spectroscopic cohort of techniques can assess kinetic phenomena which take place in the long femtosecond and picosecond time scale, much faster than nanosecond flash photolysis. Therefore, phenomena such as electron vibrational relaxion to S_1 electronic level of electrons which have been further promoted can be monitored. All these phenomena take place before fluorescence emission of the chromophore, which is usually in the nanosecond scale.

The laser system employed for the transient absorption experiments was based on an amplified Ti:Sapphire laser (Coherent Libra), with 1 kHz repetition rate, ∼5 mJ output energy, central wavelength of 800 nm and pulse duration of 100 fs.[217] In order to synchronize the pump and the probe beams at such fast time scales, the 800 nm laser beam was split in order to generate the two light sources. A home-built optical parametric amplifier (OPA) allowed the generation of narrowband (∼ 10 nm) pump pulses of 600 nm. A broadband white-light continuum probe pulse, covering the 540 − 1015 nm wavelength range, was generated by focusing a fraction of the laser output into a 2-mm-thick sapphire plate. Pump and probe pulses were time delayed with respect to each other by a computer-controlled motorised translation stage. Pump and probe pulses, with relative polarisation set to the magic angle, were focused onto the 1-mm-thick sample cuvette. The transmitted probe beam was sent to a spectrometer equipped with a charge-coupled device (CCD) sensor capable of recording spectra at the full 1 kHz laser repetition rate. The pump beam was modulated at 500 Hz by a mechanical chopper synchronised with the laser. Differential transmission (ΔT/T) spectra as a function of probe wavelength, λ, and pump-probe delay, t, were obtained by subtracting transmission when the probe is on or off, according to the chopper. ΔT/T was transformed to ΔA by means of Equation 6. Furthermore, global analysis[218] of kinetics recorded in the whole

probed spectral range were applied. Figure 17 presents a very simplified scheme of the optical setup.

$$\Delta A = -log\left(\frac{\Delta T}{T} + 1\right) \qquad Eq.6$$

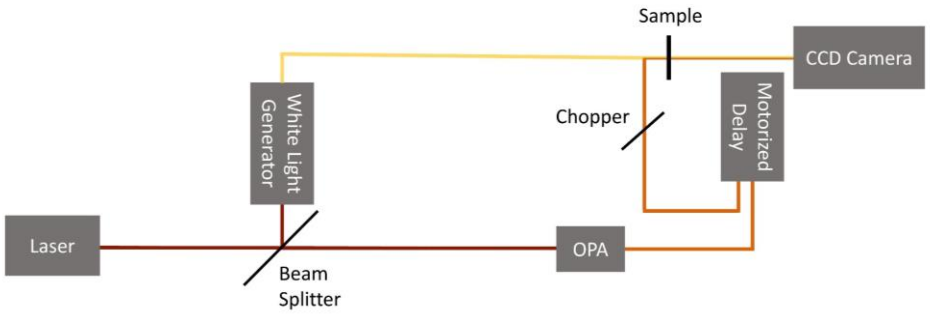

Figure 17. Schematic femtosecond transient absorption spectroscopy setup.

3.2.3 Fluorescence Correlation Spectroscopy

Fluorescence correlation spectroscopy (FCS) is a technique which correlates fluctuations of fluorescence intensity in a small finite volume along time. It measures fluorescence emitted from 1 μm^3. Due to its great sensitivity, FCS can be considered a single molecule technique. Indeed, FCS measures fluorescence fluctuations in this volume emitted from molecules, particles (or any emissive entity in general) which travel freely through this fixed volume. By correlating the time it takes for molecules to enter, emit and leave the confocal volume, the diffusion coefficient of the emissive particle can be determined. Once the diffusion coefficient is known, it is relatively simple to find the size of the emitting particle.

The autocorrelation function G(t) is the parameter which correlates each time series with itself shifted by time τ (Equation 7):

$$G(\tau) = \frac{1}{N}\sum_{i=1}^{n} \rho_i \left(1 + \frac{\tau}{\tau_i}\right)^{-1} \cdot \left(1 + \frac{\tau}{\tau_i \cdot \kappa^2}\right)^{-1/2} \qquad Eq.7$$

Where k is a geometrical factor from the instrument and τ_i the diffusion time.

Simplifying to a spherical shape, the diffusion coefficient and the size of the particle can be determined with Equations 8 and 9:

$$D_i = \frac{{\varpi_0}^2}{4 \cdot \tau_i} \quad Eq.8 \qquad r = \frac{\kappa_B \cdot T}{6 \cdot \pi \cdot \eta \cdot D} \quad Eq.9$$

where ω_0 corresponds to a geometrical factor of the equipment (0.375 μm for the instrument used) τ_i corresponds to the diffusion time, k_B is the Boltzmann constant, T the temperature in kelvins, η the viscosity of the solvent and D the diffusion coefficient.

FCS experiments were performed using a Microtime 200 system from PicoQuant (Berlin, Germany), based on an inverted confocal microscope (Olympus IX70) and equipped with two SPADs (single photon avalanche diodes). Excitation was achieved by using a 405 nm picosecond diode laser. Fluorescence emission by the photosensitizers was collected through a band-pass filter and split with a 50/50 splitter between the two detection channels. When determining diffusion coefficients, the SPAD detectors were placed in cross-correlation mode, eliminating signals which are not common for the two detectors.

The latter experiments performed (when stated) included a filter in front of each detector. A 700LP long pass filter (Omega Optical) was placed in front of detector 1 and a 640BP20 Rapid Band bandpass filter (Omega Optical; CW=640nm, FWHM=20nm) was placed in front of detector 2.

The photosensitizer concentration was kept in the nanomolar range, so that only a few molecules (always below 10) were detected in the confocal volume. Figure 18 presents a diagram of the experimental setup.

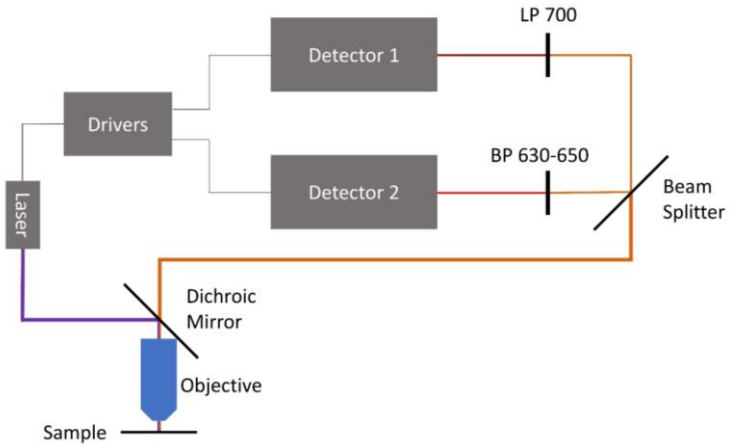

Figure 18. Diagram of the experimental setup for FCS experiments.

3.2.4 Microbial strains

The microorganisms tested in Chapter 3 are *Staphylococcus aureus* ATCC 29213, *Escherichia coli* ATCC 25922, and C*andida albicans* ATCC 10231. Also, gentamicin resistant *Escherichia coli* DH5α which was kindly donated by Dr. Montserrat Llagostera from the Universitat Autònoma de Barcelona, was used to perform photoinactivations.

3.2.5 Neoplastic cell lines and photodynamic inactivation studies

The cancerous cell line used to assess antineoplastic activity was HeLa (EUCELLBANK 0037) from the human cervix epithelial adenocarcinoma. These cells, which grow in a monolayer manner, were cultivated in "Dulbecco's Modified Eagle's Medium" (DMEM) supplemented with 1% (v/v) of L-glutamine, with 10% (v/v) of bovine foetal serum and 1% (v/v) of penicillin/streptomycin. Cells were seeded in T-25 flasks and let grow up to 90% before subculturing at 37 °C in a humid atmosphere with 5% CO_2.

Antineoplastic Uptake Assay

Uptake assays were performed by monitoring porphycene fluorescence after incubating the cells with the photosensitizers.

7,000 cells per well were seeded in 96-well plates and were left to grow during 24 hours until achieving the desired confluence. Porphycene derivatives were diluted in PBS and DMEM (previously supplemented) in a 1:10 (v/v) proportion obtaining a final 1 μM concentration. The

culture medium was changed for the one containing the photosensitizer at different times. After incubating the desired time, cells were washed with culture medium thrice, followed by the addition of 2% sodium dodecylsulphate (SDS) to dissolve the cellular content.

Fluorescent spectra were obtained by exciting at 380 nm and reading at 635 nm using a Synergy H1 Hybrid plate reader (BioTek Instruments, Inc., Winooski, VT, USA). In order to normalize the amount of cells in each well, protein quantification was performed using the bicinchoninic acid assay with bovine serum albumin as reference.[219]

Antineoplastic Photodynamic Inactivation

7,000 cells per well were seeded in 96-well plates and were left to grow during 24 hours until the desired confluence was achieved. Porphycene derivatives were diluted in PBS and DMEM (previously supplemented) in a 1:10 (v/v) proportion obtaining the final concentration desired. The culture medium was changed for the one containing the photosensitizer and left to incubate during the optimal time for each compound determined in the uptake assay. After incubation, cells were washed with culture medium thrice to eliminate the drug fraction which had not been uptaken. Culture medium was reconstituted followed by illumination of the 96-well plate from the top. After letting the cells grow for 24 hours in the incubator, the media was removed and changed for 100 μL of complete medium with 0.05 $mg \cdot ml^{-1}$ of 3-(4,5-dimethylthiazol-2-yl)-2,5-diphenyltetrazolium bromide (MTT) for 3 hours. Then, the media was removed and changed for 100 μl of DMSO in order to lyse the cells.

Cell viability was quantified by colourimetry, using Synergy H1 Hybrid plate reader (BioTek Instruments, Inc., Winooski, VT, USA) to read absorbance at 526 nm. Live cells can metabolize MTT, yielding the coloured formazan, which is formed by MTT reduction by succinate dehydrogenase enzyme in mitochondria.[220]

3.2.6 Microscopic techniques

Stimulated Emission Depletion Microscopy

Stimulated emission depletion (STED) microscopy has been performed using a custom-made setup equipped with a supercontinuum pulsed laser source (ALP-710-745-SC, Fianium LTD, Southampton, UK) previously described.[83] The excitation wavelength was selected by means of an Acousto-optic Tuneable Filter, while the STED wavelength was predefined by the laser outputs, in particular the 750 nm output. The laser presented a repetition frequency of 20 MHz and a pulse width of about 100 ps. In all the experiments, 405 nm was used for excitation and 750 nm as STED beam. The doughnut shape of the STED beam is formed by a vortex phase plate (RPC Photonics Inc., Rochester, NY, USA). The beams are scanned on the sample by galvanometer mirrors (Till-photonics, FEI Munich GmbH, Germany), focused by a HCX PL APO CS 100×1.4NA oil (Leica Microsystems, Mannheim, Germany) objective and fluorescence was collected by an avalanche photodiode (SPCM-AQRH-13-FC, Excelitas Technologies, Vaudreuil-Dorion, Quebec, Canada) in the spectral window 630-730 nm.[221] The bacteria were incubated at a concentration of 8 μM in PBS during 30 minutes. They were later placed on a cover slip which had previously been treated with poly-lysine. After 5 minutes of incubation, the cover slip was washed with water to eliminate the excess salt and unbound bacteria and then sealed against a glass slide. Figure 17 presents a diagram of how a STED microscope functions.[222]

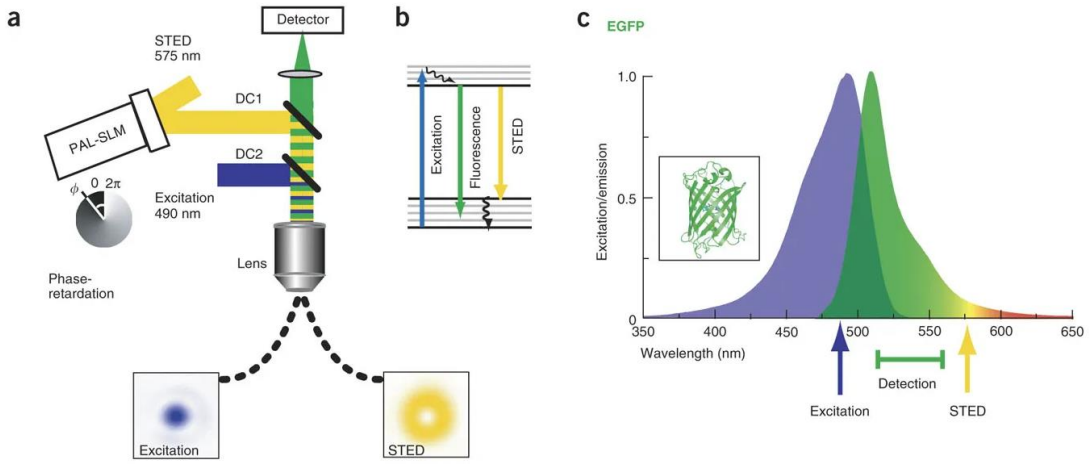

Figure 19. STimulated Emission Depletion microscopy scheme imaging GFP. a: Microscope setup presenting the excitation beam in blue and the doughnut-like STED beam in yellow. b: Jablonski diagram representing the photophysical phenomena involved in STED microscopy (excitation, fluorescence and stimulated emission). c: Spectral overlap of excitation and emission spectra of GFP indicating where excitation and depletion are taking place. Figure adapted from reference [222].

Confocal Spinning Disk Microscopy

HeLa cells were incubated in complete medium with the photosensitizers during 12 hours at 8 μM. Portacin and Porphonium were co-incubated with MitoTracker Green FM (Invitrogen) and Porbutyl with CellMask Green Plasma Membrane Stain (Invitrogen) for 30 minutes. Cells were then thoroughly washed with PBS and finally reconstituted with phenol red-free complete medium. Spinning disk confocal microscopy utilizes multiple pinholes to project a series of parallel excitation light beams onto the specimen in a multiplexed pattern that was subsequently detected after fluorescence emission passed through the same pinholes.

The main features of this technique are the high-speed imaging of living cells and lower photobleaching and phototoxicity due to multiple excitations that needed only a low level of laser power at the specimen to fully excite fluorescence (Figure 20).

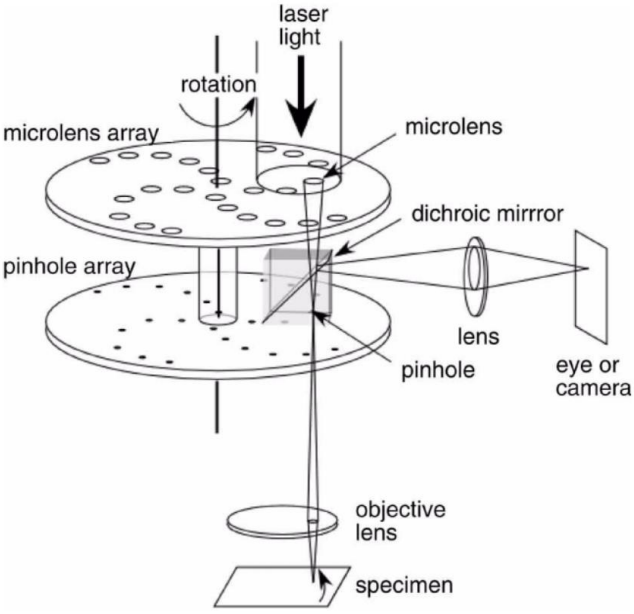

Figure 20. Inner structure of a Spinning Disk Confocal Microscopy. Adapted from source [223].

The microscope was composed by a confocal unit Nikon TiE inverted Microscope equipped with an Okolab incubation system and four excitation lasers (405, 488, 561, and 640 nm). The system was equipped with a Yokogawa CSU-X1 spinning disk containing about 20 000 pinholes and a second spinning disk containing the same number of microlenses to focus the excitation laser light. The fluorescence light was collected by an Andor EMCCD camera Ixon 897. Therefore, the specimens were imaged by sequentially exciting the photosensitizers at 405 nm and the trackers at 488 nm, while detecting fluorescence in the spectral windows of 620-750 nm and 510-540 nm, respectively.

3.3. Results

3.3.1 Photophysical Characterization of Portacin, Porphonium and Porbutyl

Absorbance and Fluorescent properties

Figure 21 presents the absorption and fluorescent spectra of 9-ITMPo, Portacin, Porphonium and Porbutyl in methanol, in which we observe the characteristic Soret and Q-bands of asymmetric porphycenes.[182] In comparison with the 9-ITMPo precursor, the conjugates show a large bathochromic shift in both absorption and fluorescence.

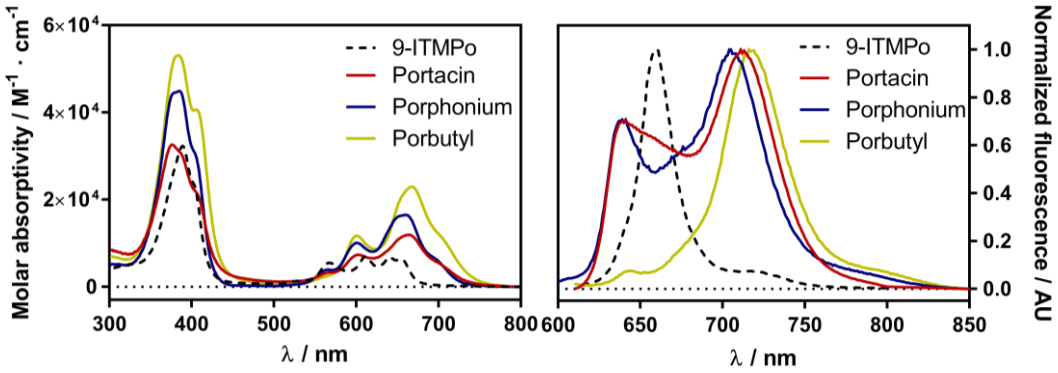

Figure 21. Absorption (left) and fluorescence (right) spectra of 9-ITMPo (black dotted line), Portacin (red), Porphonium (blue) and Porbutyl (yellow) in methanol.

The observed spectral changes of all three conjugates correlate with the results described by Planas and co-workers for fused tetraphenylporphycenes,[189] in which the absorbance and fluorescence are shifted to the near-IR as a result of an expansion of the electronic system from 18π to 22π electrons.

Some spectral differences can be observed between the different conjugates. Looking at the Soret band, Porbutyl presents a band-split which appears as a shoulder in Portacin and Porphonium. Also, at the Q-bands, Porbutyl presents a slightly larger bathochromic shift than its analogues, probably due to the inductive electron effect from the alkyl chain. Even though Porphonium has the same alkyl chain in its structure as Porbutyl, the formal charge at its tip lying delocalized between the phosphorous and phenyl residues prevents the inductive effect

from taking place. Portacin simply cannot present this inductive effect since it lacks an alkyl chain.

Regarding fluorescence, the conjugates exhibit two emission bands in comparison to the single band from 9-ITMPo. The fluorescence bands of the three compounds do not have the same ratio despite being dissolved in the same solvent, indicating that the inner molecular structure play a key role in determining the 18π-22π ratio. Portacin and Porphonium present two clear bands, while it seems that Porbutyl practically does not emit from the 18π chromophore (at 640 nm).

Taking advantage of the solubility of Portacin in aqueous environments, this conjugate was characterized also in phosphate-buffered saline (PBS; pH 7.4) and DMSO (Figure 22).

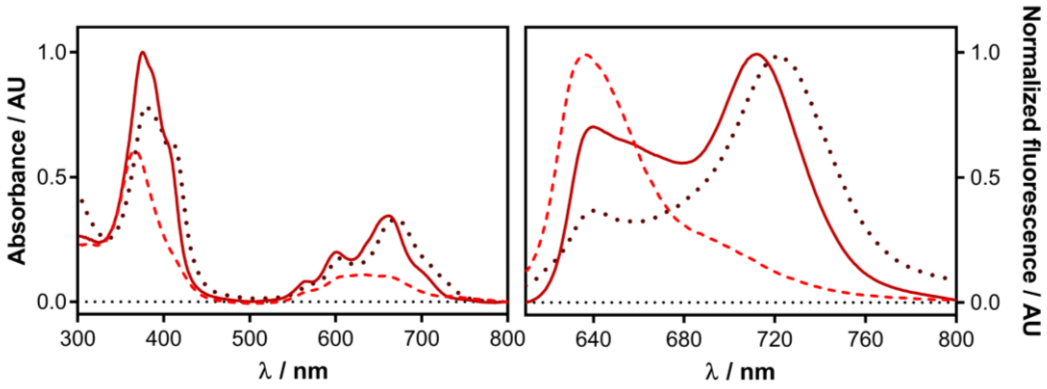

Figure 22. Absorption (left) and fluorescence (right) spectra of Portacin in PBS (red dashed line), methanol (solid dark red line) and dimethyl sulfoxide (brown dotted line).

As shown in Figure 22, the absorption spectra in PBS suffers a blue-shift as well as a loss of its structured bands and exhibiting lower molar absorption coefficients, which is consistent with the aggregation that several porphyrin-like compounds tend to experience in aqueous media.[187] In DMSO, there is a slight red-shift typical of DMSO and also an important splitting of the Soret band, just like that of Porbutyl in methanol (Figure 21).

The fluorescence spectra in PBS presents a single emission band at 640 nm, while a gradual conversion to the near-IR absorbing species (maximum emission at 715 nm) is observed when non-aqueous and less polar solvents are used (MeOH and DMSO). The equilibrium between the

two inner-chromophores are clearly influenced by the different solvents, owing to their different hydrogen bond donating (HBD) capacity. The 18π is favoured by strong HBD solvents such as PBS (involving a charge separation), while the 22π system is promoted in non-HBD like DMSO.[190] Methanol presents an intermediate profile since it is weak-HBD solvent.

This interpretation was further supported by studying Porbutyl (which is insoluble in water) in non-aqueous solvents with different HBD capacity (Figure 23).

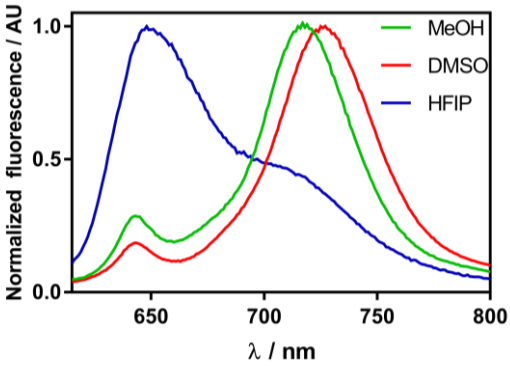

Figure 23. Fluorescence emission of Porbutyl in methanol (green), DMSO (red) and hexafluoro-2-propanol (blue) excited at 600 nm.

As previously shown, Porbutyl in methanol proved to emit very little fluorescence from the 18π chromophore. On one hand, DMSO (which is a non-HBD solvent) only further enhanced this phenomenon, favouring even more the emission from the NIR chromophore. On the other hand, the strong hydrogen donating solvent hexafluoro-2-propanol (HFIP) greatly enhanced the 640 nm emission, following the same trend as for Portacin but with a strong organic HBD solvent. Therefore, it is actually the robust aromatic structure of Porbutyl which prevents methanol from stabilizing even a fraction of the 18π system.

This indeed confirms that the ratio of the two emissions reflects the equilibrium between the 18-π and 22-π chromophores and suggests that the polar antibiotic can stabilize the zwitterionic 18-π system, likely by forming hydrogen bonds through its free amino groups. Porphonium is also an amphiphilic compound with a formal positive charge which may also be able to interrupt

the aromaticity of the 22π electronic system. Figure 24 presents a tentative explanation for the stabilization of the 18π form by the phosphonium cation and gentamicin.

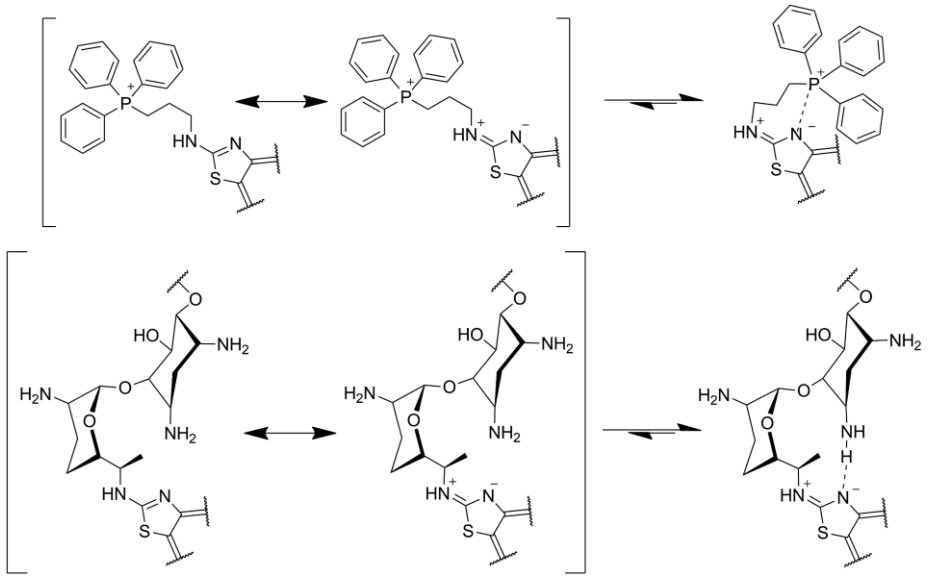

Figure 24. Stabilization of the 18π structure due to the aromaticity interruption by electronic interaction of the formal cation on the triphenylphosphonium and gentamicin's amino groups.

Excitation fluorescence spectra of Portacin in methanol were performed to each fluorescent band (Figure 25), revealing the absorption spectra of the two distinct chromophores.

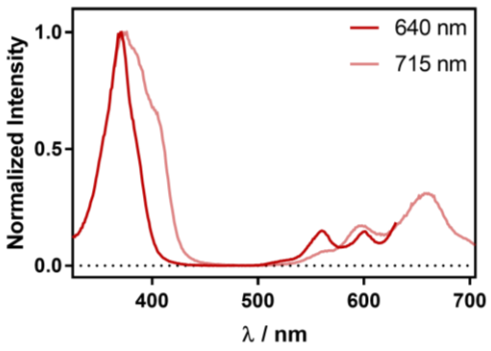

Figure 25 Excitation fluorescence spectra of Portacin observing at 640 nm (red) and at 715 nm (pink).

The fluorescence excitation spectrum indicates that the emission originates from a monomeric species with 18π or 22π electronic system, as observed previously for a related porphycene.[187] The spectrum from the 640 nm band presented a similar absorption spectrum to that of a conventional porphycene (like 9-ITMPo shown in Figure 21), whilst a broader Soret band (like

the one presented by Porbutyl in methanol or Portacin in DMSO) and Q-bands further shifted to the infrared appearing from the 715 nm band.

The ratios between the two emissive species are not the same, depending greatly on the acidity and polarity of the environment, as well as on the own structure of the molecule. The absorption spectrum will be therefore a weighted sum of the individual absorption spectrum of either electronic system.

These two emissions were further examined by time-resolved fluorescence (TRF) analysis (Figure 26).

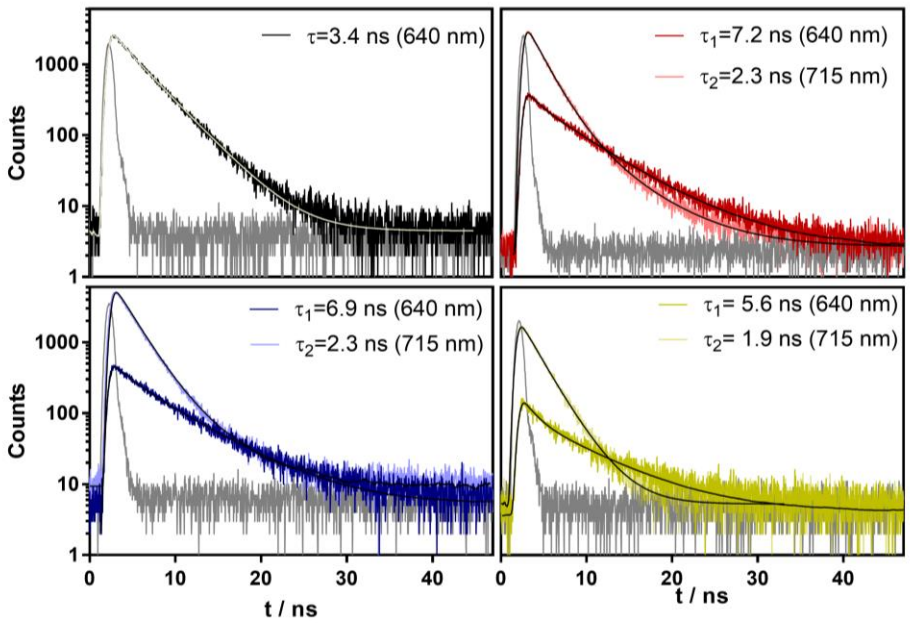

Figure 26. Time-resolved fluorescence decays at 640 and 715 nm of 9-ITMPo (Black; top left), Portacin (red; top right), Porphonium (blue; bottom left) and Porbutyl (yellow; bottom right) exciting at 596 nm. The instrument response function (IRF) is represented in grey.

While 9-ITMPo fluorescence decays with monoexponential kinetics (τ_s = 3.4 ns), the three porphycene conjugates decay with biexponential kinetics indicating two different populations of the excited singlet state of the PS. Along with Time Resolve Emission Spectra (TRES) shown in Figure 27, a pattern behaviour was observed in which a longer emitting fluorescence (ranging from 5.6 ns to 7.2 ns; Table 1) originated from the 18π structure, while shorter fluorescence

lifetimes (ranging from 1.9 ns to 2.3 ns; Table 1) from the 22π chromophore. This phenomena was already described by Planas when studying other expanded porphycenes.[190]

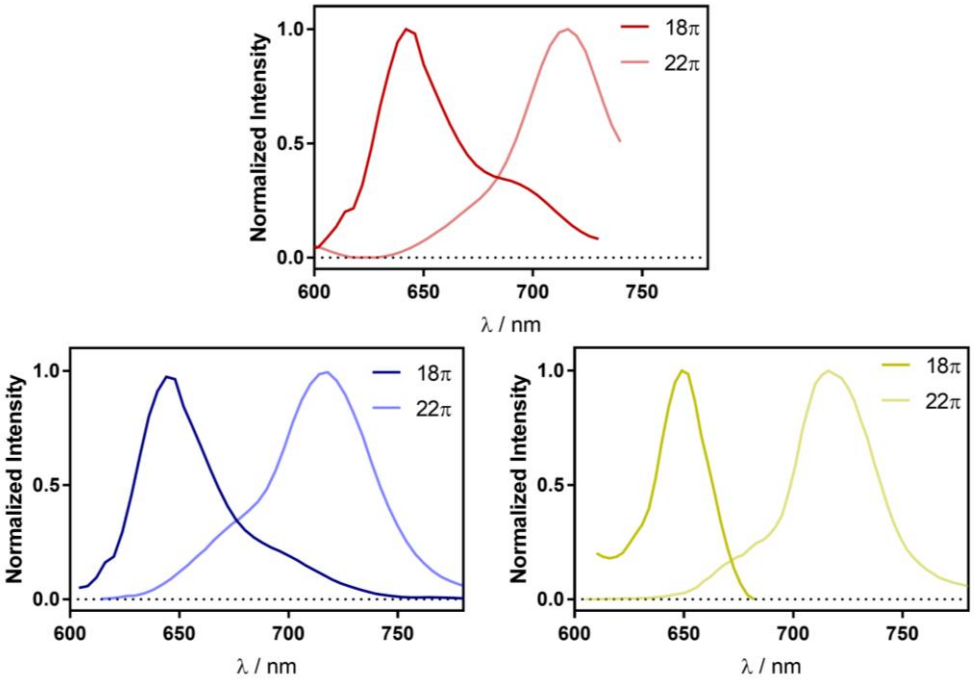

Figure 27. Time Resolved Emission Spectra of Portacin (top; red), Porphonium (bottom left, blue) and Porbutyl (bottom right, yellow) exciting at 596 nm in methanol. The darker colour represents the 18π chromophore and the lighter colour represents the 22π chromophore.

Time resolved fluorescence was also attempted after incubating the photosensitizers with *S. aureus*, and even though differences in the relative amplitudes between chromophores were expected due to the hydrophobicity of the bacterial wall, no major changes were detected in comparison with the results obtained in organic solvent or PBS.

The fluorescent quantum yields were determined in methanol using tetraphenylporphyrin[165] in toluene as reference. All conjugates presented similar quantum yields, between 0.06 and 0.15 (Table 1). The solubility of Portacin in water permitted to measure its fluorescence yield in PBS, resulting in 0.02, 5 times lower than the fluorescence quantum yield in methanol. This reduction is due to the aggregation of the photosensitizer in water, as reflected also in the absorbance spectrum.

Triplet lifetime and Φ_Δ Quantification by Direct Phosphorescence Detection (1275 nm)

Continuing with the photophysical characterization, the lifetime of the triplet states of the conjugates were measured by nanosecond laser flash photolysis in deaerated methanol. Figure 28 presents the transient absorption variation spectra of 9-ITMPo (grey; top left), Portacin (red; top right) and Porbutyl (yellow; bottom right) excited at 355 nm and observed at 600 nm.

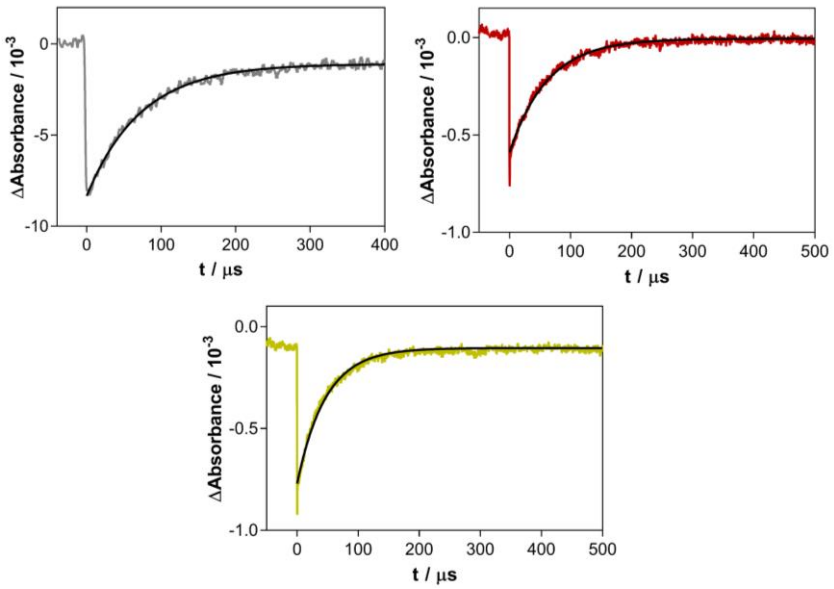

Figure 28. Transient absorption of 9-ITMPo (grey; top left), Portacin (red; top right) and Porbutyl (yellow; bottom) excited at 355 nm and observed at 600 nm under an argon atmosphere.

The signals were fitted with monoexponential curves, determining the lifetimes to be 74, 66 and 47 μs respectively. Since two chromophores exist, one would expect to find two distinct triplet lifetimes (one for either chromophore). Monoexponential curves fitted adequately the signal, indicating that the lifetime of the two chromophores are either very similar and that the measuring system is not able to distinguish between such close values or that there is an interconversion between the two species faster than the decay of both chromophores. In these cases, a monoexponential decay is also observed.

Φ_Δ Determination by Direct Phosphorescence Detection at 1275 nm

The ability of the expanded porphycenes to sensitise the production of $^1O_2$ was studied in methanol (Figure 29).

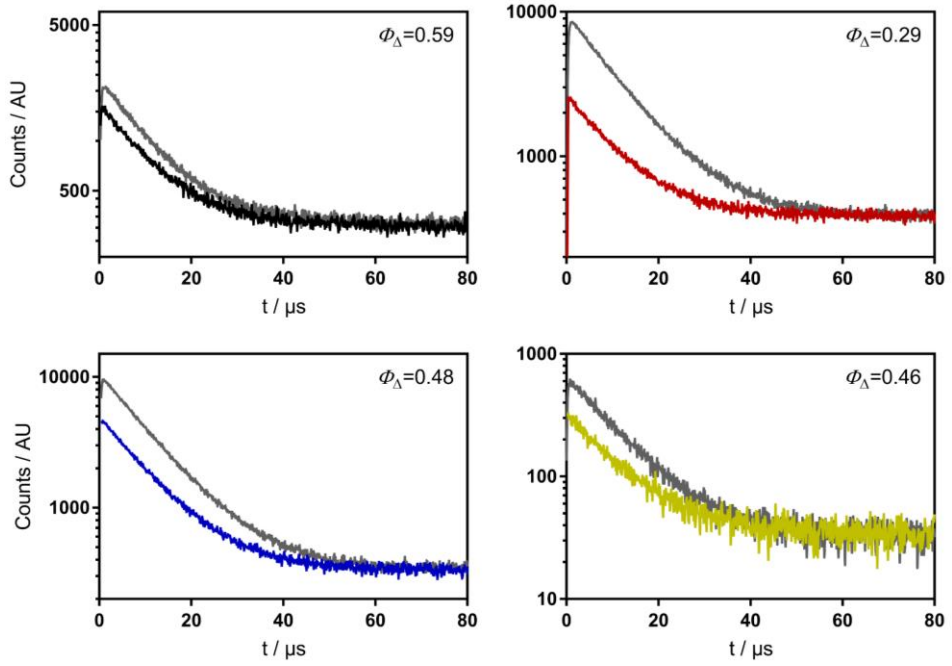

Figure 29. Singlet oxygen quantum yield determination by direct detection of phosphorescence at 1275 nm of 9-ITMPo (grey; top left), Portacin (red; top right), Porphonium (blue; bottom left) and Porbutyl (yellow; bottom right). The grey line represents the signal emitted from an optically matched solution of Phenalenone (reference).[166]

The yields observed reflect a general reduction in the efficiency of the energy transfer towards oxygen after cyclization. 9-ITMPo presents a Φ_Δ of 0.59, while the conjugates do not exceed the 50% efficiency. Signals from all conjugates were quenched after adding sodium azide, proving that the signal recorded is originated from singlet oxygen phosphorescence.[224] This trend was previously reported by Planas and co-workers for the tetraphenylporphycene analogues,[189] and despite being measured then in acetone, the Φ_Δ values observed for the tetra(methoxyethyl)porphycenes are higher, indicating an improved sensitization when introducing the alkyl chains. Notoriously, the Φ_Δ of Portacin is considerably lower than those of Porphonium and Porbutyl. This could be due to photoinduced electron transfer (PET) quenching of the thiazoloporphycene excited states from the free electron pairs of the primary amines present in gentamicin. This phenomenon has been previously reported in other amino-

substituted porphyrinoids.[225,226] The amino group directly attached to thiazoloporphycene ring is not expected to participate in the PET process due to the delocalization of its electron pair across the macrocycle, as observed with Porphonium and Porbutyl which share this linking amine group with Portacin.

Having observed the lower Φ_Δ of Portacin in methanol, the $^1O_2$ production was further studied in different solvents and different pH. Φ_Δ was measured in heavy water, methanol and dimethyl sulfoxide (DMSO) at neutral, acidic (by adding a drop of diluted acetic acid) and basic (by adding a drop of diluted sodium carbonate) conditions in each solvent. Figure 30 presents the phosphorescent transient signals of singlet oxygen of Portacin and an optically matched reference (PNS in PBS, PN in MeOH and C_{60} for DMSO) in the mentioned conditions, and the yield determined.

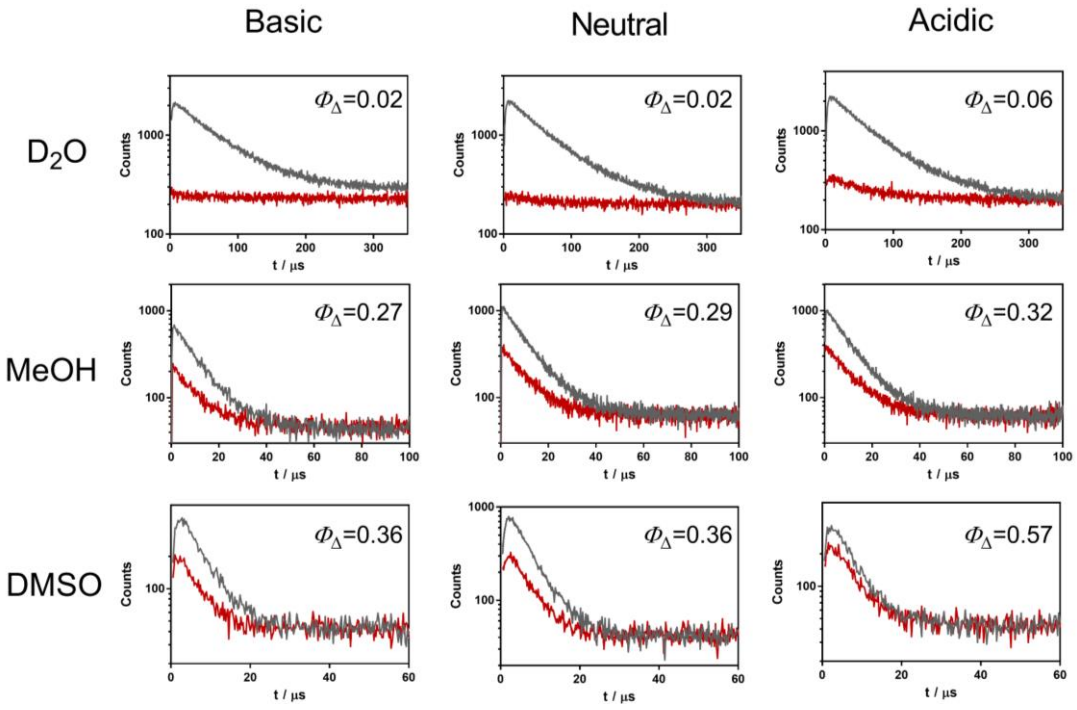

Figure 30. Singlet oxygen quantum yields of Portacin in air-saturated heavy water (top), methanol (middle) and dimethyl sulfoxide (bottom) in basic (left), neutral (centre) and acidic (right) pH by adding diluted sodium carbonate and acetic acid (respectively). PNS was used as reference in heavy water (Φ_Δ =1.03)[167]; PN was used as reference in methanol (Φ_Δ=0.97)[166] and Fullerene C_{60} used as reference in dimethyl sulfoxide (Φ_Δ=1).[227]

The Φ_Δ of Portacin presents different efficiencies depending on the H-bond donor properties of the solvent and on the protonation or deprotonation of the amines of gentamicin. To begin, the Φ_Δ in heavy water is very low (Φ_Δ = 0.02) due to the aggregation of the compound (phenomena already described previously). The addition of sodium carbonate did not induce a change in the quantum yield, but acetic acid enhanced it yield. This increase is due to the protonation of the free amines in gentamicin which can undergo PET, and therefore reducing the capacity of the photosensitizer to generate $^1O_2$. Since carbonate did not change the Φ_Δ it can be said that the amines of gentamicin have their free electron pair available in physiological medium. The increased Φ_Δ in methanol indicates that the compound is non-aggregated in this solvent. As in water, amine protonation induces an increase in the Φ_Δ while no difference was observed in basic conditions. Regarding dimethyl sulfoxide, there is a further increase in the Φ_Δ in comparison with methanol in "neutral" conditions. As before, the addition of base did not change the Φ_Δ yield but acetic acid did increase it up to values close to those of 9-ITMPo. DMSO presented the highest Φ_Δ of the series and also did not present the ability to form hydrogen bonds with its solute.

As mentioned previously, water and methanol are strong H-bond donors and can partially stabilize the 18π zwitterionic form of the photosensitizer. This zwitterionic form presents a formal negative charge on the thiazole ring[190] and, due to its proximity to the photosensitizer, it may easily undergo photoinduced electron transfer. Since DMSO cannot stabilize this zwitterionic form, PET takes place to a lesser extent and might even be suppressed after protonating gentamicin's amines.

To sum up, the photophysical properties of 9-ITMPo, Portacin, Porphonium and Porbutyl have been summarized in Table 1.

Table 1. Summary of the photophysical properties of 9-ITMPo, Portacin, Porphonium and Porbutyl in methanol.

PS	λ_{Abs}/nm	ε / M^{-1} cm^{-1}	λ_{Fluo}/nm	Φ_F	τ_S/ ns	Φ_Δ	τ_T/µs
9-ITMPo	640	$6.8 \cdot 10^3$	659	0.26	3.4	0.59	74
Portacin	664	$1.2 \cdot 10^4$	643; 713	0.10 ± 0.02	τ_1 = 7,2; τ_2 = 2.3	0.29 ± 0.02	66
Porphonium	660	$1.7 \cdot 10^4$	639; 705	0.12	τ_1 = 6.9; τ_2 =2.3	0.48 ± 0.02	-
Porbutyl	667	$2.3 \cdot 10^4$	640; 716	0.06	τ_1 = 5.6; τ_2 = 1.9	0.46 ± 0.02	47

3.3.2 Femtosecond Laser Flash Photolysis

The femtosecond flash photolysis measurements were performed at the Politecnico di Milano in collaboration with Professor Giulio Cerullo and Dr. Margherita Maiuri. Figure 31 presents an example of the raw data obtained by femtosecond flash photolysis. The 3D scheme shows how light transmittance ($\Delta T/T$) from the probe changes according to wavelengths and time lapses.

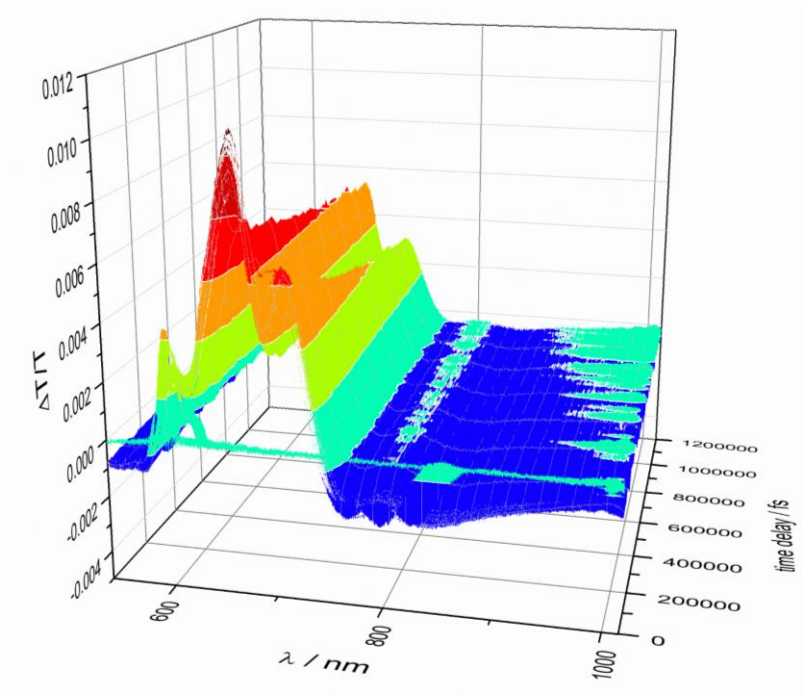

Figure 31. Femtosecond Flash Photolysis of Portacin in methanol.

The three porphycene conjugates and their precursor 2,7,12,17-tetrakis(methoxyethyl)porphycene (TMPo) were analysed with this technique. Data from these 3D plots were processed in order to obtain absorbance variations at different time delays and selected wavelengths (kinetics); and absorbance variation at different wavelengths but fixed time scale (spectra). Measures were performed in methanol where the compounds are completely unaggregated, and in PBS in the presence of *S. aureus*. Since Portacin is soluble in water, this conjugate was also analysed alone in PBS.

Figure 32 presents the kinetic profiles of TMPo (A), Portacin (B), Porphonium (C) and Porbutyl (D) in methanol, along with a global exponential fitting to all wavelengths represented with a black line.

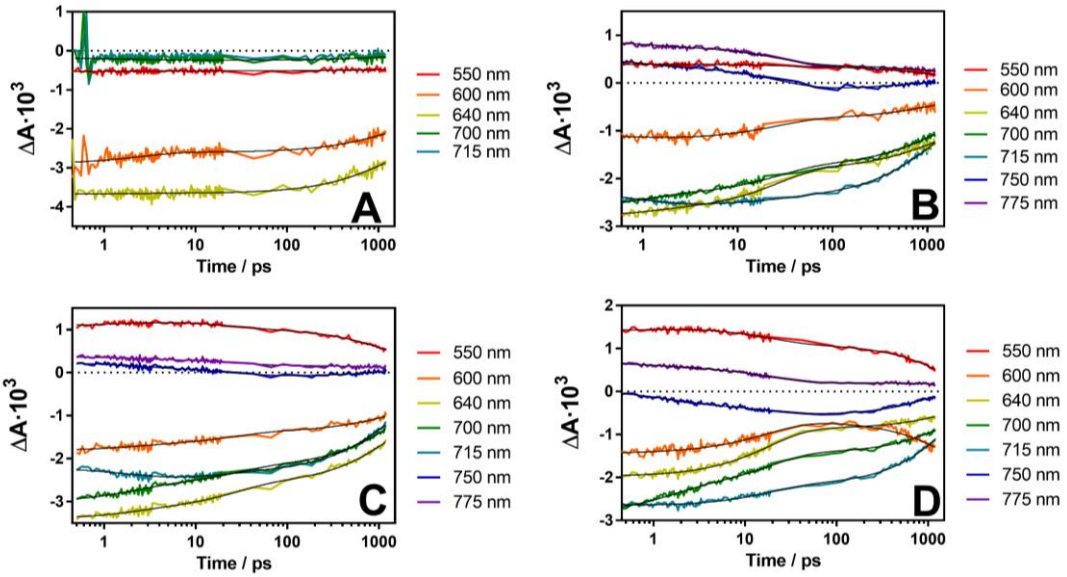

Figure 32. Femtosecond kinetic transient absorption in methanol of TMPo (A; top left), Portacin (B; top right), Porphonium (C; bottom left) and Porbutyl (D; bottom right) at several wavelengths and their exponential decay fittings.

At a glance, we observe a rich photophysics in this ultrafast time scale. The photophysics presented by TMPo (A) is simpler than that of the conjugates due to the presence of only one chromophore. As presented in Table 2, a 2-exponential decay for TMPo and a 3-exponential decay for the conjugates were required to achieve adequate fitting.

Table 2. Lifetime of ultrafast processes of TMPo and Portacin, Porphonium and Porbutyl in methanol.

PS	τ_1 / ps	τ_2 / ps	τ_3 / ns
TMPo	2.5	N/A	1.2
Portacin	1.0	26	1.1
Porphonium	2.0	27	1.4
Porbutyl	1.4	18	2.5

The lifetimes fitted present 2 shared decays in all compounds in the order of the picoseconds and of the nanoseconds. Also, and due to inherent more complex photochemistry, the 3 conjugates present a singular additional decay in the order of tens of picoseconds which is not found in the precursor, TMPo. The lifetimes in the picosecond range correspond to vibrational relaxations from higher electronic levels down to S_1. The decay with a lifetime of 20 ps is not found in TMPo, indicating that this longer lifetime may be assigned to the 22π species.

The longest lifetime corresponds to the lifetime of S_1, which as measured by TRF, is of a few nanoseconds. These values obtained are not quantitatively reliable since the flash photolysis measuring conditions only ranged until 1.2 ns. If the system could measure beyond more reliable values would be obtained, which should be completely comparable to those observed by TRF.

Figure 33 stems from setting the time variable at 1.2 ps from the 3D plot and examining the spectrum-like graph (blue line) in methanol. The green line represents the absorbance spectra of the compounds, and the red one a qualitative subtraction from the previous.

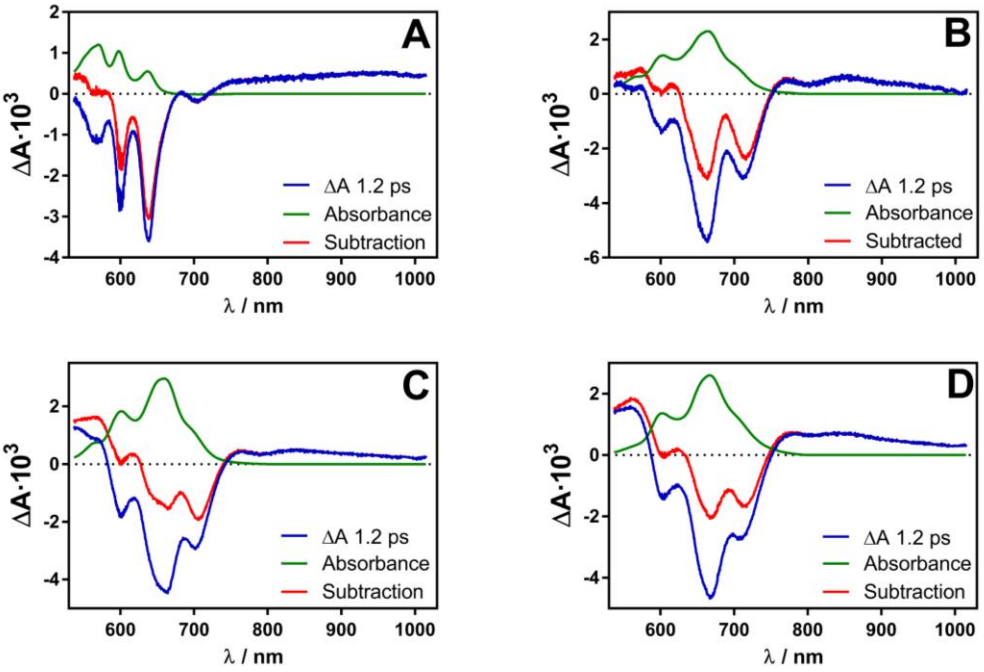

Figure 33. Femtosecond spectral transient absorption in methanol of TMPo (A; top left), Portacin (B; top right), Porphonium (C; bottom left) and Porbutyl (D; bottom right) at 1.2 ps, representing the absorption variation at 1.2 ps (blue), the absorption spectra of the compound (green) and a qualitative subtraction of both spectra (red).

The signal recorded presents a large negative range which mirrors quite accurately that of the absorption, and a milder positive signal on either side of the depleted area. The mirror image obtained with a negative sign is due to the depletion of the ground state, whilst the positive bands correspond to excited state absorption.

The qualitative subtraction was performed by "normalizing" the subtraction at the highest energy band absorption maximum in order to eliminate the large ground state depletion. The ground state depletion may occlude weaker phenomena also taking place.

The red line presents a continuous excited state absorption along the light spectra analysed, to which some depleting signals are overlaid. Portacin (B), Porphonium (C) and Porbutyl (D) present a depleting band at approximately 710 nm, and most notably, at 620 nm for TMPo which corresponds to stimulated emission. The other minor negative bands are also a result of stimulated emission which takes place at other specific wavelengths where there is a quantumly defined energy gap.

Qualitatively speaking, TMPo presents a much larger ΔA signal than its normalized absorption, indicating an efficient light stimulated emission. In large contrast, stimulated emission from the conjugates is milder most likely due to an overlap of stimulated emission with excited state absorption. This competition between processes results in a reduction of stimulated emission.

Despite knowing that most photosensitizers are insoluble in water (and in this case only Portacin is water-soluble), femtosecond spectroscopy was attempted in an aqueous environment in the presence of *S. aureus* in PBS. Figure 34 presents the kinetic profiles in aqueous media of Portacin in PBS (A) and Portacin (B), Porphonium (C) and Porbutyl (D) in the presence of *S. aureus*, along with a global exponential fitting to all wavelengths represented with a black line.

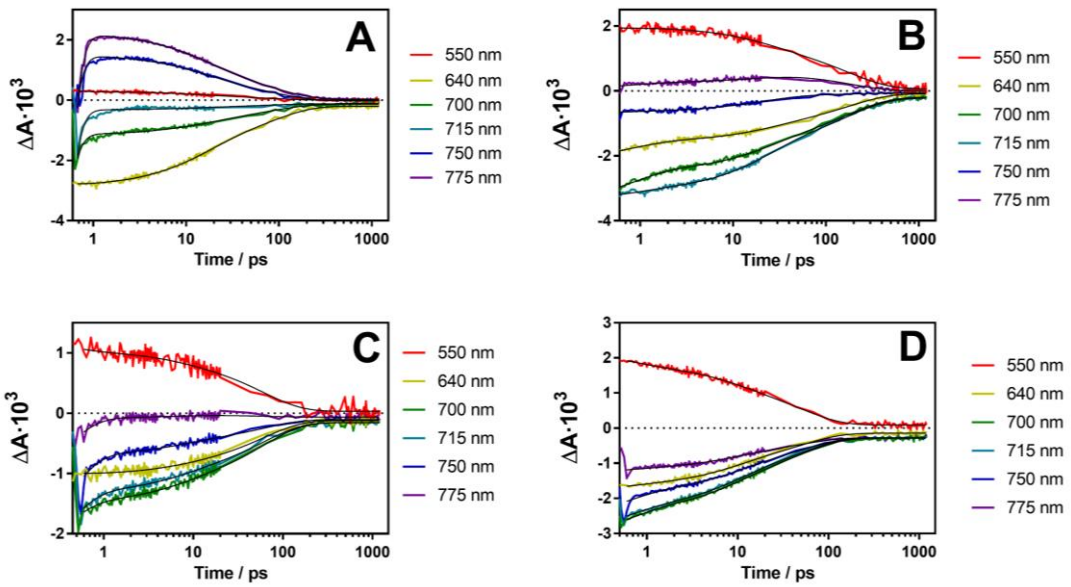

Figure 34. Femtosecond kinetic transient absorption in PBS of Portacin (A; top left) and in the presence of S. aureus of Portacin (B; top right), Porphonium (C; bottom left) and Porbutyl (D; bottom right) at several wavelengths and their exponential decay fittings.

The comparison between Portacin in methanol (Figure 32, section B) with Portacin in PBS (Figure 34, section A) exemplifies how the rich photochemistry observed in methanol (which lasts up to the nanosecond range) is cut short down to some hundreds of picoseconds. This lifetime reduction of the photophysical phenomena is due to the aggregation of the compound and explains experimentally the empirically well-known loss of photophysical activity of hydrophobic photosensitizers in aqueous media. Aggregated molecules in water present therefore faster non-radiative decay pathways which reduce all other slower processes. Fluorescence is mostly lost due to the short lifetime of the first singlet excited state. Of course, any intersystem crossing phenomena is also affected, and therefore the singlet oxygen quantum yield is also smaller.

The addition of bacteria of the system (Figure 34) resulted in a partial disaggregation of the photosensitizers due to the binding of the compounds to *S. aureus*, which was reflected in the recovery of the photophysical properties (for Porphonium and Porbutyl) and a slight time lengthening in the lifetimes of Portacin. Table 3 presents the lifetimes of these measurements.

Table 3. Lifetime of ultrafast processes of Portacin in PBS and Portacin, Porphonium and Porbutyl incubated with S. aureus.

	PS	τ_1 / ps	τ_2 / ps	τ_3 / ns
PBS	**Portacin**	0.11	14	0.08
Bacteria	**Portacin**	0.79	21	0.18
	Porphonium	0.30	6	0.06
	Porbutyl	0.54	8	0.05

Fitting 3-exponential decays to the signals revealed lifetimes approximately 2 orders of magnitude shorter than those in methanol. The porphycene conjugates find a hydrophobic environment at the cell wall, being able then to disaggregate and partially recover their properties. Figure 35 stems from setting the time variable at 1.2 ps from the 3D plot and examining the spectrum-like graph (blue line) in an aqueous environment. The green line represents the absorbance spectra of the compounds, and the red one a qualitative subtraction of the previous.

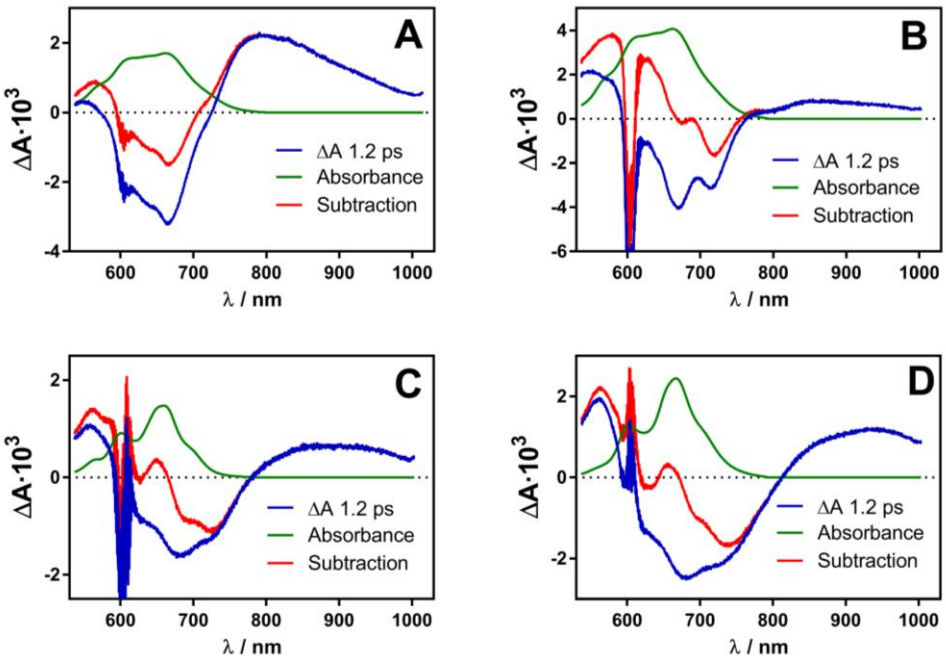

Figure 35. Femtosecond spectral transient absorption in PBS of Portacin (A; top left) and incubated with S. aureus of Portacin (B; top right), Porphonium (C; bottom left) and Porbutyl (D; bottom right) at 1.2 ps. The absorption variation at 1.2 ps is represented in blue, the absorption spectra of Portacin in PBS and of Porphonium and Porbutyl in methanol in green and the qualitative subtraction of both spectra in red.

The comparison between Portacin in methanol and PBS (Figure 33 section B and Figure 35 section A) show how the ΔA signal loses its structure due to aggregation in the same way its absorbance spectra does. Also, there is an increase in the ΔA beyond 750 nm in PBS which is probably due to, in addition to the monomer excited-state absorption, absorption of aggregates or exciplexes. Once bacteria are added into the system, the signal recovers its structure, proving once more the binding to a hydrophobic region on the bacteria. Also, the three "solvents" share a minimum at approximately 665 nm and 710 nm, corresponding to stimulated emission.

Porphonium and Porbutyl show a similar pattern, presenting a ΔA minimum at 680 nm and a second relative minimum at approximately 730 nm corresponding to stimulated emission. There is also a large absorption beyond 800 nm corresponding to absorption of aggregates and of excites states.

A final comparison of transients at 640 nm and 715 nm between solvents and bacteria are represented in Figure 36.

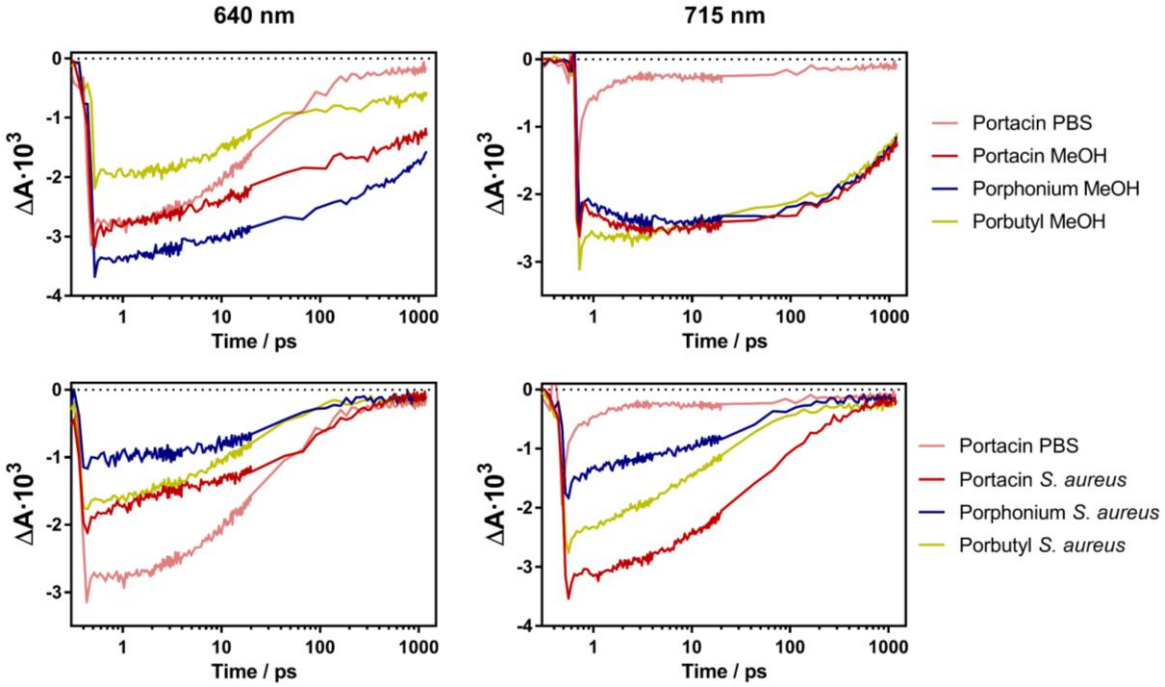

Figure 36. Femtosecond Flash photolysis of Portacin (red), Porphonium (blue) and Porbutyl (yellow) in methanol, incubated with S. aureus and, only for Portacin, in PBS as a comparison. Left graphs represent transients at 640 nm and right ones at 715 nm.

Figure 36 represents transients which appear in previous figures but correspond to the fluorescent maxima of the conjugates and can help to establish interesting comparisons. As mentioned previously, the solvent in which the conjugate is found conditions its photophysical properties by enhancing one or other chromophore within the molecule. In methanol, the three conjugates present large decays both at 640 nm and 715 nm, but Portacin in PBS does not. This is coherent with other spectroscopic measures such as fluorescence, in which the emission is observed only from 640 nm, from the 18π chromophore. Once bacteria are added, the photophysics of Portacin at 715 nm is recovered, once again, due to the apolar environment found at the bacteria which promotes the 22π chromophore.

3.3.3 Fluorescence Correlation Spectroscopy

Fluorescence correlation spectroscopy (FCS) is a spectroscopic technique which also permitted to evidence interaction between the photosensitizers and bacteria.

Figure 37 presents the results after performing an FCS correlation to the three expanded porphycene photosensitizers in PBS. Molecules were excited at 405 nm and all fluorescence was registered from 510 nm to longer wavelengths.

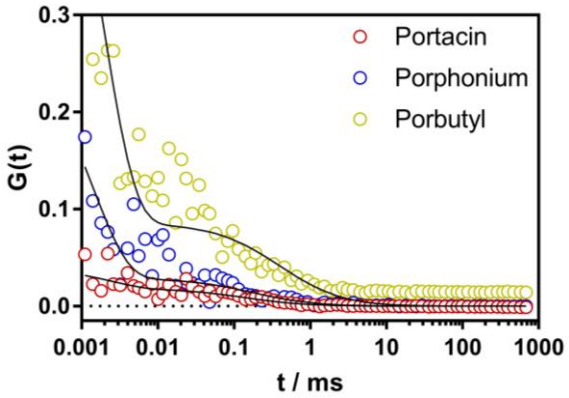

Figure 37. Fluorescence correlation spectroscopy of Portacin (red), Porphonium (blue) and Porbutyl (yellow) in PBS. Fitting curves are represented in black.

G(t) is a parameter which depends inversely on the number of molecules which go through the confocal volume, and therefore can be different depending on the concentration of the sample.

Table 4 presents the diffusion time (τ_i), the diffusion coefficient (D) and the radius (r) of the diffusing particles.

Table 4. Diffusion times (τ_i), diffusion coefficients (D), and radius' (r) of Portacin, Porphonium and Porbutyl determined by FCS in PBS.

Photosensitizer	τ_i / ms	D_i / $\mu m^2 \cdot s^{-1}$	r / Å
Portacin	0.14	250	11
Porphonium	0.18	200	14
Porbutyl	6.32	6	492

The radius values obtained for Portacin and Porphonium match nicely those calculated computationally with the software Chem3D (radii of 13 and 10 Å for Portacin and Porphonium respectively), whilst the radius determined for Porbutyl is much larger than the computational value, also of 10 Å. This difference in the radius of the molecule can be attributed to aggregation of Porbutyl in aqueous solvents. Large aggregates instead of monomers circulate through the confocal volume.

The three conjugates were tested also in bacteria. Specifically, Portacin was incubated with *S. aureus* and *E. coli* for 30 minutes before running FCS (Figure 38).

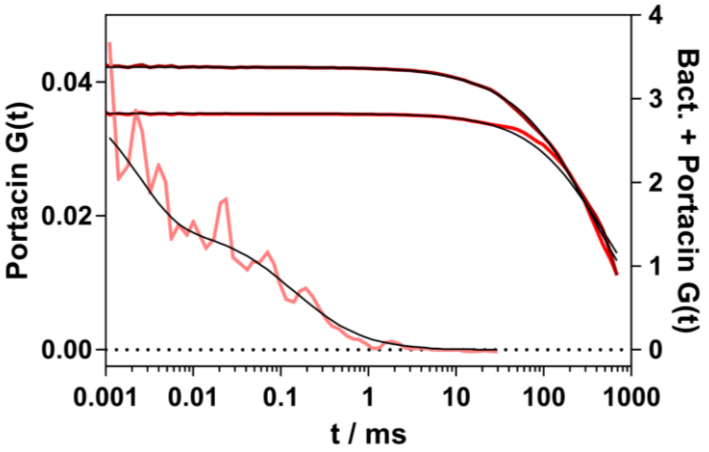

Figure 38. Fluorescence correlation spectroscopy of Portacin in PBS (light red), incubated in S. aureus (bright red) and in E. coli (dark red). Fitting curves are represented in black.

The plot revealed a huge decrease in the diffusion coefficient which is due to Portacin attaching to the bacteria. Whether this attachment is only superficial to the wall or further internalized is unknown. The diffusion coefficients of the bacteria labelled with Portacin were of 0.07 $\mu m^2 \cdot s^{-1}$ for *S. aureus* and of 0.10 $\mu m^2 \cdot s^{-1}$ for *E. coli*, which correspond to 4.0 and 2.9 μm in radius respectively. These sizes are rather larger than expected for *S. aureus* and *E. coli* (which are usually of approximately 1 μm[228] and 2 μm[229] respectively) probably due to errors while fitting, or maybe due to the agglomeration of more than one bacterial cell together.

A modification was introduced into the instrument, which consisted in adding two different filters in front of each detector. The role of the two detectors is to be able to reduce background random noise when measuring by performing a cross-correlation analysis between the two detectors. By introducing the filters, we can take advantage of the two emissive chromophores within the same molecule. A band pass filter (BP 630-650 nm) was used to select the 640 nm fluorescence emission from the 18π chromophore and a long pass filter (LP 700 nm) to measure the emission at 715 nm from the 22π system.

The three porphycene conjugates were incubated with bacteria and studied in this dual detection manner. Figure 39 presents the Multichannel Scaling trace for all conjugates in PBS (left) and incubated in *S. aureus* (right), which represents the photons detected throughout the acquisition time.

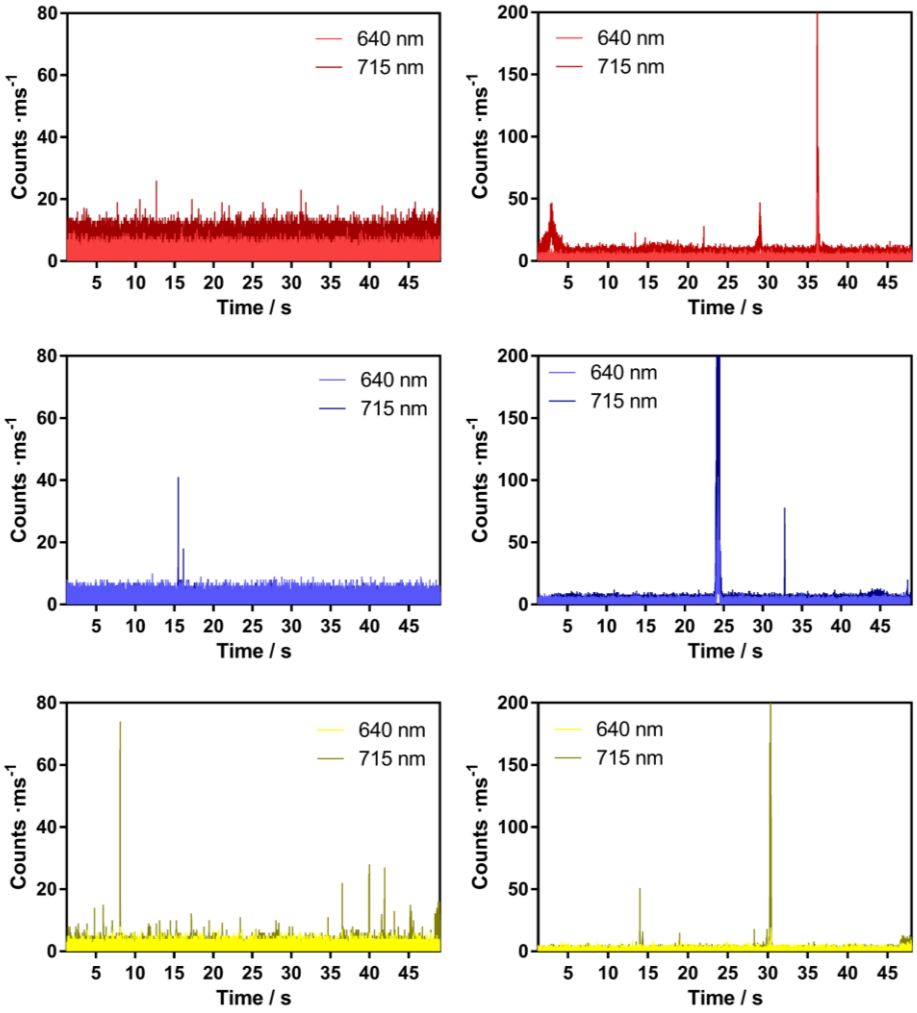

Figure 39. Multichannel scaling trace of Portacin (top, red), Porphonium (middle, blue) and Porbutyl (bottom, yellow) in PBS (left) and incubated in S. aureus (right).

The figure reveals how Portacin and Porphonium in PBS generate a relatively low, constant and homogeneous signal at both detectors (counts per millisecond), which contrasts with the spikes observed at 715 nm by Porbutyl. The 18π chromophore is promoted in PBS in all chromophores, and therefore most of the signal detected is at this wavelength. Porbutyl, due to its insolubility, aggregates and therefore is also enabled to emit from the 715 nm chromophore. This formation of aggregates, which of course will be larger in size than single molecules, is in agreement with the small diffusion coefficient determined previously.

The addition of bacteria enhances the spikes observed at 715 nm up to an order of magnitude in counts. This is indicative of bacteria that have uptaken the drug and diffuses through the confocal volume. The hydrophobic environment which can be found at the bacterial wall

promotes the emission from the 22π system, which is reflected in the number of counts detected at this wavelength.

The FCS trace obtained from these measures also detects how the emission from the 22π chromophore is greatly enhanced when bacteria travel through the confocal volume (Figure 40).

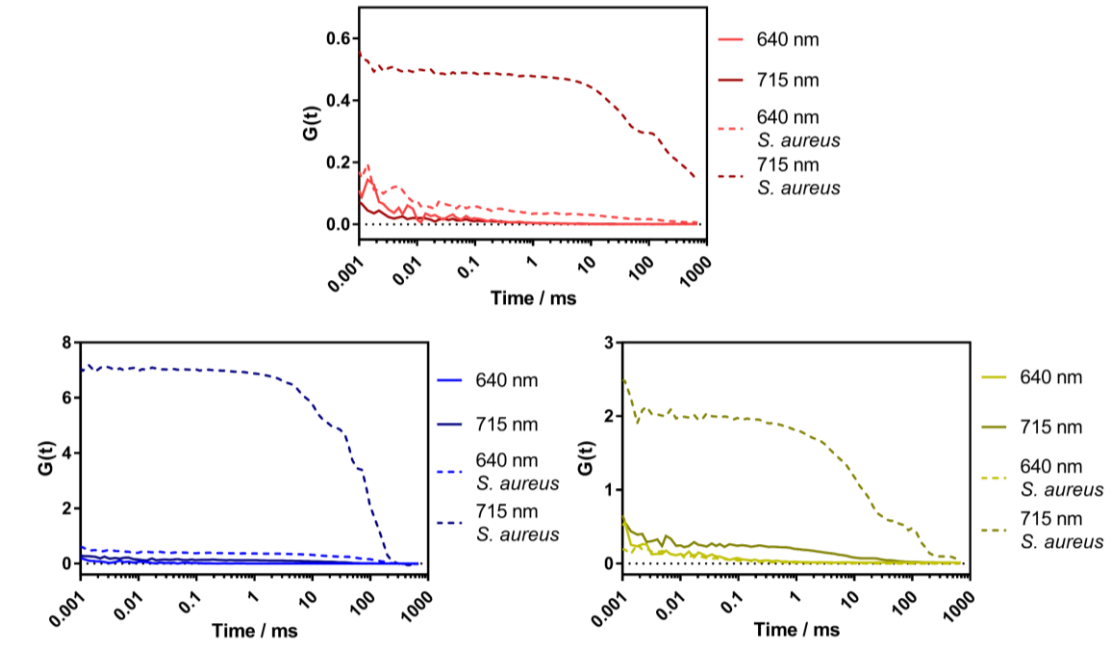

Figure 40. FCS trace of Portacin (top, red), Porphonium (bottom left, blue) and Porbutyl (bottom right yellow) in PBS (solid lines) and after a 30-minute incubation with S. aureus (dotted lines).

In all cases, the autocorrelation signal at 715 nm in bacteria grows vastly due to the fewer number of times a bacterium flows through the confocal volume in comparison to free photosensitizers in solution. The sensitivity to polarity presented by 2-aminothiazoloporphycenes is responsible for the singular increase of the deep red emission. Emission at 640 nm is not promoted when bound to bacteria, which can be associated to the free diffusing photosensitizers in solution.

As with femtosecond spectroscopy, FCS also enabled to spectroscopically detect drug-bacteria interaction harnessing the different spectral emission of expanded porphycenes according to polarity.

3.3.4 Antibacterial in vitro assays

Portacin: Antibiotic-photosensitizer conjugate mechanism of action

Tests against *Escherichia coli* (Gram-negative) were performed in order to assess and study the potential and mechanism of action of Portacin as a novel photosensitizer-antibiotic conjugate.

A first proof of concept experiment was performed on *E. coli* (Figure 41). 8 μM solutions of gentamicin, Porbutyl, Portacin (covalently bound) and an equimolar mixture of Porbutyl and gentamicin (individual elements non-covalently bound) were incubated for 30 minutes in PBS.

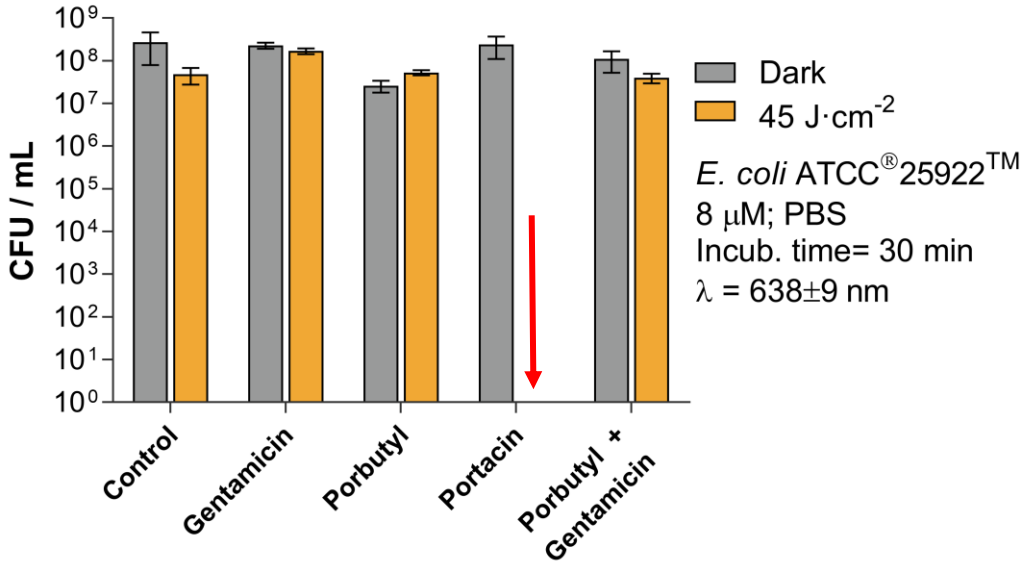

Figure 41. E. coli photoinactivation studies in PBS at 8 μM upon red light irradiation (λ = 638 ± 9 nm) (orange bars). Grey bars represent dark controls. Light doses: 45 J·cm^{-2}. Incubation time: 30 minutes. Data correspond to the mean ± SD after performing three replicates.

Surprisingly, only Portacin was able to completely eliminate the strain without showing any dark toxicity, while no effect whatsoever was inflicted by either Porbutyl and gentamicin alone nor combined. Regarding the antibiotic concentration used (8 μM, 3.8 μg/ml), it is close to the reported minimum inhibitory concentration (MIC; 4 μg/ml).[230] However, MIC values are determined at inoculum sizes (CFUs·mL^{-1}) 100-1000-fold more diluted than those used in this work and, in addition, the antimicrobial effect is measured after incubating the

drug for 24 h, while only 30 min contact was allowed in our experiments. Therefore, the lack of dark toxicity (effect of the antibiotic) is not surprising.

Stemming from the results observed, the antibiotic moiety of the conjugate does not seem to exert any bactericidal effect; all cell death being attributable to the photodynamic activity of the porphycene. Rather, gentamicin enhances the solubility of the porphycene and endows it with amphiphilic character. We suspect that this allows the conjugate to cross the bacterial wall, causing damage not only to the outer wall, as the butyl conjugate would also do, but also to the inside of the bacteria, and therefore exhibiting a larger biological activity. This experiment clearly indicates that, despite presenting a lower Φ_Δ than Porbutyl in methanol, the amphiphilic nature of Portacin is the key factor which permits to inactivate *E. coli* efficiently.

To further investigate the mechanism of action of Portacin, inactivations were performed against *E. coli* DH5α resistant to gentamicin. The resistance to this antibiotic was checked by means of an antibiogram. Antibiograms are used in clinics to check whether a strain is sensitive or resistant to a certain antibiotic. On a plate prepared for confluent growth, an empty "halo" around a disk loaded with antibiotic indicates susceptibility to that antibiotic, whilst growth around it shows resistance. Figure 42 presents the antibiograms performed on the two *E. coli* strains. ATCC 25922 appears to be sensitive to gentamicin at 10 $\mu g \cdot ml^{-1}$ whilst the strain *E. coli* DH5α is resistant to gentamicin at the same concentration.

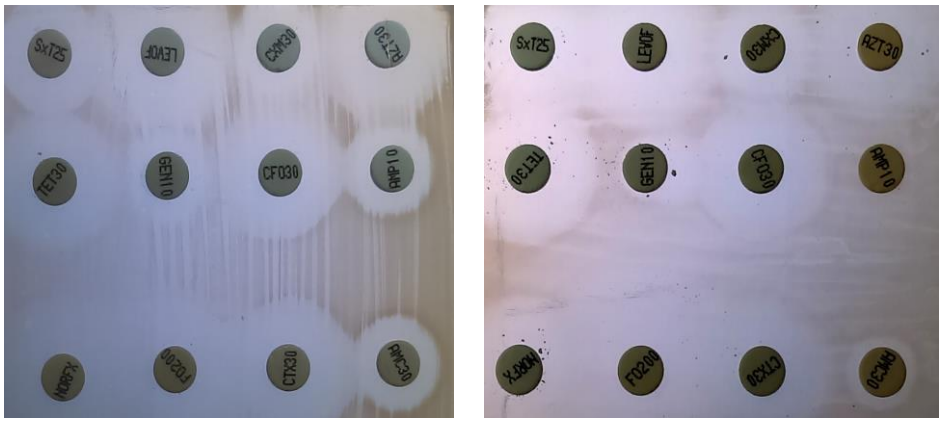

Figure 42. Antibiograms of E. coli ATCC 25922 (left) and E. coli DH5α (right) with 12 different antibiotics. Gentamicin is tested at 10 μg·ml^{-1} expressed as "GEN10".

This *E. coli* DH5α strain is known empirically to be resistant to gentamicin, so unfortunately the resistance mechanism is unknown. Figure 43 presents the photoinactivation of both *E. coli* strains at concentrations ranging from 8 to 8000 nM at 30 and 45 J·cm^{-2}.

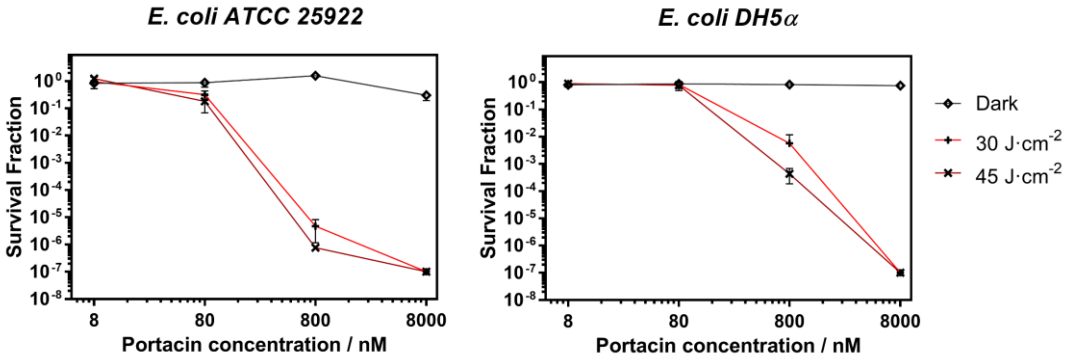

Figure 43. Photoinactivation of E. coli ATCC 25922 (left) and E. coli DH5α (right) with Portacin with concentrations ranging from 8 to 8000 nM upon red light illumination (λ = 660 ± 10 nm). Fluences of 30 J·cm^{-2} (light red) and 45 J·cm^{-2} (dark red) were applied, whilst the dark control is represented in grey. Incubation was performed in PBS for 30 minutes. Data correspond to the mean ± SD after performing three replicates.

The two inactivation profiles present similar patterns, but for the concentration at 800 nM at which the resistant strain presents less cell death (2-log). Both strains need 8 μM of Portacin to fully inactivate the strains, while 80 nM practically does not induce any effect. From this result it can be inferred that the bacterial resistance does not change dramatically the effect of the treatment, proving that PDT is indeed a feasible alternative to antibiotics when these become inefficient. Of the three resistance mechanisms mentioned in the

introduction, efflux pumps or enzymes that modify gentamicin seem to be the most likely mechanisms. Knowing that gentamicin in the conjugate exerts little to no effect (Figure 41), to which a modifying enzyme would not cause any reduction in photodynamic activity, an efflux pump seems to be the most probable resistance mechanism in this strain.

Antibacterial broad-spectrum study of Portacin, Porphonium and Porbutyl

A full inactivation profile of Portacin, Porphonium and Porbutyl was obtained against *S. aureus* ATCC 29213 and *E. coli* ATCC 25922 by varying concentrations and light doses. Figure 44 presents the results obtained.

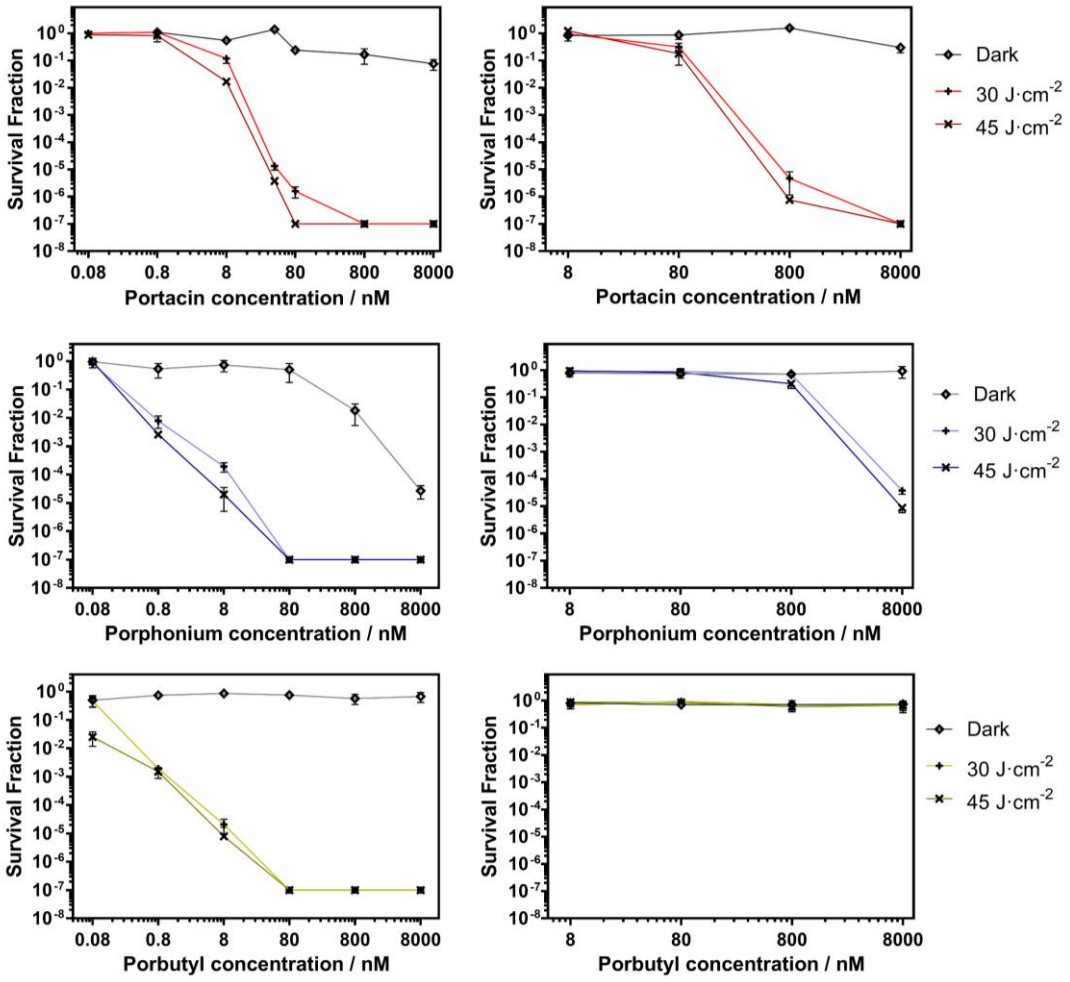

Figure 44. Photoinactivation studies in PBS of S. aureus ATCC 29213 (left) and E. coli ATCC 25922 (right) using Portacin (top; red), Porphonium (middle, blue) and Porbutyl (bottom, yellow) upon red light irradiation (λ = 660 ± 10 nm) after a 30-minute incubation. Data correspond to the mean ± SD after performing three replicates.

A first view of the results indicates how the three compounds inactivate *S. aureus,* being Porbutyl the most active compound against this strain. The greater inactivation capacity of apolar PSs on Gram-positive bacteria in comparison with amphiphilic and polar compounds follows the opposite trend in Gram-negative bacteria. As the photosensitizers become less amphiphilic (Portacin>Porphonium>Porbutyl), they turn less efficient against *E. coli* to the extent that Porbutyl does not induce any cell death. Noteworthy, Porphonium is the only compound which presents some dark toxicity against *S. aureus* at higher concentrations, whilst the others are innocuous in absence of light.

80 nM and 30 J·cm^{-2} of Porphonium and Porbutyl were the concentration/fluence ratio presenting the highest antibacterial activity for *S. aureus*. Portacin, instead, needed of 45 J·cm^{-2} at 80 nM for full eradication or a concentration of 800 nM for 30 J·cm^{-2}. In *E. coli*, complete killing by Portacin was observed at 800 nM upon irradiation with 45 J·cm^{-2} of red light, whereas, a smaller killing efficiency (5-log10) was detected when exposed to 30 J cm^{-2}. At 8 μM, Porphonium achieves a 5-log cell death with 45 J·cm^{-2} while, as mentioned previously, Porbutyl does not inflict any damage. The greater susceptibility of Gram-positive bacteria in comparison to Gram-negative ones is vastly described in literature.[204,231,232]

Further information on the mechanistic action of Portacin can be extracted from the sensitivity to *E. coli* and *S. aureus*. Following the photoinactivation protocol, an assay with gentamicin against these two strains was performed (Figure 45). The two strains were sensitive to this treatment, despite not achieving a full inactivation (probably due to the little uptake time of the antibiotic). In contrast with the tendency observed for the photoinactivations with the conjugate, *S. aureus* seemed to be less sensitive to the lone antibiotic than *E. coli*. This further proves the lack of activity of the antibiotic, and therefore leaving to the photosensitizer all biological insult.

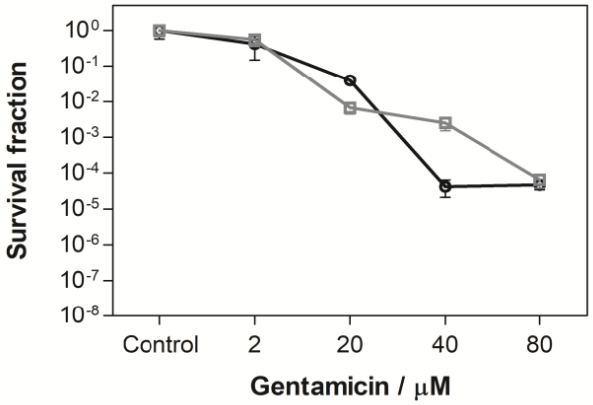

Figure 45. Inactivation of S. aureus ATCC 29213 (grey) and E. coli ATCC 25922 (black) with gentamicin without irradiation.

The promising results achieved when conjugating porphycenes are evidenced when compared to previous antibacterial studies reported in the literature which used TMPo. For instance, Masiera and co-workers required 5 μM of TMPo in Pluronic F 127 solution and 54 J·cm^{-2} light-dose to effectively inactive *E. faecalis*,[183] or Polo et al. observed about 4-log of bacterial lethality using 1 μM of TMPo linked to oligomeric polylysine residues in Gram-positive (*S. aureus*) and Gram-negative (*E. coli*) bacteria.[185] Other cationic porphycenes, in which pyridinium or alkylammonium groups have been introduced into the substituents in the β positions, present similar trends against these microorganisms but achieving complete cell death at concentrations in the order of the few micromoles at comparable fluences.[187,188]

Other published articles reporting tetrapyrrole antimicrobial conjugates with antibiotics and peptides show similar trends to the ones presented by expanded porphycenes. Apolar photosensitizing precursors present high activity against Gram-positive bacteria while their amphiphilic conjugated counterparts excel against Gram-negative bacteria, just as described by Dosselli.[13,121,191]

Also in this field, Huang and co-workers described the conjugation of vancomycin to a chlorin which had previously been derivatized with a cationic polymer.[194] The introduction of vancomycin did not exert any effect on *E. faecium*, proving the loss of activity of the

antibiotic just like with gentamicin in Portacin. Probably, the direct conjugation of vancomycin to the photosensitizer (without the cationic polymer) would enhance the performance of the chlorin. Cahan and co-workers reported an interesting polar photosensitizer-antibiotic conjugate obtained from Rose Bengal and penicillanic acid and kanamycin respectively. Due to the different type of photosensitizer used, this conjugate will be discussed at the end of this chapter.[193]

Porphonium presents a functional group which has been little exploited for in antimicrobial purposes, while it has been vastly used in cancer due to its ability to cross organelle bilayers. PPh_3^+ has been used against bacteria linked to chitosan (endowing the polymer with a net cationic charge)[233] and also linked to an alkyl chain.[234] The cationic polymer was able to inactivate both *S. aureus* and *E. coli*, while the moiety linked to the chain was capable of inactivating *Bacillus subtilis* (a Gram-positive bacteria) and leaving *E. coli* unharmed.

In PDT applications, even fewer applications have been described. Kirakci and co-workers present a molybdenum complex derivatized with PPh_3^+ or a pyridinium group, in which only the first was able to induce significative strain inactivation to Gram-positive bacteria at 10 μM. Both compounds were unable to affect Gram-negative ones.[235] Also, Stoica and co-workers presented several curcumin derivatives for PDT applications. The PPh_3^+ derivative actually hampered the photodynamic effect of the photosensitizer.[236]

A final interesting study published consisted of derivatizing phenalenone and perylene with PPh_3^+.[79] These blue-absorbing conjugates presented great activity at low concentrations and low light doses. The phenalenone derivative needed of 5μM and 1.2 $J \cdot cm^{-2}$ of 420 nm light to inactivate *S. aureus* completely, and 10 μM under the same light conditions to inactivate *E. faecalis*. The perylene derivative required of similar concentrations but higher fluences (10 $J \cdot cm^{-2}$) in order to inactivate the same strains. Both compounds were totally ineffective against *E. coli* under the experimental conditions tested.

3.3.5 Stimulated Emission Depletion Microscopy of Bacteria

According to Abbe, the resolution of a focusing light is limited by diffraction; the shorter the wavelength, the greater the resolution.[237] This is particularly inconvenient for live-cell microscopy which cannot use high frequency radiation (UV or X-Ray) since these are harmful for cells, while the use of electron microscopy is of course ruled out since samples cannot be alive for this type of microscopy. To sum up, under visible light we will not be able to discern between objects smaller than 250 nm, which is the size of the smallest resolution achievable with an optical lens.[238]

Therefore, one of the challenges still in live-cell microscopy is beating the diffraction limit of light and being able to see further down within a cell. Different sub-diffraction techniques have been developed such as STochastic Optical Reconstruction Microscopy (STORM), Photo Activated Localization Microscopy (PALM) or Stimulated Emission Depletion (STED).[238]

STED microscopy is a fluorescence super resolution microscopical technique developed by Stefan Hell at the beginning of the 2000s.[34,239] This technique is able to break the diffraction of light by reducing the point spread function of an emissive point by stimulating the fluorescence emission of nearby molecules, keeping them dark, and therefore, detecting only fluorescence from molecules in a much smaller area.

Instrumentally, an auxiliary beam with the shape of a doughnut is added to the standard excitation beam leaving an unaltered centre. The power of the STED beam will determine the size of the point spread function, the stronger the beam, smaller the centre of the doughnut.[240] Not all fluorophores are amenable to undergo STED microscopy, only those which present stimulated emission phenomena and, most importantly, that either ground or excited state molecular absorption does not overlap the STED beam. Strong intensity beams are needed for STED to work, and therefore photobleaching phenomena are usual. In quantum dots (which are less likely to photobleach), reports have stated that a resolution in the tens of nanometres have

been achieved using CdSe@ZnS quantum dots.[241,242] Examples of organic dyes which are used for STED microscopy are ATTO647,[240] rhodamine[243] and even hypericin.[83]

Despite thinking at first that expanded porphycenes would not be fit for STED microscopy due to its absorption towards the deep red, the results observed in Milano proved that some stimulated emission could be induced. Keeping in mind that expanded porphycenes would not be the best STED candidate molecule, STED microscopy assays were performed on *E. coli* and *S. aureus* at the Centre for Human Technologies of the Istituto Italiano di Tecnologia in Genova in collaboration with Professor Paolo Bianchini and Dr. Michele Oneto.

Portacin was incubated in *S. aureus* and *E. coli* for 30 minutes and placed onto a glass slide which had previously been treated with poly-lysine. Figure 46 presents the images obtained using STED microscopy. Excitation was performed at 405 nm, STED auxiliary beam was of 750 nm and fluorescence was captured from 640 to 730 nm.

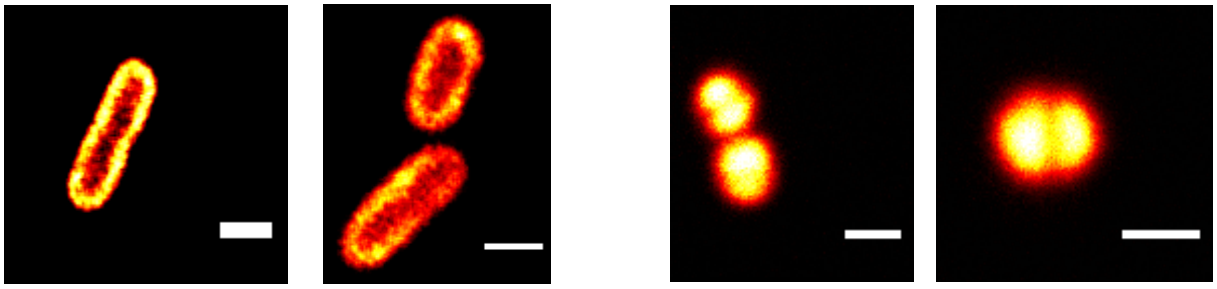

Figure 46. STimulated Emission Depletion images of E. coli (left) and S. aureus (right) incubated with Portacin. The size bar is of 1 μM long.

To our surprise, STED was feasible after performing gated fluorescence which enabled to reduce the background noise. The images shown in Figure 46 present typical rod-shape expected for *E. coli* and *cocci* shape for *S. aureus*. Shape aside, the most noticeable difference between the images from each bacterium was the different distribution of Portacin within the cell at the same incubation time. *S. aureus* presented a very homogeneous distribution of the photosensitizer, being very intense in the centre (the cytoplasm) and gradually fading away when moving away from the bacteria. In contrast, *E. coli* showed a major drug accumulation at the bacterial wall,

while weaker fluorescent signal was observed in the cytoplasm. This distinct accumulation is due to the nature of the bacterial wall. Gram-positive walls are much more porous and present a lower negative potential than its Gram-negative counterpart. Furthermore, the different uptake can justify the different susceptibility of either bacteria to PDT, being the bacteria with greater uptake the most affected one, which is in great agreement with the literature that states that Gram-positive bacteria are more susceptible to PDT than Gram-negative ones. Stemming from this uneven uptake of the photosensitizer, maybe longer incubation times when treating *E. coli* would be advisable in order to enhance the bacterial photoinactivation.

Unfortunately, Porphonium and Porbutyl imaging was unsuccessful since a home-made STED design was used instead of the Leica equipment used for Portacin. Expanded porphycenes are not the best STED dyes due to the pumping of the ground state, which resulted in high background noise. Super-resolution images of Porphonium and Porbutyl were not obtained.

3.3.6 Photoinactivation studies on *Candida albicans*

The three expanded porphycenes were tested against *Candida albicans* ATCC 10231 which was chosen as a yeast model. Figure 47 presents the photoinactivation resulting from incubating this microorganism for 30 minutes and irradiated with red light at different concentrations.

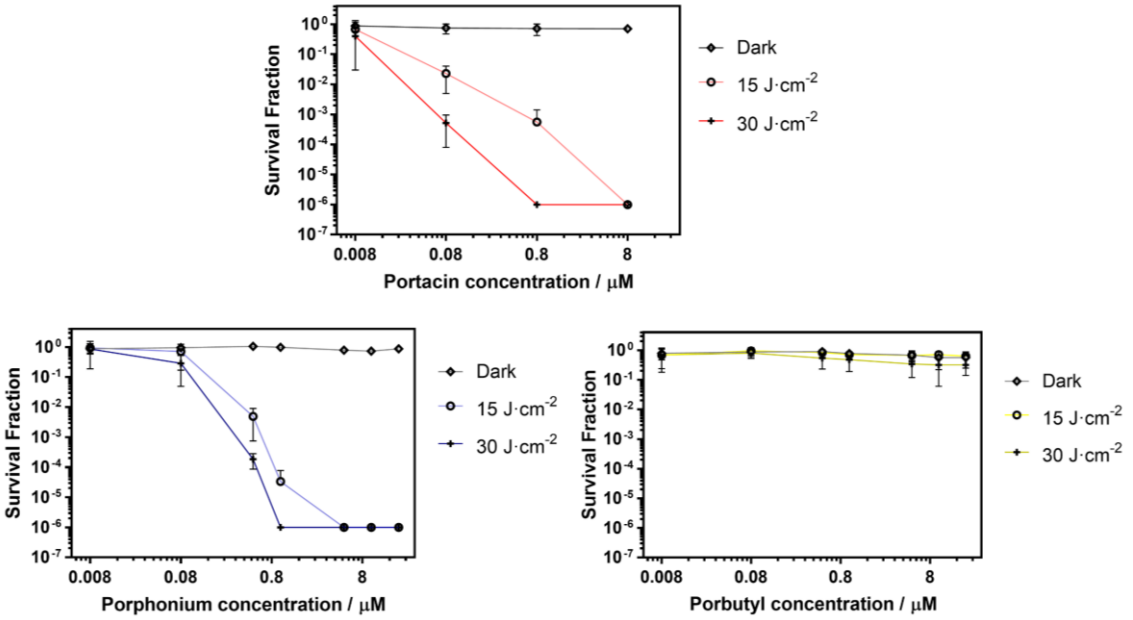

Figure 47. Photoinactivation of Candida albicans ATCC 10231 with Portacin (top, red), Porphonium (bottom left, blue) and Porbutyl (bottom right, yellow) irradiated with red light (λ=660 nm ±10 nm) at concentrations ranging from 0.008 to 20 μM and fluences of 15 and 30 J·cm-2. Dark controls are represented in grey.

Portacin and Porphonium presented similar activity, where complete photoinactivation takes place at 0.8 μM with 30 J·cm^{-2} of red light. Still, Portacin induces a 3-log cell death at only 80 nM. In sharp contrast, Porbutyl does not present any activity even at 20 μM. None of the compounds present any dark toxicity in the evaluated range.

Many reports have photoinactivated *Candida albicans* with a large variety of photosensitizers such as hypericin,[81,244] phenothiazinium salts,[245] 5-aminolevulinic acid,[246] phthalocyanines[247], porphycenes[187,188] and even fullerenes.[96] Most photosensitizers induced complete cell death using concentrations in the order of the few micromols using approximately between 15 and 50 J·cm^{-2} of light. Notably, hypericin required only of 0.63 μM to inactivate *C. albicans*,[244] slightly lower than the 0.8 μM determined for Portacin and Porphonium.

Fungi are known to present lower uptakes of hydrophobic molecules in comparison with hydrophilic-charged ones.[248] This reason can justify the lack of activity of Porbutyl, but it is in complete contrast with the high activity demonstrated by hypericin, which is an apolar compound with very low solubility in physiological media. Hypericin presents interaction with many biomolecules, especially proteins such as apomyoglobin and β-lactoglobulin,[83,249] and furthermore, it is produced naturally by plants so there must be a high interaction between the photosensitizer and biological components.

3.3.7 Expanded Porphycenes against Hela cells

Cancer and antimicrobial PDT share the same goal (to kill unwanted cells), but are in the need of different requirements, such as the type of photosensitizers. Porphycene conjugates were also tested against HeLa cells to evaluate their activity against cancer. The experiments were performed in collaboration with Ms. Mireia Jordà.

The first step performed was to determine the incubation time at which the uptake of photosensitizer is highest, in order to induce a greater outcome. This was performed incubating cells with the drug at the highest non-toxic concentration in the dark. Figure 48 presents the uptake for 24 hours resulting from incubating the tumoral cells with 1 μM of Porphonium. Assays were performed in triplicate.

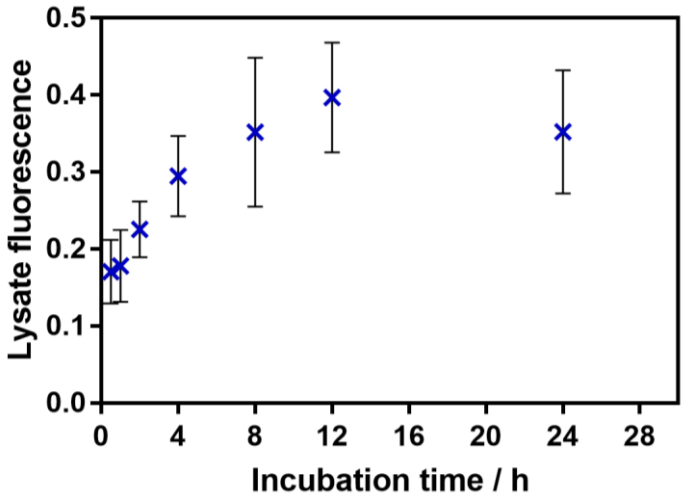

Figure 48. Porphonium uptake by HeLa cells at 1 μM for 24 hours.

The results indicate that the highest concentration Porphonium inside the cells was after 12 hours of incubation. The fluorescence measures of the lysate present a considerably large error measure due to the little fluorescence of Porphonium in PBS. Worse again, uptake assays of Portacin and Porbutyl were not successful when trying to quantify precisely the uptake values, since the results were barely distinguishable from the background noise. Qualitatively, uptake values were greater after incubation during 12 hours for Porbutyl and 24 hours for Portacin (data not shown).

After determining the optimal uptake time for each compound, cell viability assays were performed. HeLa cells were incubated during the adequate time, supernatant removed to eliminate the excess photosensitizer which had not entered the cell, and then irradiate them with red light. 24 hours later, cell viability was quantified by MTT assay. Live cells will metabolize MTT, developing a purple colour which can be determined spectrophotometrically. The results obtained normalized to control cells are presented in Figure 49.

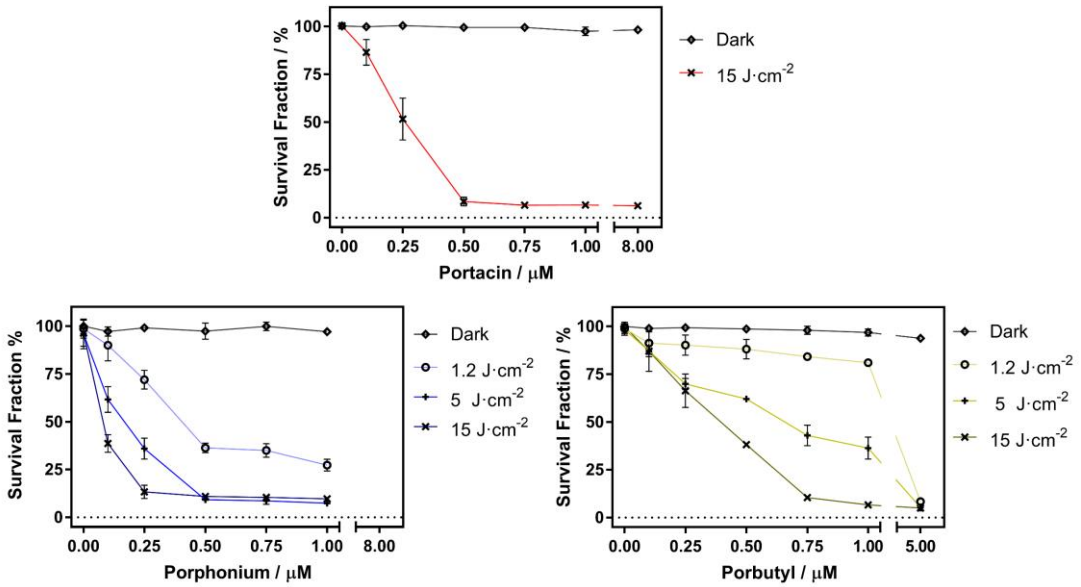

Figure 49. HeLa cells inactivation with Portacin (top, red), Porphonium (bottom left, blue) and Porbutyl (bottom right, yellow) with red light (λ=660 nm ±10 nm) at concentrations ranging from 0.1 to 8 μM. Dark controls are represented in grey.

The results show how the three compounds are active against HeLa cells under illumination, whilst none of the conjugates present any dark toxicity at the tested concentrations. Most notably, out of the three compounds Porphonium presented the highest activity since it can reduce cell viability to 13% at only 0.25 μM under 15 J·cm^{-2} of light, while Portacin and Porbutyl required of concentrations of 0.50 and 0.75 μM respectively under the same fluence.

The EC_{50} values (concentration at which cell viability is reduced to 50%) of the three compounds under 15 J·cm^{-2} of red light were of 0.07, 0.25 and 0.35 μM for Porphonium, Portacin, and Porbutyl respectively. At 1.2 J·cm^{-2} (ten times less light), Porphonium reduced cell viability to

36% at 0.50 μM, while at the same concentration Porbutyl only inactivated 12% of cells. Portacin was only evaluated at 15 $J \cdot cm^{-2}$.

None of the photoinactivations performed actually achieves a 100% cell death, there is always an approximate 10% which remains. At first, the explanation attributed to this fact was the residual noise of the fluorimeter, and therefore blank tested was performed. A well without cells was treated with MTT as any other well and did not develop any colour, proving that indeed the signal read on the fluorimeter correspond to live cells. This residual activity could be attributed to cells that, instead of undergoing apoptosis as a result of cell damage, repaired this damage and became somehow resistant to the treatment. Previous studies have already reported this phenomema.[50]

The higher activity of Porphonium can be explained thanks to the lipophilic cation in its structure. Unlike aPDT, excessively hydrophilic compounds (specially charged) will find it harder to cross the cell plasma membrane than other moderately hydrophobic.[156] The longer uptake for Portacin may be justified also for this hydrophilicity. Furthermore, in addition to the moderate hydrophilicity, once inside the cell the triphenylphosphonium group may target the photosensitizer to mitochondria and improve the photoinactivation outcome.

The inactivation results obtained are similar to those of other reported porphycenes such as Py_3MeO-TBPo described by Ruiz-Gonzalez and coworkers,[250] and Temocene described by García-Díaz.[102,251,252] Porphonium (which presented the best results in this trio) and the porphycenes mentioned already reported requiring under 1 μM and only up to 5 $J \cdot cm^{-2}$ to induce up to 90% cell death.

3.3.8 Spinning Disk Confocal Microscopy on HeLa Cells

Spinning disk confocal microscopy was the microscopic technique used to determine the subcellular localization of the three expanded porphycenes in HeLa cells since these are fluorescent, also in physiological media. This microscopic technique is based on confocal microscopy, to which a simultaneous point-illumination system has been incorporated. The physical spinning disk introduced enables to irradiate many points at the same time, therefore obtaining images much faster than standard confocal microscopy, with less photobleaching, but with slightly less resolution.

In order to determine the subcellular localization of the three expanded porphycenes, co-localization assays were performed by adding commercial dyes that target different organelles along with the fluorescent photosensitizer.

Portacin

Portacin and MitoTracker green (which do not have overlapping spectra) were incubated in HeLa cells for 12 hours and 30 minutes respectively. After a thorough wash, cells were illuminated at 405 nm to excite Portacin and at 488 nm for MitoTracker Green (Figure 50).

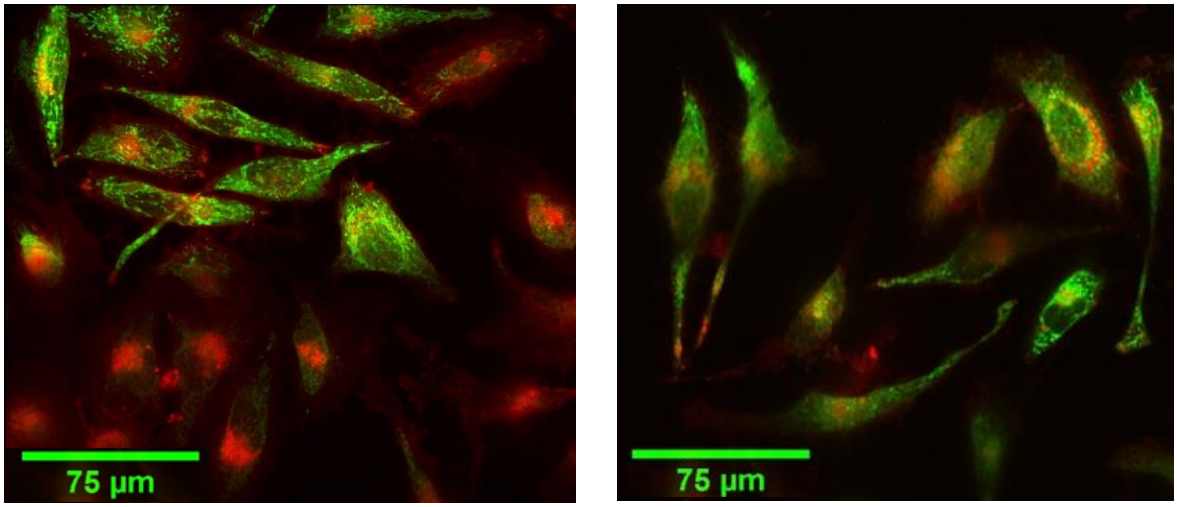

Figure 50. Spinning disk microscopy composite of HeLa cells incubated with MitoTracker Green (green) excited at 488 nm and with Portacin (red) excited at 405 nm. Emission were collected at 515 nm for MitoTracker Green and from 620 to 750 nm for Portacin.

The labelling has been successful since the cells presented both fluorescence emissions and the background appears clear. MitoTracker Green presents a bright fluorescence signal, while Portacin's is weaker. At a first glance, we observe that Portacin and MitoTracker green are capable of crossing the cytoplasmic membrane, but without entering the nucleus. Also, they do not seem to co-localize together. Figure 51 presents a zoom in on two specific regions of interest to further examine this phenomenon.

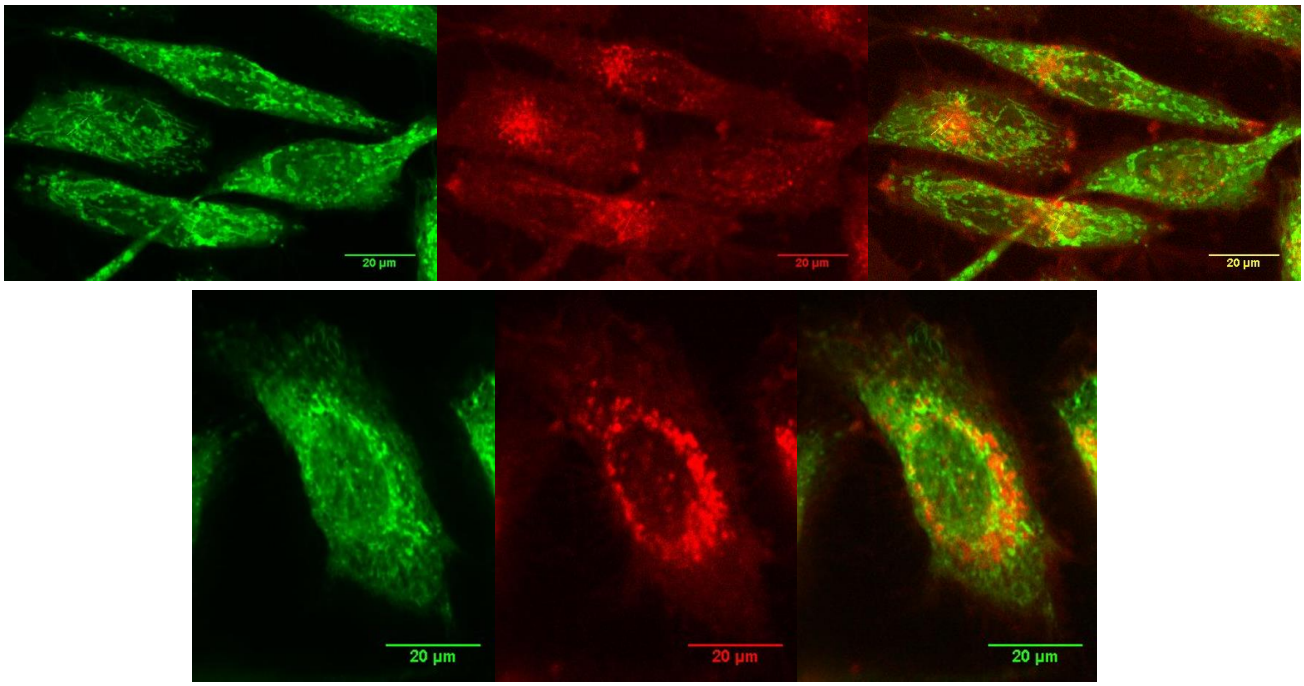

Figure 51. Spinning disk microscopy of HeLa cells incubated with MitoTracker Green (left, excited at 488 nm), Portacin (middle, excited at 405 nm) and the composite of the two images (right).

Judging from MitoTracker green, mitochondria appear homogeneously distributed throughout the cell with a certain accumulation around the nucleus. Portacin, on the other hand, seems to present the majority of its signal from nearby the nucleus, but not colocalized with MitoTracker green. This distribution pattern maybe indicative of an accumulation in the endoplasmic reticulum, since this organelle is found linked to the nucleus so it can perform important roles in protein synthesis, modification and delivery towards other organelles.[253]

The Pearson correlation coefficient (PCC) and Mander's overlap coefficients (MOC) were calculated in order to attempt the quantification of the colocalization. A PCC value of 1 indicates a complete colocalization, a value of 0 indicates a random distribution, while -1 is indicative a

perfect negative correlation. The MOC, on the other hand, is a pair of values which establishes the percentage of overlapping of one signal with the second, and vice versa. In the case of Portacin, the PCC calculated is of 0.72 while, regarding MOC, the fraction of Portacin overlapping MitoTracker is of 95%, but the fraction of MitoTracker overlapping Portacin is of only 43%.

These values are in agreement with the observations performed qualitatively. Portacin does not localize in mitochondria but localizes around the nucleus where many mitochondria are found along with the endoplasmic reticulum.

Porphonium

Porphonium's subcellular localization was analysed in the same manner as Portacin. The photosensitizer was co-incubated with MitoTracker green in HeLa cells and were imaged using spinning disk microscopy. Figure 52 presents the composite of the green fluorescence from MitoTracker (colour green) and that from Porphonium in red. The mixture of these two colours yields the yellowish colour observed.

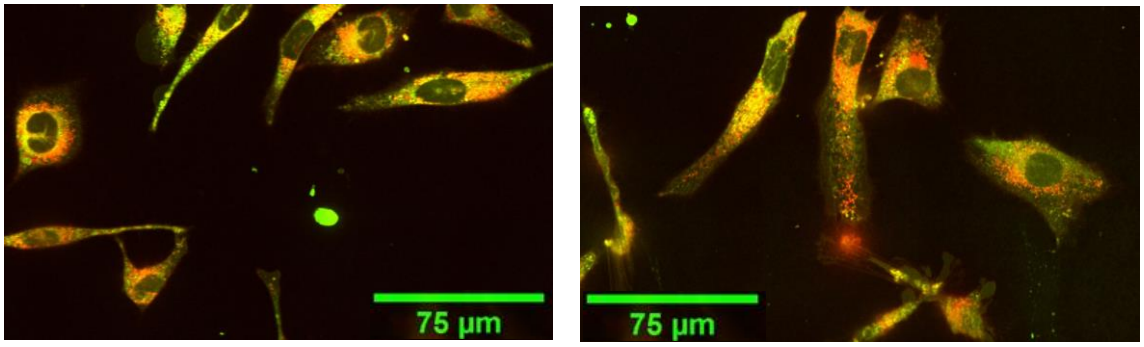

Figure 52. Spinning disk microscopy composite of HeLa cells incubated with MitoTracker Green (green) excited at 488 nm and with Porphonium (red) excited at 405 nm. Emission were collected at 515 nm for MitoTracker Green and from 620 to 750 nm for Porphonium.

As in the previous experiment, both compounds enter the cell and cannot access the nucleus. Regarding subcellular localization, we observe a greater overlap between MitoTracker green and Porphonium inside the cell. Figure 53 presents a zoom towards a region of interest.

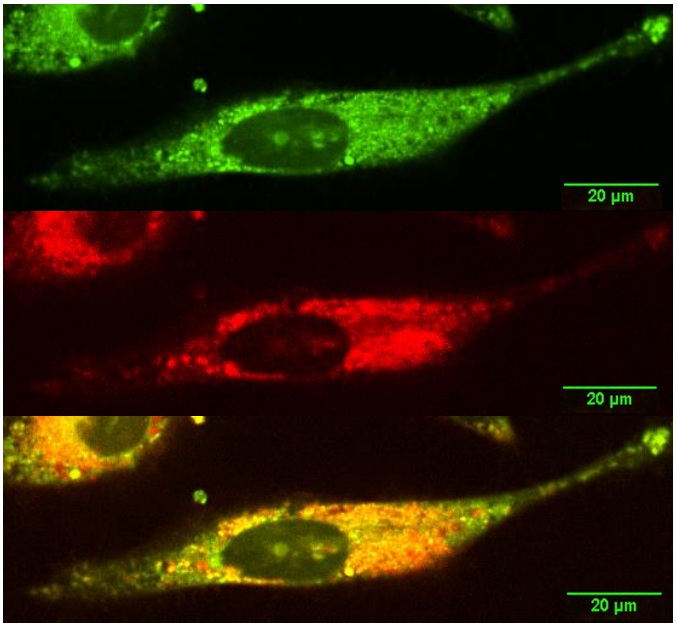

Figure 53. Spinning disk microscopy of HeLa cells incubated with MitoTracker Green (top, excited at 488 nm), Porphonium (middle, excited at 405 nm) and the composite of the two images (bottom).

The evident yellow colour stemming from the green and red mixture of emissions seen in the image is indicative of a greater colocalization than for Portacin.

As with the previous Portacin, MitoTracker can be found ubiquitously since mitochondria are spread across the whole cell, even at the very tips away from the nucleus, while Porphonium seems to once again accumulate close by to the nucleus, but without entering it. Once again, accumulation in the endoplasmic reticulum seems likely, but presenting a greater accumulation in mitochondria than Portacin.

The PCC value obtained from the image is of 0.83, greater than the value observed for Portacin. The MOC values are of 96% for Porphonium overlapping MitoTracker and of 63% for MitoTracker overlapping Porphonium. Just as for the PCC value, the higher MOC values indicate a greater colocalization in mitochondria in Porphonium than in Portacin. This enhanced colocalization is due to the triphenylphosphonium moiety in the expanded porphycene structure.

Porbutyl

Unlike the previous two compounds, Porbutyl is much more apolar and, therefore, instead of tracking mitochondria, the plasmatic membrane was stained to elucidate whether the photosensitizer binds to the membrane or is capable of entering into the cytosol (Figure 54).

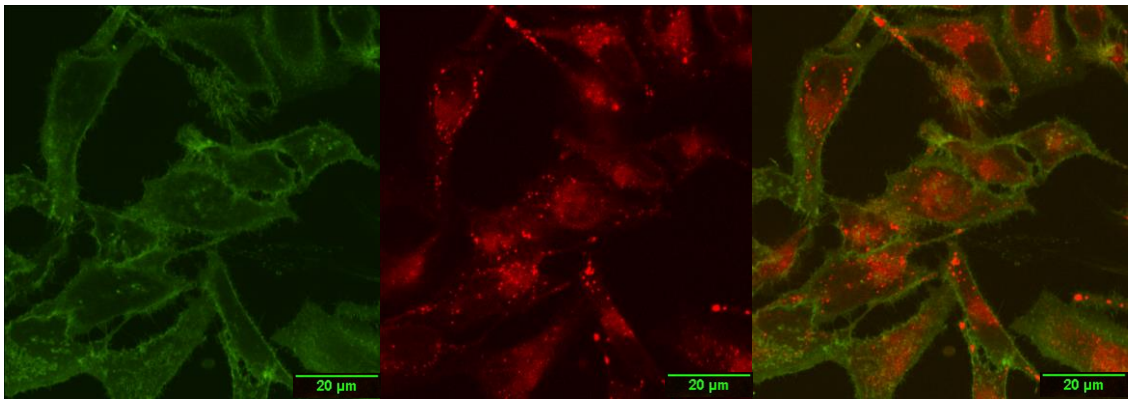

Figure 54. Spinning disk microscopy of HeLa cells incubated with Cell Mask Green (left, excited at 488 nm), Porbutyl (middle, excited at 405 nm) and the composite of the two images (right).

Porbutyl presents a completely different pattern than Portacin and Porphonium. Cell Mask green stains the cell membrane very nicely (left image in Figure 54), while Porbutyl appears to be accumulated in spheres within the cell. It seems that Porbutyl is mainly trapped inside endosomes within the cell (most likely lysosomes). Also, stemming from the dim red emission around the nucleus, it could be claimed that some smaller fraction of the compound could accumulate, as the other compounds, in the endoplasmic reticulum.

A nice image that can be obtained when staining the membrane are 3D plots. In this particular case, Porbutyl was found aggregated within the cell, as seen in Figure 55.

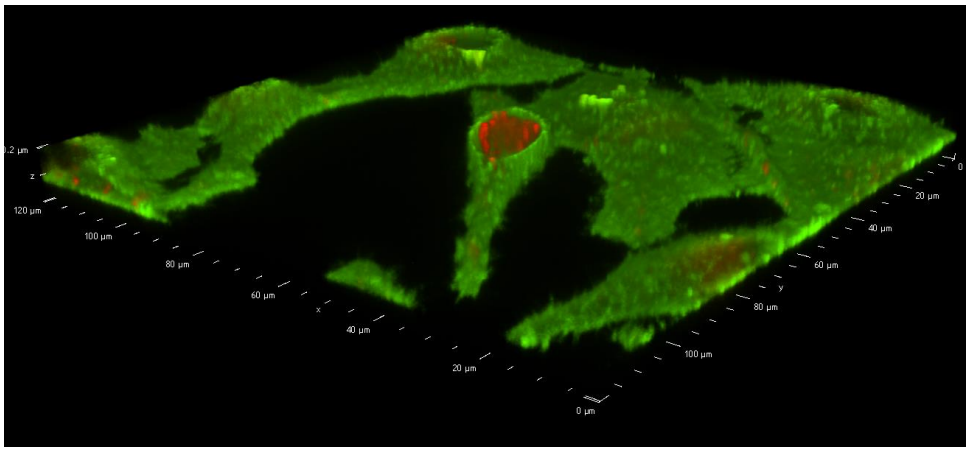

Figure 55. Spinning disk microscopy 3D model of HeLa cells incubated with Cell Mask Green (green excited at 488 nm and Porbutyl (red, excited at 405 nm).

To a greater or lesser extent, all porphycene conjugates present accumulation in the endoplasmic reticulum, as already stated by previous studies with porphycenes derivatives as photosensitizers.[254,255] The introduction of the triphenylphosphonium functional group into the photosensitizer had per goal to target mitochondria, objective which has been partially achieved since there is a greater accumulation there than seen in Portacin or Porbutyl. Other authors claim that for some molecules maybe more than one triphenylphosphonium moiety must be introduced to achieve a selective target to mitochondria, such as stated by Gilson in 2019.[159] Further imaging showed cell blebbing as a result of illumination, indicating that the most probable cell death pathway is apoptosis.

In comparison with other Porphycene derivatives, Ruiz-Gonzalez and García-Díaz published reports showing accumulation in lysosomes.[102,250] Of the three expanded porphycenes, Porbutyl seems to accumulate in endosomes, while in contrast, those charged expanded porphycenes which seem to majorly accumulate in the ER and partially in mitochondria (only Porphonium).

3.3.9 Rose Bengal – Gentamicin Conjugate

After this discussion on porphycenes, another analogous compound studied was Rose Bengal – Gentamicin conjugate (RBG). This compound is exactly like Portacin but changing the expanded Porphycene for Rose Bengal (RB) (Figure 56).

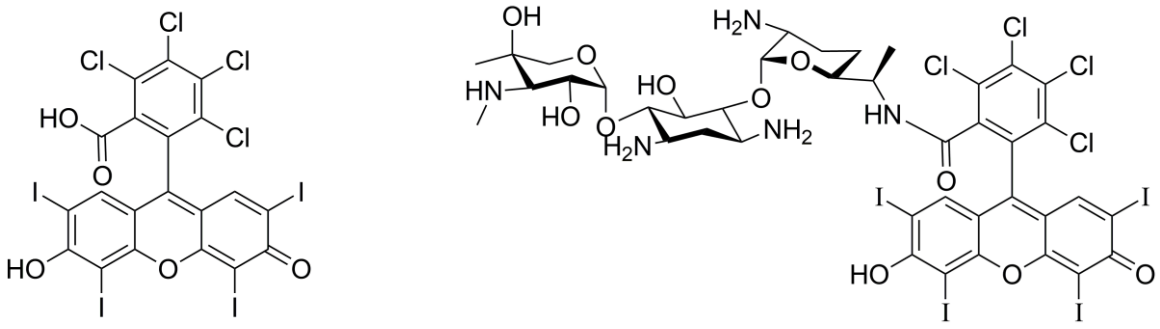

Figure 56. Molecular structures of Rose Bengal (left) and of Rose Bengal – Gentamicin conjugate (right).

Rose Bengal (RB) is a xanthene, from the same family as fluorescein, rhodamine and eosin. It has been synthetically prepared and, unlike fluorescein and rhodamine which have fluorescent quantum yields close to 1, the heavy atoms in its structure promote intersystem crossing and, therefore, is capable of generating singlet oxygen in good yields (0.75 in water).[42] Despite having a high singlet oxygen quantum yield, it is prone to bleaching and it is negatively charged at physiological pH. Also, it is in clinical trials for the treatment of psoriasis, dermatitis, melanoma and breastcancer.[70]

The anionic charge is a negative feature for inactivating Gram-negative microorganisms since there is static repulsion between the photosensitizer and the bacterial cell wall. Therefore, conjugation of Rose Bengal to gentamicin will yield a polar compound lacking the anionic charge from the acid group.

Photophysical Characterization of RBG

Absorption and fluorescence emission spectra of the precursor Rose Bengal and of the conjugate in PBS are presented in Figure 57.

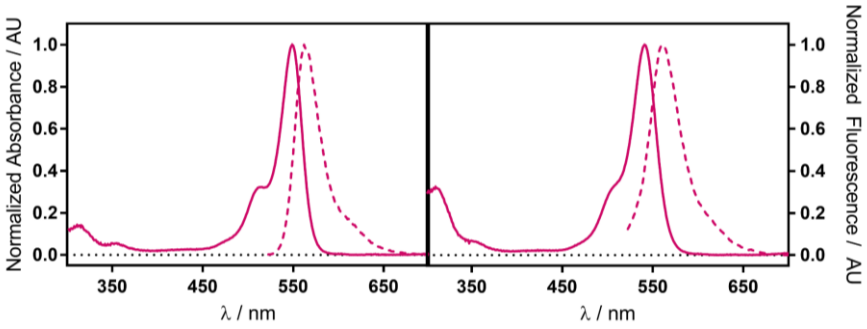

Figure 57. Absorbance (solid line) and Fluorescence (dotted line) spectra of Rose Bengal (left) and the Rose Bengal-Gentamicin conjugate (right) in PBS.

Both absorption and fluorescence present very similar spectra since the conjugation little affects Rose Bengal as a chromophore. In addition to the slight blue-shift of the conjugate in comparison to RB, there is an increase in the ultraviolet absorption due to the presence of the sugars that form gentamicin.

Table 5 summarizes the maximum wavelength absorption and emission, as well as the fluorescence and singlet oxygen quantum yields of RB and RBG in PBS and MeOH.

Table 5. Photophysical properties of Rose Bengal and the Rose Bengal-Gentamicin conjugate in PBS and MeOH.

Compound	λ_a / nm		λ_e / nm		Φ_F		Φ_Δ	
	PBS	MeOH	PBS	MeOH	PBS	MeOH	PBS	MeOH
RB	550	557	562	568	0.018[256]	0.08[256]	0.75[42]	0.76[42]
RBG	541	560	558	577	0.003	0.06	0.74	0.46

The table shows how both RB and RBG suffer a red shift in absorption and fluorescence when they are dissolved in methanol. Rose Bengal was used as reference to calculate the fluorescence and singlet oxygen quantum yields of the conjugate. The fluorescence quantum yield of the conjugate is lower than RB in both solvents, especially in PBS where the compound is practically

non-fluorescent (Φ_F=0.003). Regarding the singlet oxygen yields, the conjugation practically does not affect the singlet oxygen production in PBS, whilst in methanol it is reduced by 40%. This distinct behaviour in the Φ_Δ according to the solvent may be due to the availability of the free electron pairs in the amines present in gentamicin when dissolved in methanol. This phenomenon would not take place in PBS since at physiological pH these same amines would be protonated, and therefore electron transfer could not take place. As with Portacin, we do see a reduction in Φ_Δ when dissolved in methanol, but not in Porphonium and Porbutyl, which do not have these free pair electrons. A final comparison between the Φ_Δ of Portacin and RBG in PBS could unfortunately not be performed since Portacin partially aggregates in PBS, and therefore losing grand part of its photosensitizing capacity.

Antibacterial Studies of RBG

As with Portacin, bacterial inactivations with RB and RBG were performed against *S. aureus* and *E. coli* in order to test their biological activity. The inactivation against the two bacterial strains offer valuable information when willing to understand the mechanism of action of the Rose Bengal-Gentamicin conjugate (Figure 58).

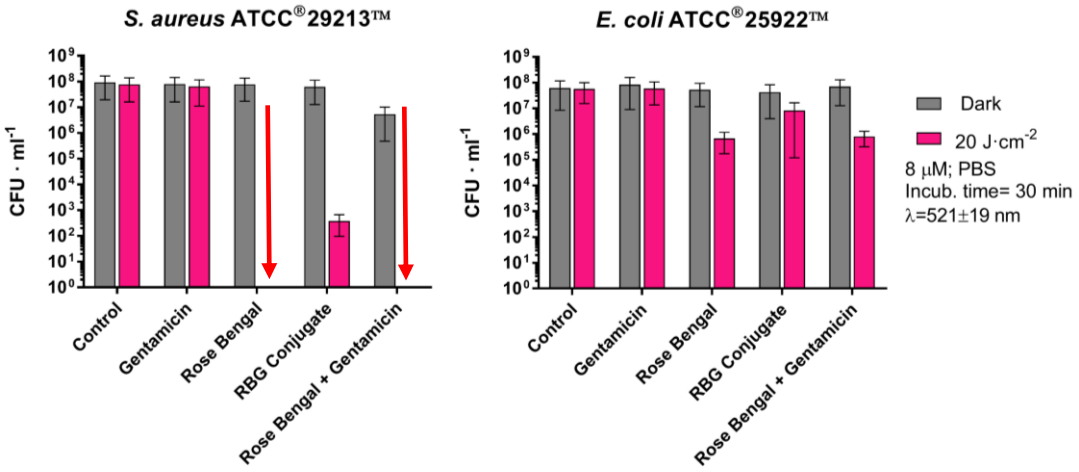

Figure 58. S. aureus ATCC 29213 (left) and E. coli ATCC 29522 (right) photoinactivation studies in PBS at 8 μM upon green light illumination (λ = 521 ± 19 nm) (pink bars). Grey bars represent dark controls. Light doses: 20 J·cm^{-2}. Incubation time: 30 minutes. Data correspond to the mean ± SD after performing two replicates. A red arrow indicates complete strain inactivation.

The analysis of the individual elements show how gentamicin alone does not induce any bacterial death in either strain, while RB is active. Rose Bengal, while being non-cytotoxic in the dark, is well known to efficiently inactivate *S. aureus*, while it has a harder time in inactivating *E. coli,* as reflected in Figure 58.[257,258] In these conditions, Rose Bengal inactivates the Gram-positive strain completely, while it can only induce 2-log cell death to the Gram-negative one.

Using Gentamicin and Rose Bengal in combination (without being covalently bound) has already been described by Pérez-Laguna in 2018 and by Cahan in 2010, proving that the minimum inhibitory concentration against *S. aureus* could be lowered while achieving the same disinfection results.[193,258] In our case, an additive effect between antibiotic and photosensitizer could not be appreciated since a complete inactivation is already achieved by Rose Bengal alone, but nonetheless, it is clear that the Rose Bengal-Gentamicin conjugate is less efficient inactivating than Rose Bengal alone. Also, the addition of Rose Bengal and Gentamicin separately in the dark also induces a 1.5-log cell death.

As mentioned previously, Rose Bengal has a lesser impact on *E. coli* viability due to its different bacterial wall. The outer membrane and the high negative potential in the cell diminish Rose Bengal uptake. The addition of Gentamicin to Rose Bengal does not enhance cell inactivating (obtaining a similar outcome as the photosensitizer alone), while the covalently binding of the two elements in fact hamper the disinfection effect.

Cahan presented a similar conjugate, which only differed in a hexyl chain separating the antibiotic from the photosensitizer. In contrast to the results obtained with RBG, the conjugate with the linker shows a high activity against *S. aureus*, requiring only 0.078 μM and 2 $J \cdot cm^{-2}$ for a complete inactivation of the strain. This contrast in activity may be due to the presence of the linker which allows the two parts to function without interference. *E. coli*, on the other hand, needed of 20 μM and 16 $J \cdot cm^{-2}$ for cell inactivation, agreeing with the results observed herein.

To sum up, photosensitizer-antibiotic conjugates must be carefully designed in order to obtain an improved photoactive drug. Broad-spectrum conjugates have been observed when yielding an amphiphilic compound. Also, when conjugating, the biological properties of the antibiotic may be lost due to steric hindrance preventing its action, while the increase in molecular weight entailed may hamper its uptake specially in Gram-negative bacteria.[194,259]

CHAPTER 4

Hypericin: A Natural and Efficient Photosensitizer

This chapter will verse on the use of Hypericin as a photosensitizer in antimicrobial Photodynamic therapy.

The first part consists in a comparison between pure Hypericin and a hydrophilic plant extract from *Hypericum perforatum*, which has been partially adapted from *Pietro Delcanale, Cormac Hally, Santi Nonell, Silvia Bonardi, Cristiano Viappiani and Stefania Abbruzzetti; Photodynamic action of Hypericum perforatum hydrophilic extract against Staphylococcus aureus, in Photochem. Photobio. Sci., 2020, 19, 324-331.*

The second part continues the research on the βLG-Hyp complex begun by Dr. Beatriz Rodriguez-Amigo (not yet published), in which the biological impact of adding retinoic acid to the b-lactoglobulin-Hypericin complex on *S. aureus* photoinactivations are assessed.[260]

"Experience is merely the name men gave to their mistakes"

— Oscar Wilde, The Picture of Dorian Gray

4.1 Introduction

4.1.1 Hypericin, a naturally occurring Photosensitizer

Unguents, ointments and infusions of the aerial parts of plants from the *Hypericum* genus have been used for centuries as a traditional medicinal treatment of several afflictions.[261] Up to six major natural groups can be found in these plants.[262] The biological activity relies mostly on tetraketones (such as Hyperforin) and naphthodianthrones, like Hypericin (Hyp) and pseudohypericin,[263] in which several studies have associated the antidepressant and antibacterial effects (in the dark) to Hyperforin[264,265] and the phototoxic properties to Hyp.[266]

Hyp (Figure 59), which is a secondary metabolite found in *Hypericum perforatum* (Saint John's Wort), has an intense red colour and is largely insoluble at room temperature, forming aggregates in water. Its absorption and specially the fluorescence spectra changes significantly depending on the polarity of its microenvironment.[267,268] In addition, it is one of the most potent natural photosensitizers found in nature since it is able to efficiently generate superoxide and singlet oxygen (Hyp presents a Φ_Δ of 0.36 in ethanol).[269]

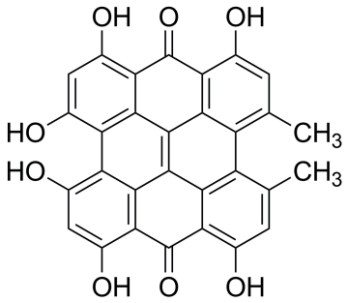

Figure 59. Hypericin (7,14-dione-1,3,4,6,8,13-hexahydroxy-10,11-dimethylphenanthrol[1,10,9,8-opgra] perylene) molecular structure.

Hyp can be extracted and purified from *Hypericum perforatum*, but the low amount of photosensitizer in each flower make this process expensive and inefficient, to which alternative synthetic approaches have been developed.[270] After defining the molecular structure in 1953 by Brockmann, a total synthesis process was published in 1957 by the same authors. Further on, semisynthetic and biosynthetic strategies have also been pursued always aiming to reduce the number of steps and cost of the process.[271]

Despite the costly and tedious obtention procedures, the phototoxicity presented by Hyp has opened a whole new world of applications in PDT. Hyp has been successfully tested against bacteria, [83,104,272–274] fungi, [81,244] cancer cells[82,275–277] and even virus[278,279] when illuminated.

Due to its lipophilicity, one of the main drawbacks of this compound is its aggregation in aqueous environments, which seriously compromises its photophysical properties presented in organic solvents. Many studies have delivered Hyp in ethanol or other organic solvents (assuming the consequences of aggregation in physiological media), while others have engineered ways to deliver the photosensitizer disaggregated either modifying the molecular structure[280] or using nanoparticles, and therefore most likely to preserve their photophysical properties. Biodegradable nanoparticles,[281] liposomes,[282–284] proteins like albumins, apomyoglobin and β-lactoglobulin (βLG),[104,273,285] and also formulations with polyvinylpyrrolidone[286]have been used as drug delivery carriers.[104,249] Figure 60 presents how βLG can accommodate Hyp into its structure.

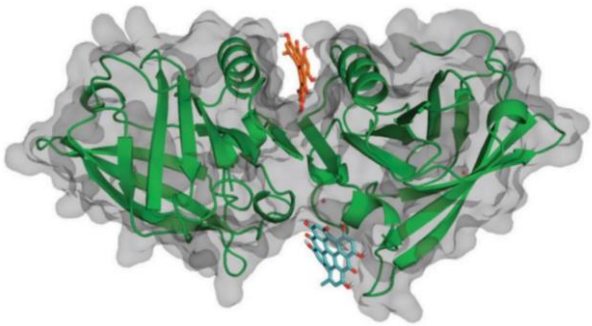

Figure 60. βLG model accommodating two hypericin molecules within its hydrophobic cavities. Figure adapted from reference[104].

4.1.2 Acne Treatments

Hyp has been used to treat many different types of infections, being acne one of these.[280] *Acne vulgaris* is a chronic inflammatory disease of the pilosebaceous unit-hair follicles of the skin associated with a sebaceous gland. It results from an altered keratinisation, inflammation, and bacterial colonisation of hair follicles by *Propionibacterium acnes*, while other bacterial strains present in the skin microbiota may also be involved, such as *Staphylococcus aureus*.[287,288]

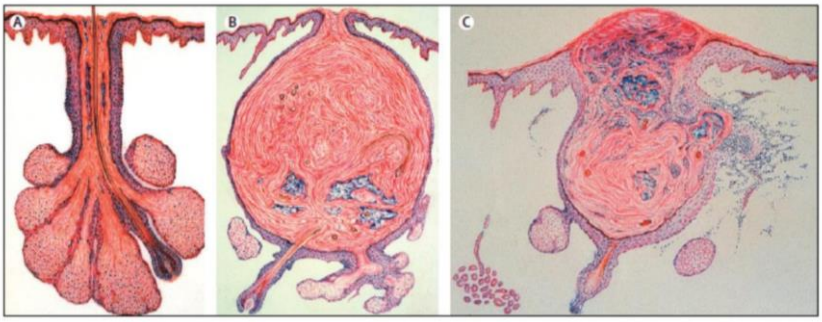

Figure 61. Normal sebaceous follicle (A) and comedone (B), and inflammatory acne lesion with rupture of the follicular wall and secondary inflammation (C). Adapted from reference [287].

Around 630 million people worldwide suffer from this condition, mostly teenagers, which can be painful and frequently cause significant embarrassment and anxiety in affected patients.[289] It accumulates on areas with greater amount of sebaceous glands, such as face, neck, chest, upper arms and back causing non-inflammatory injuries (comedones) or inflammatory injuries (papules, pustules and large red bumps) which may end up in various degrees of scarring.[287,290]

Several approaches, both topical and systemic, are attempted to overcome *acne vulgaris*. Systemic oral contraceptive pills can be used to reduce androgen-levels causing a reduction in sebum production,[287] while retinoids, namely all-trans-retinoic acid (tretinoin) and 13-cis-retinoic acid (isotretinoin) are used to diminish inflammation and normalize the desquamation of the follicular epithelium (even though they can cause depression and teratogenesis in pregnant women).[291,292] A third flank tackled regarding *acne vulgaris* is the antimicrobial one, in which benzoyl peroxide and antibiotics, such as clindamycin and erythromycin, are used to disinfect skin afflicted by *acne vulgaris*. Combination therapies with different type of drugs are used to treat acne.[287,290]

Following the pervasive current trend, microbial resistance to antibiotics has also been detected in acne and therefore alternatives to these treatments must be developed.[293,294] In this regard, photodynamic therapy (PDT) may have a lot to say, since as mentioned previously, combination therapy of photosensitizers with regular drugs can help tackling afflictions. PDT has been already

attempted *in vitro* and *in vivo* successfully to treat acne either alone or in combination with antibiotics.[295–299]

As previously mentioned, part of this chapter stems from research performed previously by Dr. Beatriz Rodriguez-Amigo (not yet published).[260] Having already described the photophysical properties and biological activity of the binary complex between βLG and Hyp,[104] her research continued to investigate the optical properties of a ternary complex formed by adding Retinoic Acid (RA) to the βLG formulation (Figure 62).

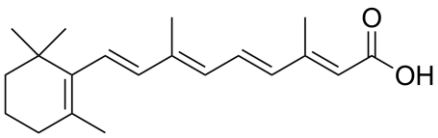

Figure 62. Molecular structure of retinoic acid or Tretinoin.

Both Hyp and RA are highly hydrophobic and, therefore, very insoluble in water. βLG can accommodate the two molecules within its cavities,[104,300] making it an ideal vehicle for the two active compounds. The goal behind this double payload is to have Hyp disinfect the affected area from undesired bacteria using light and the retinoid to diminish skin inflammation.

The photophysical study of the ternary complex showed a positive interaction between the protein and the two molecules, proving the interaction between parts. Furthermore, quenching of fluorescence and excited triplet states from Hyp due to RA was observed (Figure 63).

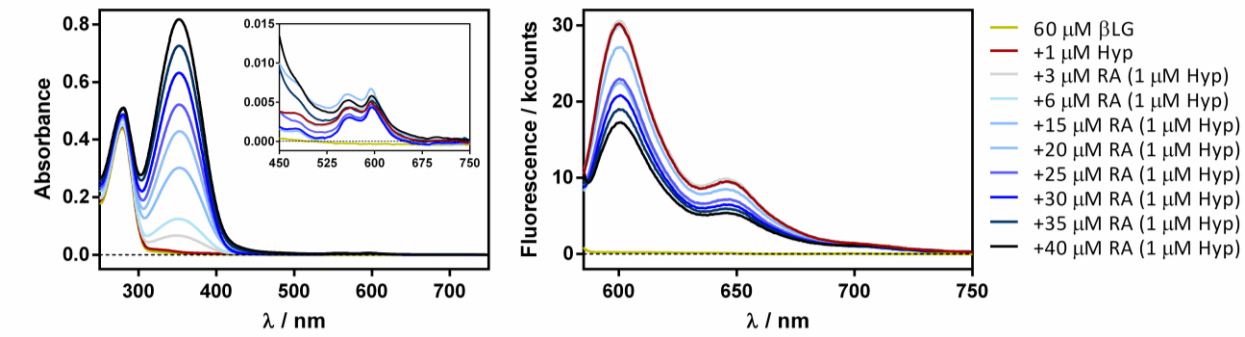

Figure 63. Fluorescence quenching of Hyp by adding RA in when complexed with βLG. Absorption (Left) and fluorescence emission (Right) spectra of Hyp-RA-βLG mixtures at increasing RA concentrations (between 0 and 50 μM). The βLG was fixed at 60 μM and Hyp at 8 μM. Adapted from Dr. Rodriguez-Amigo's doctoral thesis.[260]

The quenching phenomenon was seen to be transient because once in the presence of *S. aureus* the ternary complex disassembled, allowing Hyp to recover its photophysics. This is indeed an advantageous property by which the vehicle turns photochemically safe by adding RA (the singlet state is quenched and therefore no ROI can be formed) until it reaches its location and unloads its cargo.

After this brief introduction, this chapter will present the findings by comparing the photophysical and photodynamic properties of pure Hyp and a non-purified lyophilized hydrophilic *Hypericum perforatum* extract, and the biological activity of the ternary βLG-Hyp-RA complex will be further characterized and its activity against *S. aureus* assessed.

4.2 Materials and Methods

Plant Extract Preparation

Aboca S.p.A. kindly supplied the *Hypericum* hydrophilic extract which was prepared as described in patent n. WO 2009/106263A1. In short, *Hypericum* flowering stem was extracted with a hydroalcoholic solution (70% v/v ethanol/water) with a plant:solvent ratio of 1:13 at 40 °C for 8 hours. Ethanol was then removed under reduced pressure and a physical decantation was performed in order to separate the polar water-soluble substances from the non-hydrophilic substances by centrifugation. Finally, the clear solution was then frozen and lyophilized. The drug extract ratio range was approximately 5:1. The extract was chemically characterized by HPLC, showing a total hypericin concentration between 0.2 to 0.4%. Thus, 1 mg of the lyophilized hydrophilic extract can yield up to 1 ml solution containing about 4 μM of Hyp.

The ethanol or the DMSO solutions of the plant extract were prepared by gently grounding the lyophilized powder with a spatula. The turbid dark suspension obtained was centrifuged (10 minutes at 12 000 rpm) and the supernatant was stored. The process was repeated thrice in order to remove any insoluble compounds left in suspension. The final solution was clear with a dark red-brownish colour.

Ternary Complex Preparation

Hyp was purchased from HWI Analytik GmbH. β-Lactoglobulin (isoform B; βLG) from bovine milk, retinoic acid (tretinoin) powder and Dulbecco's phosphate-buffered saline were obtained from Sigma Aldrich. All other chemicals were commercially available reagents of at least analytical grade. Milli-Q water (Millipore Bedford, Massachusetts system, resistivity of 18 MΩ cm) was used. Hyp and RA were dissolved in DMSO and added to the desired concentration to a PBS solution of βLG. Once the complex PS-protein was prepared it was stored refrigerated in the dark.

Microbial strains

In Chapter 4, antimicrobial inactivations with the plant extract were performed with *S. aureus* ATCC 25923, whilst the biological tests using the βLG-Hyp-RA complex were done with *S. aureus* ATCC 29213.

Antimicrobial Photoinactivation Protocol

Inactivations in planktonic culture were performed as stated in Chapter 2.

For photoinactivations on biofilms, 2 µl of the bacterial culture were grown in 130 µl of TSB per well in a 96-well plate. Cell suspensions were incubated over night at 37 ± 1 ˚C. The supernatant was eliminated washing the well with sterile PBS three times and the biofilm was incubated with 150 µl of the ternary complex during 30 min at 37 ± 1 ˚C. Illumination was performed as for the planktonic conditions.

The supernatant was then eliminated, and the wells were washed twice with 150 µl of sterile PBS. Finally, the biofilm was torn by pipetting nimbly, obtaining a bacterial suspension. Cells were serially diluted, seeded on tryptic soy agar and incubated 24 h at 37 ˚C ± 1 ˚C. Experiments were carried out in duplicate for each condition, including cell controls and dark controls. Colony-forming units were counted to calculate the survival fraction. Three independent experiments were done for each photoinactivation treatment. The average and standard deviation (SD) values were calculated.

4.3 Results

4.3.1 Photodynamic action of *H. perforatum* hydrophilic extract against *S. aureus*

Photophysical Characterization

The lyophilized hydrophilic extract of *Hypericum perforatum* (aHyp) was firstly characterized photophysically once dissolved in DMSO and eliminated the non-dissolved fraction by centrifugation. Figure 64 presents the absorption spectra of pure Hyp in ethanol, in DMSO and of the aHyp in DMSO.

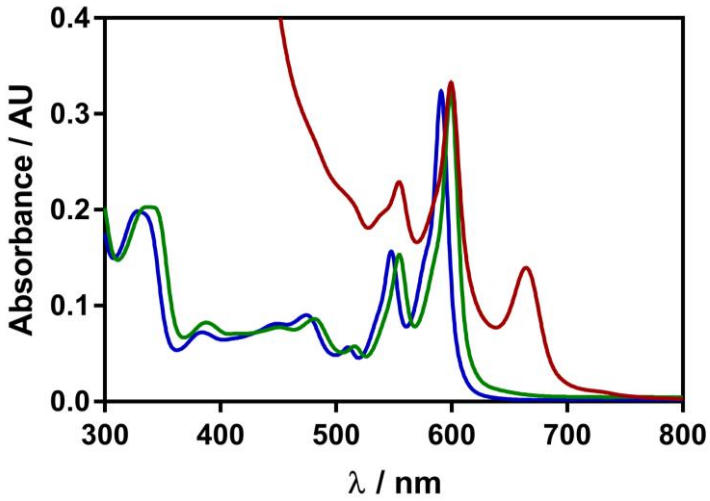

Figure 64. Absorption spectra of Hypericin in EtOH (blue) and in DMSO (green), and of aHyp also in DMSO (dark red).

Hyp presents in both ethanol (blue) and DMSO (green) similar absorption spectra, with a slight red shift typical of spectra in DMSO. aHyp in DMSO (dark red), does indeed present the two main visible absorption bands related to Hyp at exactly the same wavelengths (maxima at 555 nm and 599 nm), but also presents a maximum at 665 nm which corresponds to chlorophyll and a large non-specific absorption in the blue and UV range, indicating the presence of multiple unknown chromophores in the extract.

Regarding fluorescence, the left part of Figure 65 presents the emission spectra collected from pure Hyp in ethanol and DMSO (blue and green respectively on the left) and of aHyp in DMSO (dark red) excited at 550 nm, as well as the emission spectra of aHyp in DMSO excited at 660 nm

(yellow). The right part of Figure 65 shows the excitation spectra of aHyp in DMSO observing at 615 nm (dark red) and at 680 nm (yellow).

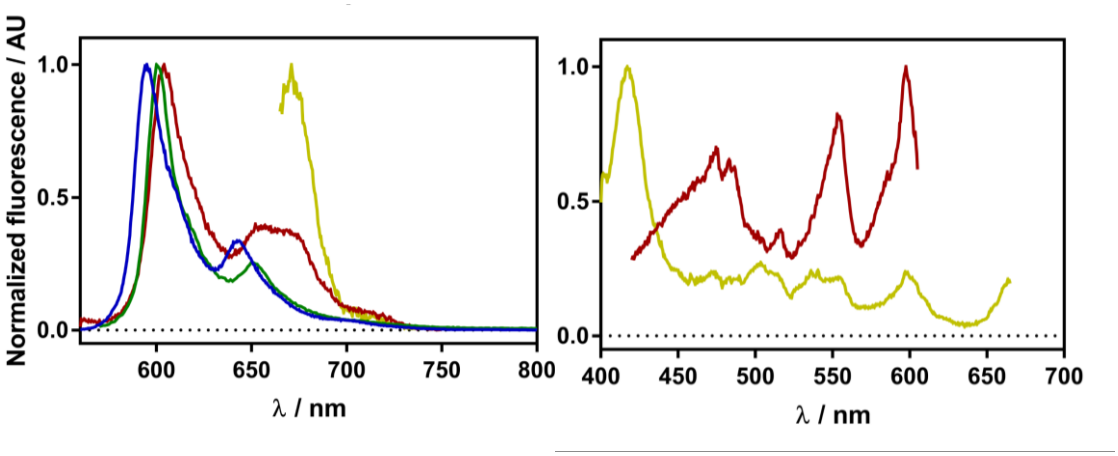

Figure 65. Left: Emission fluorescence spectra of Hypericin in ethanol (blue), DMSO (green) and of aHyp in DMSO (dark red) excited at 550 nm. aHyp in DMSO excited at 660 nm is presented in yellow. Right: Excitation fluorescence spectra of aHyp in DMSO observing at 615 nm (dark red) and at 680 nm (yellow).

The emission spectra from aHyp shows how there are mainly two fluorescent compounds which are Hyp and chlorophyll. The spectrum matches that of pure Hyp in DMSO, while emission from chlorophyll is overlapped peaking at 670 nm.[301] This can be clearly seen when chlorophyll is mainly excited at 660 nm. Also, the excitation spectrum at 615 nm (dark red) show a profile similar to that of Hyp with maxima at 599 and 555 nm. Observation at 680 nm (yellow) reveals a profile much similar to that of a chlorophyll with an intense Soret band at 417 nm. Hyp still emits fluorescence at 680 nm, which explains the minor bands in the green-orange range due to a small contribution from this chromophore.

The presence of competitive absorption from other co-solutes make it impossible to measure an accurate fluorescence quantum yield but judging by the intensities observed, the fluorescence quantum yield should be comparable to that of the pure compound. This indicates that there are no (or few) quenchers within the hydrophilic extract.

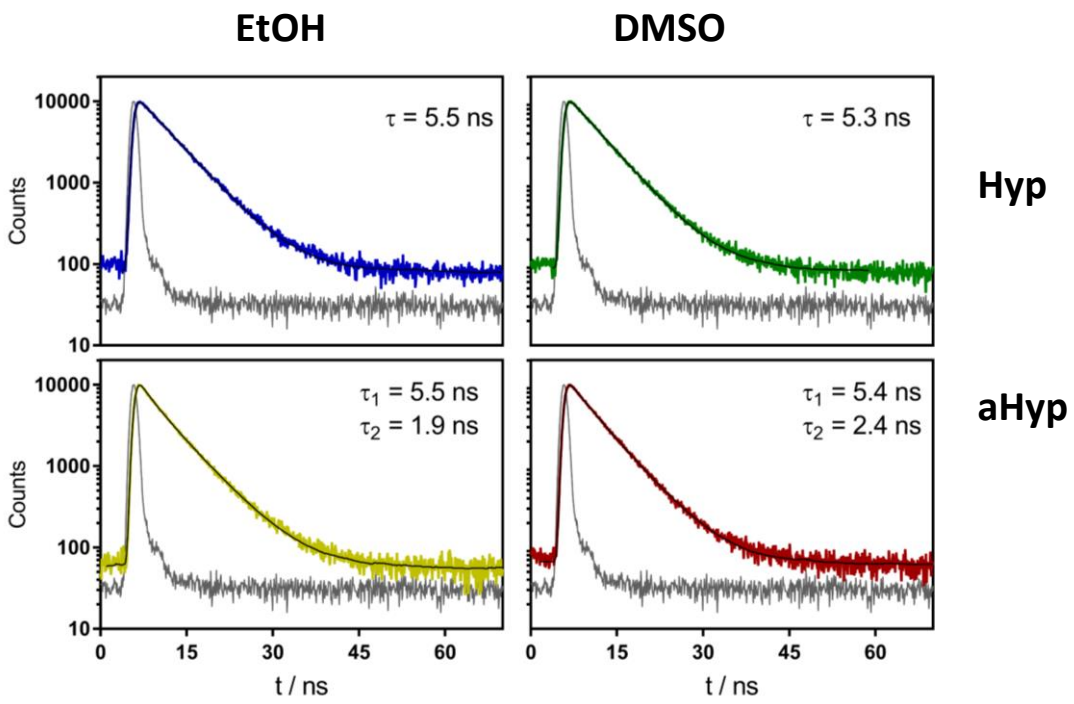

Figure 66. Time resolved fluorescence of Hypericin in EtOH and DMSO (Blue-Top Left and Green-Top Right respectively) and of aHyp in EtOH and DMSO (Yellow-Bottom Left and Dark Red-Bottom Right respectively) exciting at 600 nm and observing at 620 nm.

The TRF measurements show how Hyp presents a similar single lifetime in ethanol and DMSO (approximately 5.5 ns), while the plant extract presents two different lifetimes in both solvents. The longest lifetime matches that of Hyp, while the shorter one (1.9 ns and 2.4 ns in Ethanol and DMSO respectively) could be attributed to chlorophyll b.[302]

Triplet state measurements were also performed by nano-second laser flash photolysis, proving that triplets are formed in good yields. The triplet lifetime of the plant extract in deaerated DMSO was of 109 μs, whilst pure Hyp presented a lifetime of 170 μs, difference which was attributed to quenching by co-solutes. Just like with fluorescence, the triplet quantum yield could not be properly quantified due to the presence of other absorbing species.

Also, fluorescence microscopy imaging was performed to *S. aureus* incubated with the plant extract using N-STORM with Total Internal Reflection Imaging. The microscopy revealed binding of Hyp binding to the bacterial wall, proving interaction between drug and target.

Photodynamic Studies against *S. aureus*

The active components in any photodynamic inactivations are in fact the reactive oxygen species formed, and therefore the use of a non-purified plant extract may result in a lower activity due to the presence of natural antioxidants and other scavengers, as already reported for Hyp.[303] Despite this fact, triplets in the plant extract are formed in high yield and having microscopy images proving binding to bacteria make it reasonable to think that inactivation should be efficient. Figure 67 presents the photoinactivation of *S. aureus* using Hyp and the plant extract. Concentrations were determined spectrophotometrically to quantify Hyp in both stock solutions.

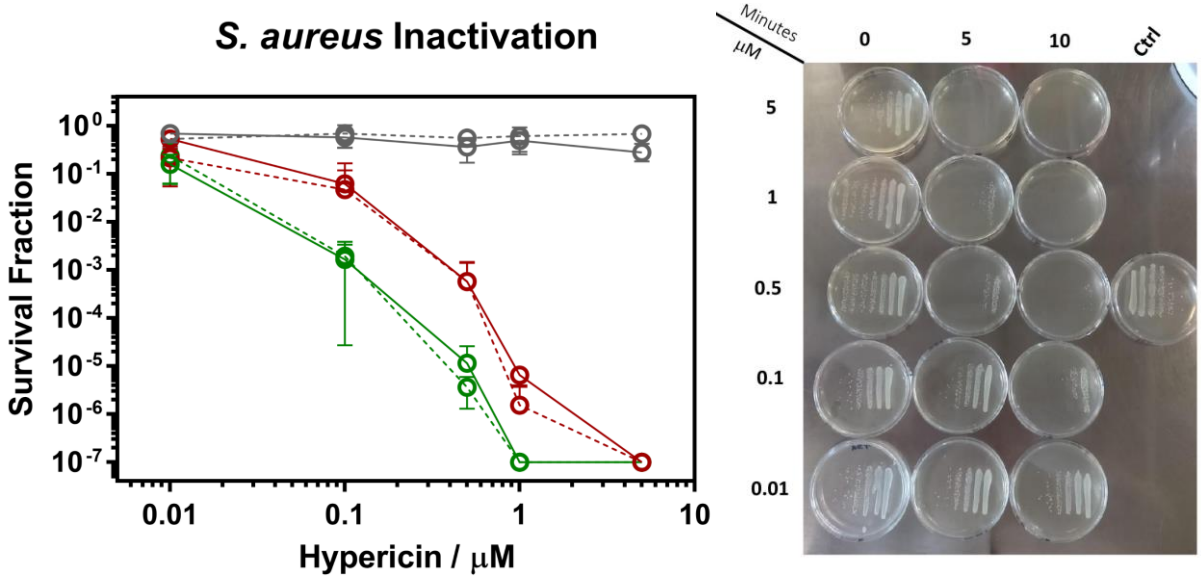

Figure 67. Left: Photoinactivation of S. aureus ATCC 25923 with Hyp (dotted lines) and aHyp (solid lines) at 4.8 (red) and 9.6 (green) J·cm^{-2} of green light (521 nm ± 19 nm). The dark controls are represented in grey. Right: Petri dishes showing for each concentration (the five rows) and exposure time (the three columns) the dilutions of the bacterial suspension from which the CFU ml^{-1} survival fraction is calculated.

Photosensitizer concentrations ranged from 0.01 to 10 μM illuminating samples with green light at increasing exposure times. Figure 67 shows that this treatment induces a relevant inactivation of the bacteria. The decrease in the number of CFU*s* upon irradiation is dependent on drug concentration and light fluence. No major difference was observed between pure Hyp and the plant extract (aHyp). A 7-log inactivation was achieved for both formulations at 1 μM after 9.6 J·cm^{-2}. A 3-log reduction was observed at 0.5 μM for the lower light dose, while at 9.6 J·cm^{-2} only needed of 0.1 μM. No dark toxicity whatsoever was detected at the concentration range tested.

DMSO and light controls (without photosensitizer) were also performed to rule out any inactivation due to light or organic solvent. Similar results were obtained by treating *S. aureus* with ethanol Hyp and aHyp solutions (data not shown).

The observed results match with those previously reported when photoinactivating Gram-positive bacteria (like *S. aureus*) with Hyp delivered in DMSO or ethanol.[104,272,273,304–307]

To sum up, non-purified solutions of lyophilized *Hypericum perforatum* present a mixture of compounds which does not affect the photochemistry of Hyp, since quenchers do not seem to be present. The spectral window left between 500 and 600 nm allows to excite the photosensitizer selectively, yielding fluorescent and triplet yields comparable to that of pure Hyp. Also, the photosensitizer is not physically entrapped or sequestered within the formulation, meaning that it is available to actuate. *Hypericum perforatum* extracts have been proved to be as active as pure Hyp when illuminating *S. aureus* with green light. Thus, it must be considered as a far cheaper alternative for bacterial disinfections, and probable many other applications.

4.3.2 Double payload in the β-lactoglobulin complex for potential acne treatment

In this subchapter the interaction between βLG and Retinoic acid will be further characterized, as the PDT inactivation assays with *S. aureus*.

Förster Energy Transfer (FRET) distance estimation between βLG and Retinoic Acid

As already proven by Dr. Beatriz Rodriguez-Amigo,[260] the addition RA does not only affect Hyp's photophysics, but also that of the protein. Fluorescence originating from βLG (mainly by tryptophan) is also quenched by the presence of the retinoid.[308] The nice spectral overlap between βLG's fluorescence and of RA absorption make it likely for a FRET-like quenching mechanism to happen. Indeed, the reduction in fluorescence intensity and lifetime when adding retinoic to the protein (Figure 68) indicates that FRET is taking place.

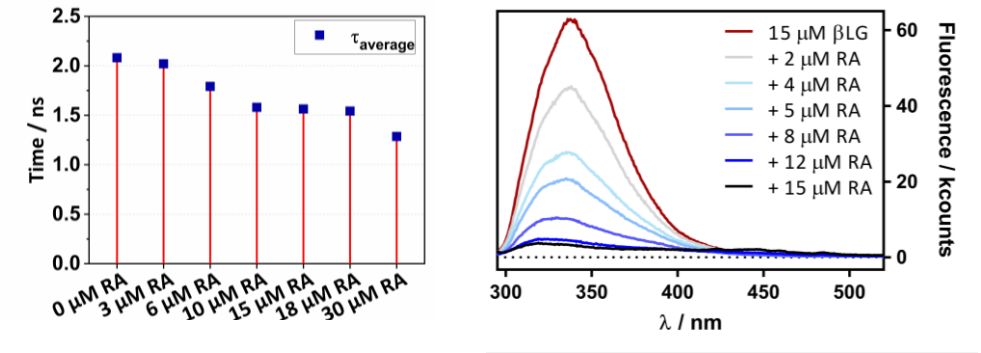

Figure 68. Fluorescence lifetime of βLG (left) and fluorescence intensity (right) with increasing concentrations of RA exciting samples at 280 nm. TRF was recorded at 349 nm. Figure adapted from Dr. Rodriguez-Amigo's thesis.[260]

One of the key parameters regarding FRET is the Förster critical distance (R_0), which defines the distance between donor and acceptor at which energy transfer has an efficiency of 0.5 (Φ_{ET}). Practically speaking, the shorter R_0, the better the energy transfer between the two chromophores is. R_0 is calculated following Equation 10:[309]

$$R_0{}^6 = \frac{9 \cdot \ln(10) \cdot \kappa^2 \cdot \Phi_F \cdot J}{128 \cdot \pi^5 \cdot n^4 \cdot N} \qquad Eq.10$$

in which κ is the orientation factor for dipole-dipole interaction, Φ_F the fluorescent quantum yield of βLG (the donor) in the absence of RA (the acceptor), *J* the spectral overlap integral between the fluorescence spectra of βLG and the molar absorption coefficients of RA, *n* the

refractive index of the medium between the Förster pair and *N* Avogadro's number. To this end, the refractive index of the protein βLG was found bibliographically (*n*=1.594),[310] the fluorescent quantum yield was measured by comparison using tryptophan as reference[311] ($\Phi_{F,\beta LG}$=0.04), parameter *J* was calculated using Equation 11[309] and the orientation factor, despite knowing that inside a protein it will be a fixed value, it has been assumed to be 2/3, which is the typical value for dyes free in solution.

$$J = \frac{\int F_d(\lambda) \cdot \varepsilon_a(\lambda) \cdot \lambda^4 \cdot d\lambda}{\int F_d(\lambda) \cdot d\lambda} \qquad Eq.11$$

Where $F_d(\lambda)$ is the normalized emission spectrum of the donor (βLG) and $\varepsilon_a(\lambda)$ the molar absorptivity of the acceptor (RA). Figure 69 presents the emission spectrum of βLG in PBS and the molar absorptivity of RA in ethanol. Since RA is insoluble in PBS and its inclusion into the protein monomerizes the molecule, it was assumed that the absorption values would be similar.

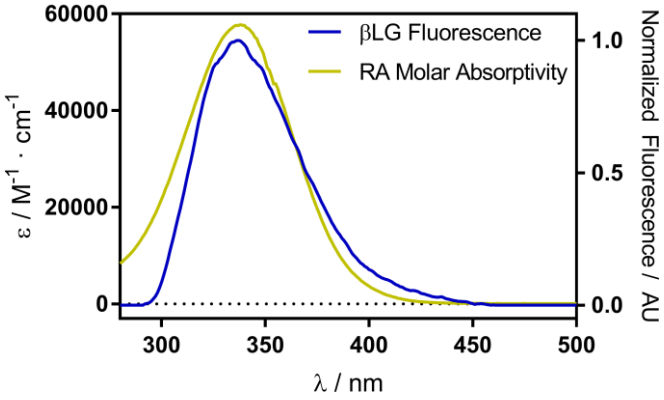

Figure 69. Spectral overlap of βLG fluorescence emission and RA molar absorptivity.

Assuming the values mentioned above, the critical distance at which 50% of the energy from the donor is transferred (R_0) resulted in 7.7 Å. The reduction in the donor's average lifetime (Figure 68) and Equation 12 were used to calculate the experimental Φ_{ET} and the actual distance between acceptor and donor.

$$\Phi_{ET} = 1 - \frac{\tau_D}{\tau_D^{\circ}} = \frac{{R_0}^6}{R + {R_0}^6} \qquad Eq.12$$

The energy transfer quantum yield resulted in 0.29 (from 2.1 to 1.5 ns), and therefore, the distance between donor and acceptor was of 9.0 Å. βLG contains two tryptophan residues within its structure, Trp19 and Trp61. Trp61, has been previously described to be quenched by a nearby cysteine bridge,[312] so it was assumed that Trp19 was the one involved in the FRET quenching process with RA.

A final computational calculation was performed in which RA was embedded into βLG. Some studies have already stated that RA enters deep into the protein calyx. [313,314] The conformation with least energy proved RA to be at a distance of 11 Å from Trp (Figure 70). The experimental and computational findings are in nice agreement with each other.

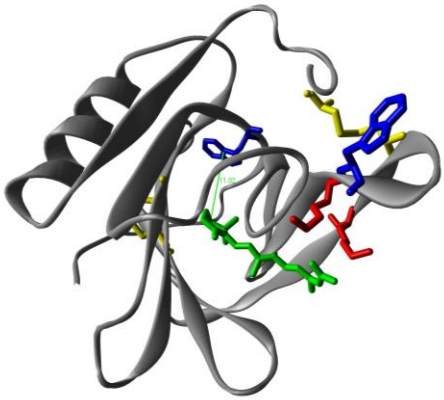

Figure 70. Representation of the main amino acids of βLG monomer involved in the interaction with RA (purple sticks). Red sticks represent some of the Lysines, blue ones the two Tryptophans present in the protein, in yellow the two Cysteines forming the disulphide bond next to Tryptophan61 and in green Retinoic Acid inside the protein. Barely noticeable, the distance between Tryptophan19 and RA (11 Å) is indicated in light green.

Antimicrobial studies

Having seen the quenching of the photophysical properties of Hyp in the ternary complex (Figure 63) and its later recovery when in the presence of bacteria[260], we performed antimicrobial inactivations to study its effects on *S. aureus*. *Propionibacterium acnes,* as main actor in acne pathogenesis, was considered for PDT but it was ruled out since it prefers anaerobic growth conditions.

Prior to using the ternary complex to inactivate bacteria, the individual components were tested independently and in combination with the others. βLG and RA did not present any cytotoxicity activity in the dark nor under green light illumination at concentrations up to 100 μM for the protein and 10 μM for the RA. Also, the dual complex βLG-RA (where protein concentration was fixed at 40 μM and RA concentration varied) did not cause significant changes in the bacteria growth, neither in darkness nor under 18 and 37 J·cm^{-2} of fluence of green light (Figure 71).

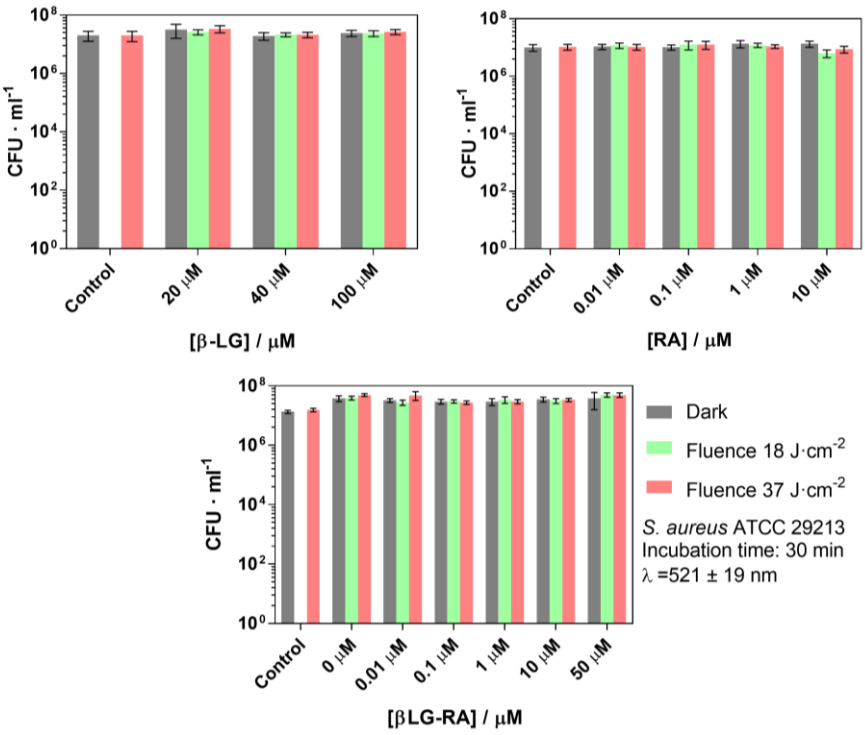

Figure 71. Photoinactivation of S. aureus ATCC 29213 with βLG (top left), RA (top right) and the binary complex βLG-RA (fixing βLG concentration at 40 μM). Coloured bars represent different green light fluences, namely, 0 (grey), 18 (green) and 37 (pink) J·cm^{-2}.

After demonstrating the innocuity of βLG and RA, Hyp was added to the complex to inactivate *S. aureus*. Figure 72 presents the inactivation of *S. aureus* using each individual component and their binary and ternary combinations. βLG was used at 40 μM, RA at 10 μM and Hyp at 4 μM under 18 and 37 J·cm^{-2} of green light (λ=521±19 nm).

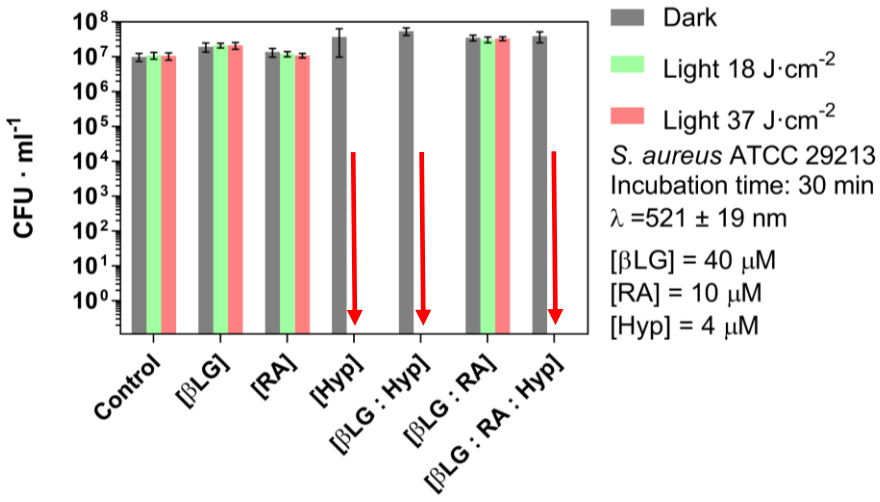

Figure 72. Photoinactivation of S. aureus ATCC 29213 with combinations of βLG, RA and Hyp at 40, 10 and 4 μM respectively. Coloured bars represent different green light fluences, namely, 0 (grey), 18 (green) and 37 (pink) J·cm^{-2}.

Only the illuminated formulations which contained Hyp were able to induce a complete eradication of the bacterial strain. No other condition, light or dark, induced any cell death whatsoever.

The results obtained are in nice agreement with previous studies performed, in the same conditions, with the binary complex βLG:Hyp.[104] 4 μM of Hyp induces a complete inactivation of the antimicrobial strain, demonstrating that RA has no effect on the outcome of the treatment. There was a concern during the design of the study about a possible reduction of the bacterial inactivation due to the introduction of a singlet oxygen scavenger such as RA.[315] The double bonds in the polyene chain of RA could readily react with ROS, and therefore reducing its effect. Since Hyp at 4 μM at fluences up to 18 and 37 J·cm^{-2} may even deplete all RA and then inactivate the bacteria, milder inactivation conditions were sought, to which RA was then added.

Figure 73 presents the photoinactivation of *S. aureus* by adding increasing concentrations of RA to the binary complex βLG-Hyp (40:1 μM). In these experimental conditions, in which a partial bacterial inactivation (reduction of 3-log units) was achieved, the addition of RA up to 50 μM caused no effect.

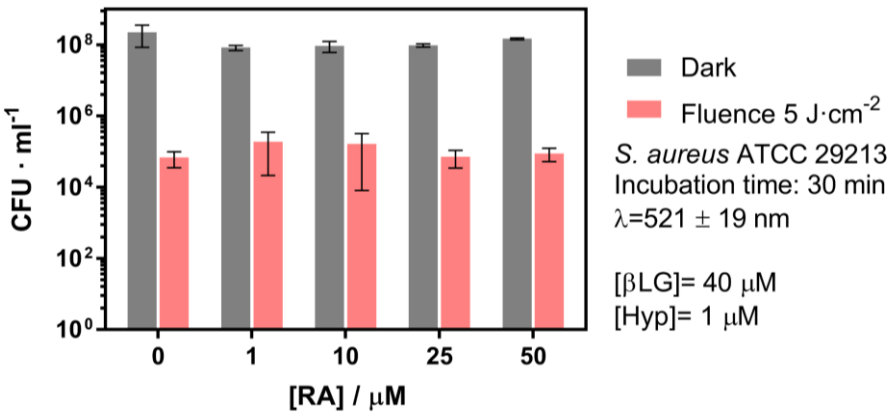

Figure 73. Photoinactivation of S. aureus ATCC 29213 with increasing concentrations of RA, from 0 to 50 μM, to βLG-Hyp complex (40:1 μM). Grey bars represent the dark controls and the pink one after a fluence of 5 J·cm^{-2} of green light.

In light of these results, it is safe to say that retinoic acid is able to quench the photophysical properties of Hyp only when it is close together within the protein. Once the cargo is unloaded to bacteria, a physical separation of the components takes place and RA loses this capacity. Singlet oxygen can travel only very short distances which further supports the distancing hypothesis.

To further understand the delivery system, an uptake assay was performed in order to assess the binding of hypericin to bacteria. After the 30-minute incubation with the ternary complex, the supernatant of the centrifuged cells was washed with PBS and the pellet resuspended three times, before finally being dissolved in DMSO to lyse the bacteria and monomerize the photosensitizer. Figure 74 presents the fluorescence spectra of Hyp before, during and after the centrifugation steps.

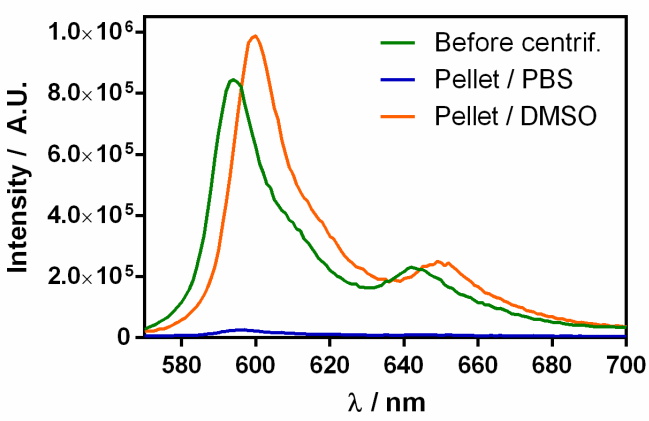

Figure 74. Fluorescence spectra of Hyp excited at 550 nm of S. aureus ATCC 29213 incubated with the ternary complex βLG-RA-Hyp immediately after incubation without washing the supernatant (Green); pellet resuspended in PBS after the first centrifugation (Blue) and the pellet resuspended in DMSO after centrifugation (Orange).

The green line shows how Hyp in PBS incubated with the bacteria before washing the supernatant presents a structured spectrum, indicating that the photosensitizer is in a monomeric form either in the protein complex or attached to the bacteria. Once the supernatant had been cleaned and the pellet resuspended in PBS (in which βLG was removed from the supernatant) the fluorescence lost its intensity indicating either the absence of Hyp or its high aggregation and, therefore, self-quenching of its photophysics. The latter centrifugation and resuspension of the pellet in DMSO dissolves the bacterial cells, and Hyp is therefore monomerized once again, recovering its fluorescence emission. This recovery proves that the photosensitizer was either attached or internalized in the bacteria. The fluorescence spectrum presents the typical bathochromic shift expected for DMSO.

In addition, the uptake of Hyp by the cells was monitored at different RA concentration. Hypericin in bacteria was quantified by interpolating in a calibration curve obtained by fluorescence. Figure 75 shows how the uptake of the photosensitizer is independent from the amount of RA. The introduction up to 50 μM of RA does not interfere with Hyp uptake by cells which stays invariable at approximately 0.6 μM 15% (uptake).

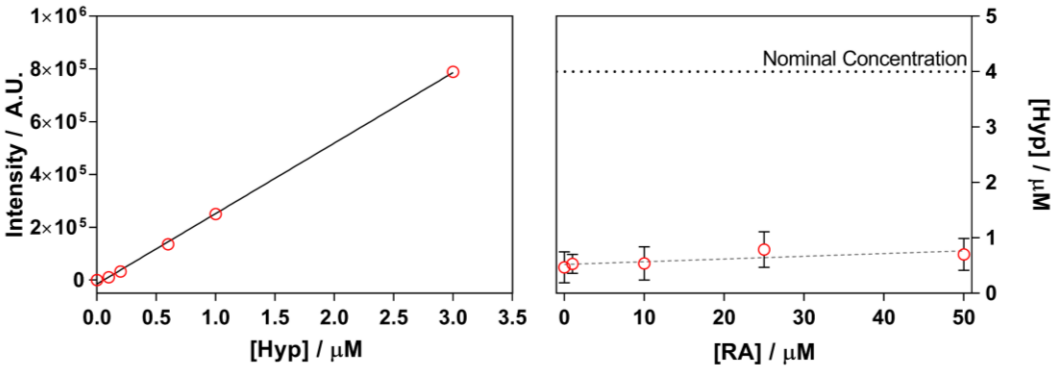

Figure 75. Fluorescence calibration curve of Hyp in DMSO (left) and uptake concentrations of Hyp by S. aureus (right) at increasing RA concentrations.

Staphylococcus aureus biofilms were also tested with the ternary complex formed by Hyp, RA and βLG in the same conditions as were used in planktonic cultures. Bearing in mind that biofilms may need from 10 to 1000 times more concentration in order to induce cell death,[316] Hyp concentrations were tested from 8 μM up to 400 μM (100-fold higher). Even the incubation time was increased up to 24 hours (as described in previous studies),[317] but under the same fluences (18 and 37 $J \cdot cm^{-2}$), no cell death was induced onto the bacterial culture whatsoever (data not shown).

These results demonstrate that neither concentration nor the incubation period can enhance Hyp uptake by *S. aureus* biofilm culture. On account of this phaenomenon, it can be concluded that *S. aureus* biofilm cultures shows a high resistance to Hyp penetration, making it impossible to photoinactivate as proposed. Maybe the addition of coadjuvants would permeabilise the extracellular matrix and facilitate biofilm eradication.[318]

Other published studies, which also pursue the goal of treating acne with PDT, have proved its feasibility *in vitro*, *in vivo* and in clinical trials. De Annunzio and co-workers used methylene blue, curcumin and chlorin Ce6 for the inactivation of *P. acnes*, for which 3.3 $J \cdot cm^{-2}$ and 2.6 μM of Ce6 were required to fully inactivate the strain.[319] Another study using Ce6 published by Jeon and co-workers presents susceptibility of *P. acnes*, despite achieving only 2-log cell death and

presenting dark toxicity, at 0.8 μM.[320] A later study by the same group proves also an anti-inflammatory effect of Ce6 in HaCaT cells, showing that one compound can treat both inflammation and infection at the same time.[296]

Another Korean study approaches a dual therapy treatment for acne using lipase-sensitive liposomes to deliver erythromycin and Pheophorbide A to obtain an enhanced effect on *P. acnes* infections *in vitro* and *in vivo*.[298] Finally, Xu and co-workers tested in clinical trials a combination of minocycline and ALA in "moderate to severe facial acne", in which they saw an improvement of the clinical outcome and in quality of life of the patients when using the combined therapy in comparison with the antibiotic alone.[299]

To sum up, this study is very preliminary when speaking of treating acne but has potential to be further developed successfully. The ternary complex formulation does not inhibit the pharmacological activity of Hyp against *S. aureus* and furthermore, its photophysical properties are silenced (i.e., quenched) by RA while not in contact with bacteria. A hypothetical cream using a photochemically safe and non-invasive drug carrier would be able to benefit from the double payload disinfecting the affected hair follicles with Hypericin-mediated PDT and decreasing inflammation with RA.

CHAPTER 5

General Discussion

Many advances have been achieved in Photodynamic Therapy since its discovery in 1900. One of the clearest examples of this development is the classification of photosensitizers in "generations". The shortcomings of first-generation photosensitizers were rapidly overcome through the development of synthetic drugs endowed with enhanced absorption in the red, solubility in physiological environments, photostability, etc. Both porphycenes and Hypericin (even though it is a natural product) can be included in the second-generation of photosensitizers.

One of the first goals of this thesis was to study the introduction of an antibiotic as a targeting element towards bacteria,[197] while also benefiting from the antibiotic's bactericidal activity. What initially began as developing a third-generation photosensitizer (introducing a targeting element) has resulted in a second-generation study since it has been proven that Portacin does not present selectivity towards bacteria. In addition to the cancer results presented (performed with a 12-hour incubation of the photodrugs), another preliminary assay in HeLa cells was performed (incubating the photosensitizers during only 30 minutes to mimic the aPDT protocol) which shows that phototoxicity against human cells in these conditions is harsh (data not shown). These *in vitro* results should be continued with *in vivo* assays in order to assess whether the damage caused on the surrounding eukaryotic cells is "tolerable" that is, if the benefits obtained from the treatment will ever compensate the collateral negative effects, or if the photosensitizer needs a selectivity enhancer for this application.

The improved properties observed for the expanded porphycene conjugates such as the large bathochromic shift into the optical window range, their theranostic potential, the broad microbiological action of Portacin and the high activity of Porphonium against cancer could be further improved by conjugating these compounds with targeting elements. The use of targeting molecules such as folate[321] and small proteins like lectins (targeting the Oncofoetal Thomsen–Friedenreich disaccharide for example)[127] and antibody fragments (such as nanobodies)[118] for

cancer treatments, and sugars like mannitol and sorbitol and p-aminobenzoic acid [322] for aPDT could prove to be effective selectivity enhancers. Alternatively, nanoparticles such as liposomes and micelles could be used provided that some of the aforementioned targeting agents should be incorporated.

Having found out that gentamicin does not have biological activity once conjugated to porphycene (as other antibiotics conjugated to photosensitizers), one would reconsider the propriety of using an antibiotic as a solubilizing agent for porphycene due to the antibiotic resistance it could potentially induce in bacteria. The solubilization of Portacin is due to the amines present in the aminoglycoside, which probably would not be achieved with standard glycosides that have alcohol groups since these are not ionized in physiological media. Since most natural aminoglycosides present bactericidal effects, a synthetic conjugate would be needed to which a mannitol sugar could be added at the tip for targeting purposes, yielding a tetraglycoside.

The amphiphilicity of photosensitizers is the cornerstone property which explains the broad-spectrum activity of the photosensitizers in aPDT. In this regard, just like PCI,[163] the disposition of the cationic charges introduced onto the apolar core may be one of the reasons behind the high biological activity of Portacin. Other cationic compounds described such as the ammonium and pyridinium porphycene derivatives described by Ragàs[187] and Ruiz-González[188], respectively, the cationic porphyrin series described by Caminos[231], and the bulky cationic phthalocyanines reported by Revuelta-Maza[75] need higher photosensitizer concentrations than Portacin to inactivate Gram-negative bacteria. Geometrically, the above-mentioned molecules have their cationic charges on the vertexes, stemming radially form its apolar core. Portacin, on the other hand, has a linear disposition of charges orthogonally attached to the expanded aminothiazolo ring. The separation of the polar and apolar regions of the photosensitizer may enhance the internalization of Portacin into the cytoplasm, resulting therefore in a greater inactivation.

The uptake of a photosensitizer is sometimes not enough to ensure a proper cell inactivation, since it always depends on its final cellular localization.[323] A clear example of this in aPDT can be found in Hypericin. Delcanale successfully reports STED imaging of Hypericin uptaken by *E. coli*,[83] while no efficient inactivation of Gram-negative bacteria with this photosensitizer has been reported so far.[272,286,304] The development of super-resolution optical microscopic techniques, such as STED, opens a new field in microbiology in which colocalization studies can be performed to relate uptake and accumulation patterns with treatment outcome.

Cancer PDT is very sensitive to the final subcellular localization of the photosensitizer. The addition of the triphenylphosphonium moiety into the expanded porphycene was not enough to clearly guide accumulation of the photosensitizer to mitochondria. Some studies have hinted that, for some molecules, one single triphenylphosphonium group is not enough to change its accumulation pattern.[159] Judging from the spinning disk images, this functional group is able to partially direct Porphonium towards mitochondria, while Portacin and, particularly, Porbutyl, have different accumulation patterns. The accumulation in mitochondria could explain the higher activity of this photosensitizer against HeLa cells.

One of the main drawbacks of synthetic third-generation photosensitizers are their production costs in comparison to the added medical potential obtained. Natural solutions, such as Hypericin, must still be further explored in order to benefit from what nature already provides. Hypericin, which has proven to be a great selective photosensitizer against Gram-positive bacteria and has applications in fungi and cancer afflictions, can also be used directly from its plant extract. We have proven that potential natural quenchers and antioxidants from the extract do not affect *S. aureus* inactivation, making it a far cheaper alternative than synthetic or purified natural photosensitizers. Pharmaceutical regulations may prevent the use of unknown mixture from a plant with many different components, but perhaps a health application categorized as a herbal medicinal product could be found (HMP).[324]

Hypericin-based treatments for acne seem to be advancing fast and could be found widespread in clinics soon. The use of β-lactoglobulin as a single carrier for a double pay load of retinoic acid and hypericin is a very elegant and powerful solution for a localized treatment.

The lack of selectivity observed reinforces the general need in PDT in finding better and optimized photosensitizers, especially with greater selectivity. Perfect PSs for the different applications have not yet been discovered and therefore research must continue in this field. Not only biological tests, but also research in understanding the molecular mechanism taking place within the cell is of utmost importance. In this regard, super resolution microscopy and femtosecond spectroscopy are two examples of very powerful techniques that can be further exploited to learn about the PDT mechanism of action.

Antibiotics for infections and chemotherapy for cancer will not be substituted overnight for PDT, and they may never be. However, given the synergistic effects discovered in recent years, classical treatments for each malady may be complemented with PDT, meaning that there will be combined treatments using photosensitizers and antibiotics or chemodrugs.

CHAPTER 6

Conclusions

1. *2-gentamicin-thiazolo[4,5-c]2,7,12,17-tetrakis(methoxyethyl) porphycene*, or Portacin, is a broad-spectrum antimicrobial agent, being able to efficiently inactivate *S. aureus*, *E. coli* and *C. albicans* in the sub-micromolar range. Mechanistically speaking, the biological activity observed is only due to the amphiphilic properties of the photosensitizer, while the role of the antibiotic is to solubilize porphycene. The hydrophobic polarity of the other expanded porphycenes prevent them from inactivating efficiently the Gram-negative *E. coli*.

2. The decrease in the fluorescence and singlet oxygen quantum yields of Portacin in PBS due to aggregation has been justified experimentally using Femtosecond Transient Absorption Spectroscopy. The faster decay of transient phenomena in the picosecond range, when dissolved in PBS in comparison to methanol, is a spectrophotometric evidence of the empirically observed loss of photophysical properties from aggregated hydrophobic photosensitizers in physiological environments. The incubation of the photosensitizers with *S. aureus* in PBS resulted in a partial recovery of the previously lost properties due to the accumulation in the hydrophobic bacterial wall of bacteria.

3. Femtosecond Transient Absorption Spectroscopy also proved that porphycenes and 2-aminothiazoloporphycenes can be used as probes for STED super resolution microscopy. The latter fluorophores present an overlap of stimulated emission and ground-state absorption, therefore hampering their performance. Portacin was imaged by STED in the cytoplasm of *S. aureus* while *E. coli* presented a major accumulation at the bacterial wall, justifying the different sensitivity to PDT treatments.

4. The introduction of a triphenylphosphonium moiety to porphycene partially directs the subcellular localization of *2-N-propyltriphenylphosphonium-aminothiazolo[4,5-c]-2,7,12,17-tetrakis(methoxyethyl)porphycene* towards mitochondria in HeLa cells. The higher biological activity of Porphonium in comparison with the other two porphycene derivatives can be related to the greater accumulation in this PDT-sensitive organelle.

5. A hydrophilic *Hypericum perforatum* extract has proven to be as efficient as pure Hypericin in photoinactivating *S. aureus*, showing that the presence of possible natural quenchers in the extract do not hamper the outcome of the treatment. The plant extract can be used as an economical alternative to the chemically pure Hypericin.

6. The incorporation of retinoic acid to the β-lactoglobulin-Hypericin complex does not decrease the pharmacological activity of Hypericin against *S. aureus*. The antioxidant capacity of retinoic acid does not scavenge the reactive oxygen intermediates formed by Hypericin, rendering a photochemically safe nanovehicle until delivery of the payload to bacteria.

CHAPTER 7

References

1 World Health Organization, GLOBAL HEALTH ESTIMATES SUMMARY TABLES: PROJECTION OF DEATHS BY CAUSE, AGE AND SEX, BY WORLD BANK INCOME GROUP, https://www.who.int/healthinfo/global_burden_disease/GHE_DthWBInc_Proj_2016-2060.xlsx.

2 R. C. Bone, R. A. Balk, F. B. Cerra, R. P. Dellinger, A. M. Fein, W. A. Knaus, R. M. H. Schein and W. J. Sibbald, *Chest*, 1992, **101**, 1644–1655.

3 P. Agostinis, K. Berg, K. A. Cengel, T. H. Foster, A. W. Girotti, S. O. Gollnick, S. M. Hahn, M. R. Hamblin, A. Juzeniene, D. Kessel, M. Korbelik, J. Moan, P. Mroz, D. Nowis, J. Piette, B. C. Wilson and J. Golab, *CA. Cancer J. Clin.*, 2011, **61**, 250–281.

4 A. Fleming, *Br. J. Exp. Pathol.*, 1929, 226–236.

5 J. Davies and D. Davies, *Microbiol. Mol. Biol. Rev.*, 2010, **74**, 417–433.

6 J. Yim, J. R. Smith, N. B. Singh, S. Rice, K. Stamper, C. Garcia de la Maria, A. S. Bayer, N. N. Mishra, J. M. Miró, T. T. Tran, C. A. Arias, P. Sullam and M. J. Rybak, *J. Antimicrob. Chemother.*, 2017, **72**, 2290–2296.

7 J. O'Neill, *Rev. Antimicrob. Resist. Chaired by Jim O'Neill*, 2014, 4–16.

8 E. D. Brown and G. D. Wright, *Nature*, 2016, **529**, 336–343.

9 M. P. Singh and M. Greenstein, *Curr. Opin. Drug Discov. Devel.*, 2000, **3**, 167–76.

10 C. Ghosh, P. Sarkar, R. Issa and J. Haldar, *Trends Microbiol.*, 2019, **27**, 323–338.

11 P. D. Cotter, R. P. Ross and C. Hill, *Nat. Rev. Microbiol.*, 2013, **11**, 95–105.

12 S. K. Sharma, P. Mroz, T. Dai, Y. Y. Huang, T. G. S. Denis and M. R. Hamblin, *Isr. J. Chem.*, 2012, **52**, 691–705.

13 R. Dosselli, M. Gobbo, E. Bolognini, S. Campestrini and E. Reddi, *ACS Med. Chem. Lett.*,

2010, **1**, 35–38.

14 Meade, Slattery and Garvey, *Antibiotics*, 2020, **9**, 32.

15 B. Bechinger and S. U. Gorr, *J. Dent. Res.*, 2017, **96**, 254–260.

16 A. Sulakvelidze, Z. Alavidze and J. G. Morris, *Antimicrob. Agents Chemother.*, 2001, **45**, 649–659.

17 E. Kutter, D. De Vos, G. Gvasalia, Z. Alavidze, L. Gogokhia, S. Kuhl and S. T. Abedon, *Curr. Pharm. Biotechnol.*, 2010, **11**, 69–86.

18 V. S. Gondil, K. Harjai and S. Chhibber, *Int. J. Antimicrob. Agents*, 2020, **55**, 105844.

19 M. R. Hamblin and T. Hasan, *Photochem. Photobiol. Sci.*, 2004, **3**, 436–450.

20 M. Wainwright, T. Maisch, S. Nonell, K. Plaetzer, A. Almeida, G. P. Tegos and M. R. Hamblin, *Lancet Infect. Dis.*, 2017, **17**, e49–e55.

21 T. Jurkowitsch and R. Knobler, in *Photobiology*, ed. L. O. Björn, Springer New York, New York, NY, 2nd edn., 2008, pp. 577–590.

22 E. A. Gordon Spratt, L. V. Gorcey, N. A. Soter and J. A. Brauer, *Br. J. Dermatol.*, 2015, **173**, 19–30.

23 A. P. Castano, T. N. Demidova and M. R. Hamblin, *Photodiagnosis Photodyn. Ther.*, 2004, **1**, 279–293.

24 A. P. Castano, T. N. Demidova and M. R. Hamblin, *Photodiagnosis Photodyn. Ther.*, 2005, 2, 1–23.

25 A. P. Castano, T. N. Demidova and M. R. Hamblin, *Photodiagnosis Photodyn. Ther.*, 2005, **2**, 91–106.

26 L. Benov, *Med. Princ. Pract.*, 2015, **24**, 14–28.

27 M. D. Daniell and J. S. Hill, *Aust. N. Z. J. Surg.*, 1991, **61**, 340–348.

28 B. Tian, C. Wang, S. Zhang, L. Feng and Z. Liu, *ACS Nano*, 2011, **5**, 7000–9.

29 X. Huang, P. K. Jain, I. H. El-Sayed and M. A. El-Sayed, *Lasers Med. Sci.*, 2008, **23**, 217–228.

30 K. Krumova and G. Cosa, in *Singlet Oxygen: Applications in Biosciences and Nanosciences, Volume 1*, 2016, pp. 1–21.

31 E. I. Zenkevich, E. I. Sagun, V. N. Knyukshto, A. S. Stasheuski, V. A. Galievsky, A. P. Stupak, T. Blaudeck and C. Von Borczyskowski, *J. Phys. Chem. C*, 2011, **115**, 21535–21545.

32 J. E. Brown, S. B. Brown and D. I. Vernon, *Expert Opin Investig Drugs*, 1999, **8**, 1967–1979.

33 E. Boix-Garriga, B. Rodríguez-Amigo, O. Planas and S. Nonell, in *Singlet Oxygen: Applications in Biosciences and Nanosciences*, eds. S. Nonell and C. Flors, Royal Society of Chemistry, 2016, pp. 23–46.

34 S. W. Hell, *Nat. Biotechnol.*, 2003, **21**, 1347–1355.

35 G. R. Buettner, *Arch. Biochem. Biophys.*, 1993, **300**, 535–543.

36 J. Hang, P. Ghorai, S. A. Finkenstaedt-Quinn, I. Findik, E. Sliz, K. T. Kuwata and P. H. Dussault, *J. Org. Chem.*, 2012, **77**, 1233–1243.

37 J. Hofmann, G. Just, W. Pritzkow and H. Schmidt, *J. für Prakt. Chemie/Chemiker-Zeitung*, 1992, **334**, 293–297.

38 N. I. Krinsky, *Trends Biochem. Sci.*, 1977, **30**, 35–38.

39 Y. You, *Org. Biomol. Chem.*, 2018, **16**, 4044–4060.

40 M. Bregnhøj, M. Westberg, B. F. Minaev and P. R. Ogilby, *Acc. Chem. Res.*, 2017, **50**, 1920–1927.

41 S. Nonell and C. Flors, in *Singlet Oxygen: Applications in Biosciences and Nanosciences*, eds. S. Nonell and C. Flors, Royal Society of Chemistry, 2016, pp. 7–26.

42 R. W. Redmond and J. N. Gamlin, *Photochem. Photobiol.*, 1999, **70**, 391–475.

43 S. Kim, M. Fujitsuka and T. Majima, *J. Phys. Chem. B*, 2013, **117**, 13985–13992.

44 C. Flors, M. J. Fryer, J. Waring, B. Reeder, U. Bechtold, P. M. Mullineaux, S. Nonell, M. T. Wilson and N. R. Baker, *J. Exp. Bot.*, 2006, **57**, 1725–1734.

45 W. Korytowski, G. J. Bachowski and A. W. Girotti, *Photochem. Photobiol.*, 1992, **56**, 1–8.

46 A. W. Girotti and W. Korytowski, in *Singlet Oxygen: Applications in Biosciences and Nanosciences*, eds. S. Nonell and C. Flors, Royal Society of Chemistry, Cambridge, 2016, vol. 1, pp. 409–430.

47 J.-L. Ravanat, G. R. Martinez, M. H. G. Medeiros, P. Di Mascio and J. Cadet, *Tetrahedron*, 2006, **62**, 10709–10715.

48 M. J. Davies, *Biochem. J.*, 2016, **473**, 805–825.

49 V. Rapozzi and G. Jori, *Resistance to Photodynamic Therapy in Cancer*, Springer, 2015.

50 A. Casas, C. Perotti, G. Di Venosa and A. Batlle, in *Resistance to Photodynamic Therapy in Cancer*, eds. V. Rapozzi and G. Jori, Springer International Publishing, 2015, pp. 29–63.

51 A. Juzeniene, Q. Peng and J. Moan, *Photochem. Photobiol. Sci.*, 2007, **6**, 1234–1245.

52 S. Keereweer, P. B. A. A. Van Driel, T. J. A. Snoeks, J. D. F. Kerrebijn, R. J. B. De Jong, A. L. Vahrmeijer, H. J. C. M. Sterenborg and C. W. G. M. Löwik, *Clin. Cancer Res.*, 2013, **19**, 3745–3754.

53 W. M. Star, *Phys. Med. Biol.*, 1997, **42**, 763–787.

54 R. A. Friesner, J. L. Banks, R. B. Murphy, T. A. Halgren, J. J. Klicic, D. T. Mainz, M. P. Repasky, E. H. Knoll, M. Shelley, J. K. Perry, D. E. Shaw, P. Francis and P. S. Shenkin, *J. Med. Chem.*, 2004, **47**, 1739–1749.

55 G. Jori, *J. Photochem. Photobiol. A Chem.*, 1992, **62**, 371–378.

56 M. Triesscheijn, P. Baas, J. H. M. Schellens and F. A. Stewart, *Oncologist*, 2006, **11**, 1034–1044.

57 P. Rai, S. Mallidi, X. Zheng, R. Rahmanzadeh, Y. Mir, S. Elrington, A. Khurshid and T. Hasan, *Adv. Drug Deliv. Rev.*, 2010, **62**, 1094–124.

58 H. Abrahamse and M. R. Hamblin, *Biochem. J*, 2016, **473**, 347–364.

59 S. S. Kelkar and T. M. Reineke, *Bioconjugate Chem.*, 2011, **22**, 1879–903.

60 C. Hally, B. Rodríguez-Amigo, R. Bresolí-Obach, O. Planas, J. Nos, E. Boix-Garriga, R. Ruiz-González and S. Nonell, in *Theranostics and Image Guided Drug Delivery*, ed. M. Thanou, Royal Society of Chemistry, Cambridge, 2018, pp. 86–122.

61 F. Giuntini, V. M. Chauhan, J. W. Aylott, G. A. Rosser, A. Athanasiadis, A. Beeby, A. J. MacRobert, R. A. Brown and R. W. Boyle, *Photochem. Photobiol. Sci.*, 2014, **13**, 1039–1051.

62 T. J. Dougherty, C. J. Gomer, B. W. Henderson, G. Jori, D. Kessel, M. Korbelik, J. Moan and Q. Peng, *J. Natl. Cancer Inst.*, 1998, **90**, 889–905.

63 I. Yoon, J. Z. Li and Y. K. Shim, *Clin. Endosc.*, 2013, **46**, 7–23.

64 M. el-Sharabasy, A. El-Waseef, M. Hafez and S. Salim, *Br. J. Cancer*, 1992, **65**, 409–412.

65 B. Krammer and K. Plaetzer, *Photochem. Photobiol. Sci.*, 2008, **7**, 283–289.

66 M. M. Kleinpenning, J. H. Kanis, T. Smits, P. E. J. van Erp, P. van de Kerkhof and R. M. J. P. Gerritsen, *J. Dermatolog. Treat.*, 2010, **21**, 245–251.

67 L. B. Josefsen and R. W. Boyle, *Met. Based. Drugs*, 2008, **2008**, 1–23.

68 R. Bonnett, *Chemical aspects of photodynamic therapy (Advanced Chemistry Texts, V. 1)*, Gordon and Breach Science Publishers, Amsterdam, 2000.

69 N. Kashef, Y.-Y. Huang and M. R. Hamblin, *Nanophotonics*, 2017, **0**, 1–27.

70 B. Rodríguez-Amigo, O. Planas, R. Bresolí-Obach, J. Torra, R. Ruiz-González and S. Nonell, in *Photodynamic Medicine: From Bench to Clinic*, eds. H. Kostron and T. Hasan, The Royal Society of Chemistry, 2016, pp. 23–62.

71 M. O. Senge and J. C. Brandt, *Photochem. Photobiol.*, 2011, **87**, 1240–1296.

72 B. Szyszko and L. Latos-Grażyński, *Chem. Soc. Rev.*, 2015, **44**, 3588–3616.

73 M. A. Revuelta-Maza, C. Hally, S. Nonell, G. de la Torre and T. Torres, *Chempluschem*, 2019, **84**, 673–679.

74 M. Soncin, C. Fabris, A. Busetti, D. Dei, D. Nistri, G. Roncucci and G. Jori, *Photochem. Photobiol. Sci.*, 2002, **1**, 815–819.

75 M. Á. Revuelta-Maza, P. González-Jiménez, C. Hally, M. Agut, S. Nonell, G. de la Torre and T. Torres, *Eur. J. Med. Chem.*, 2020, **187**, 111957.

76 V. F. Otvagin, A. V. Nyuchev, N. S. Kuzmina, I. D. Grishin, A. E. Gavryushin, Y. V.

Romanenko, O. I. Koifman, D. V. Belykh, N. N. Peskova, N. Y. Shilyagina, I. V. Balalaeva and A. Y. Fedorov, *Eur. J. Med. Chem.*, 2018, **144**, 740–750.

77 G. Obaid, M. Broekgaarden, A.-L. Bulin, H.-C. Huang, J. Kuriakose, J. Liu and T. Hasan, *Nanoscale*, 2016, **8**, 12471–12503.

78 E. Oliveros, S. H. Bossmann, S. Nonell, C. Martí, G. Heit, G. Tröscher, A. Neuner, C. Martínez and A. M. Braun, *New J. Chem.*, 1999, **23**, 85–93.

79 R. Bresolí-Obach, I. Gispert, D. G. Peña, S. Boga, Ó. Gulias, M. Agut, M. E. Vázquez and S. Nonell, *J. Biophotonics*, 2018, **11**, e201800054.

80 F. Cieplik, A. Späth, J. Regensburger, A. Gollmer, L. Tabenski, K.-A. Hiller, W. Bäumler, T. Maisch and G. Schmalz, *Free Radic. Biol. Med.*, 2013, **65**, 477–87.

81 A. Rezusta, P. López-Chicón, M. P. Paz-Cristobal, M. Alemany-Ribes, D. Royo-Díez, M. Agut, C. Semino, S. Nonell, M. J. Revillo, C. Aspiroz and Y. Gilaberte, *Photochem. Photobiol.*, 2012, **88**, 613–619.

82 P. Agostinis, A. Vantieghem, W. Merlevede and P. A. M. De Witte, *Int. J. Biochem. Cell Biol.*, 2002, **34**, 221–241.

83 P. Delcanale, F. Pennacchietti, G. Maestrini, B. Rodríguez-Amigo, P. Bianchini, A. Diaspro, A. Iagatti, B. Patrizi, P. Foggi, M. Agut, S. Nonell, S. Abbruzzetti and C. Viappiani, *Sci. Rep.*, 2015, **5**, 15564.

84 A. Losi, *Photochem. Photobiol.*, 2007, **83**, 1283–1300.

85 J. Torra, C. Lafaye, L. Signor, S. Aumonier, C. Flors, X. Shu, S. Nonell, G. Gotthard and A. Royant, *Sci. Rep.*, 2019, **9**, 1–10.

86 M. Westberg, M. Bregnhøj, M. Etzerodt and P. R. Ogilby, *J. Phys. Chem. B*, 2017, **121**,

9366–9371.

87 R. Yin and M. Hamblin, *Curr. Med. Chem.*, 2015, **22**, 2159–2185.

88 L. N. Dovigo, A. C. Pavarina, A. P. D. Ribeiro, I. L. Brunetti, C. A. S. Costa, D. P. Jacomassi, V. S. Bagnato and C. Kurachi, *Photochem. Photobiol.*, 2011, **87**, 895–903.

89 V. Novohradsky, A. Rovira, C. Hally, A. Galindo, G. Vigueras, A. Gandioso, M. Svitelova, R. Bresolí-Obach, H. Kostrhunova, L. Markova, J. Kasparkova, S. Nonell, J. Ruiz, V. Brabec and V. Marchán, *Angew. Chemie - Int. Ed.*, 2019, **58**, 6311–6315.

90 A. Kamkaew, S. H. Lim, H. B. Lee, L. V. Kiew, L. Y. Chug and K. Burgess, *Chem. Soc. Rev.*, 2013, **42**, 77–88.

91 S. George, M. R. Hamblin and A. Kishen, *Photochem. Photobiol. Sci.*, 2009, **8**, 788–795.

92 X. Ragàs, T. Dai, G. P. Tegos, M. Agut, S. Nonell and M. R. Hamblin, *Lasers Surg. Med.*, 2010, **42**, 384–390.

93 M. Wainwright, D. A. Phoenix, J. Marland, D. R. Wareing and F. J. Bolton, *FEMS Immunol. Med. Microbiol.*, 1997, **19**, 75–80.

94 V. Pérez-Laguna, L. Pérez-Artiaga, V. Lampaya-Pérez, I. García-Luque, S. Ballesta, S. Nonell, M. P. Paz-Cristobal, Y. Gilaberte and A. Rezusta, *Front. Microbiol.*, 2017, **8**, 1002–1011.

95 A. Jańczyk, E. Krakowska, G. Stochel and W. Macyk, *J. Am. Chem. Soc.*, 2006, **128**, 15574–5.

96 G. P. Tegos, T. N. Demidova, D. Arcila-Lopez, H. Lee, T. Wharton, H. Gali and M. R. Hamblin, *Chem. Biol.*, 2005, **12**, 1127–1135.

97 M. Alvaro, P. Atienzar, J. L. Bourdelande and H. García, *Chem. Commun.*, 2002, 3004–5.

98 M. T. Cabeen and C. Jacobs-Wagner, *Nat. Rev. Microbiol.*, 2005, **3**, 601–610.

99 M. A. Borovinskaya, R. D. Pai, W. Zhang, B. S. Schuwirth, J. M. Holton, G. Hirokawa, H. Kaji, A. Kaji and J. H. D. Cate, *Nat. Struct. Mol. Biol.*, 2007, **14**, 727–732.

100 L. B. Josefsen and R. W. Boyle, *Theranostics*, 2012, **2**, 916–966.

101 D. Bechet, P. Couleaud, C. Frochot, M.-L. L. Viriot, F. Guillemin and M. Barberi-Heyob, *Trends Biotechnol.*, 2008, **26**, 612–621.

102 M. García-Díaz, M. Kawakubo, P. Mroz, M. L. Sagristà, M. Mora, S. Nonell and M. R. Hamblin, *J. Control. Release*, 2012, **162**, 355–363.

103 H. Toledano, R. Edrei and S. Kimel, *J. Photochem. Photobiol. B*, 1998, **42**, 20–27.

104 B. Rodríguez-Amigo, P. Delcanale, G. Rotger, J. Juárez-Jiménez, S. Abbruzzetti, A. Summer, M. Agut, F. J. Luque, S. Nonell and C. Viappiani, *J. Dairy Sci.*, 2015, **98**, 89–94.

105 E. Boix-Garriga, F. Bryden, H. Savoie, M. L. Sagristá, M. Mora, R. W. Boyle and S. Nonell, *J. Porphyr. Phthalocyanines*, 2016, **20**, 1306–1318.

106 M. Kuruppuarachchi, H. Savoie, A. Lowry, C. Alonso and R. W. Boyle, *Mol. Pharm.*, 2011, **8**, 920–931.

107 M. K. Khaing Oo, Y. Yang, Y. Hu, M. Gomez, H. Du and H. Wang, *ACS Nano*, 2012, **6**, 1939–1947.

108 O. Planas, R. Bresolí-Obach, J. Nos, T. Gallavardin, R. Ruiz-González, M. Agut and S. Nonell, *Molecules*, 2015, **20**, 6284–6298.

109 K. Stockhofe, J. M. Postema, H. Schieferstein and T. L. Ross, *Pharmaceuticals*, 2014, **7**, 392–418.

110 J. Fang, H. Nakamura and H. Maeda, *Adv. Drug Deliv. Rev.*, 2011, **63**, 136–151.

111 A. K. Iyer, G. Khaled, J. Fang and H. Maeda, *Drug Discov. Today*, 2006, **11**, 812–818.

112 F. Giuntini, C. M. A. Alonso and R. W. Boyle, *Photochem. Photobiol. Sci.*, 2011, **10**, 759–91.

113 A. M. Bugaj, *Photochem. Photobiol. Sci.*, 2011, **10**, 1097–1109.

114 W. M. Sharman, J. E. van Lier and C. M. Allen, *Adv. Drug Deliv. Rev.*, 2004, **56**, 53–76.

115 N. Solban, I. Rizvi and T. Hasan, *Lasers Surg. Med.*, 2006, **38**, 522–531.

116 M. Mitsunaga, M. Ogawa, N. Kosaka, L. T. Rosenblum, P. L. Choyke and H. Kobayashi, *Nat. Med.*, 2011, **17**, 1685–1691.

117 H. Kobayashi and P. L. Choyke, *Acc. Chem. Res.*, 2019, **52**, 2332–2339.

118 R. Heukers, P. M. P. van Bergen en Henegouwen and S. Oliveira, *Nanomedicine Nanotechnology, Biol. Med.*, 2014, **10**, 1441–1451.

119 W. F. Li, G. X. Ma and X. X. Zhou, *Peptides*, 2006, **27**, 2350–2359.

120 C. L. Conway, I. Walker, A. Bell, D. J. H. Roberts, S. B. Brown and D. I. Vernon, *Photochem. Photobiol. Sci.*, 2008, **7**, 290–8.

121 R. Dosselli, C. Tampieri, R. Ruiz-González, S. De Munari, X. Ragàs, D. Sánchez-García, M. Agut, S. Nonell, E. Reddi and M. Gobbo, *J. Med. Chem.*, 2013, **56**, 1052–1063.

122 F. Selvestrel, F. Moret, D. Segat, J. H. Woodhams, G. Fracasso, I. M. R. Echevarria, L. Baù, F. Rastrelli, C. Compagnin, E. Reddi, C. Fedeli, E. Papini, R. Tavano, A. Mackenzie, M. Bovis, E. Yaghini, A. J. MacRobert, S. Zanini, A. Boscaini, M. Colombatti and F. Mancin, *Nanoscale*, 2013, **5**, 6106.

123 J. Gravier, R. Schneider, C. Frochot, T. Bastogne, F. Schmitt, J. Didelon, F. Guillemin and M. Barberi-Heyob, *J. Med. Chem.*, 2008, **51**, 3867–77.

124 F. Moret, D. Scheglmann and E. Reddi, *Photochem. Photobiol. Sci.*, 2013, **12**, 823–34.

125 D. Brevet, M. Gary-Bobo, L. Raehm, S. Richeter, O. Hocine, K. Amro, B. Loock, P. Couleaud, C. Frochot, A. Morère, P. Maillard, M. Garcia and J.-O. Durand, *Chem. Commun.*, 2009, **12**, 1475–1477.

126 J. M. Irache, H. H. Salman, C. Gamazo and S. Espuelas, *Expert Opin. Drug Deliv.*, 2008, **5**, 703–724.

127 G. Obaid, I. Chambrier, M. J. Cook and D. A. Russell, *Angew. Chemie - Int. Ed.*, 2012, **51**, 6158–6162.

128 Y. A. Shieh, S. J. Yang, M. F. Wei and M. J. Shieh, *ACS Nano*, 2010, **4**, 1433–1442.

129 Z. Tang, Z. Zhu, P. Mallikaratchy, R. Yang, K. Sefah and W. Tan, *Chem Asian J*, 2010, **5**, 783–6.

130 P. Hayley, I. Stamati, G. Yahioglu, M. Butt and M. Deonarain, *Antibodies*, 2013, **2**, 270–305.

131 A. L. Nelson, *MAbs*, 2010, **2**, 77–83.

132 M. Ritchie, L. Tchistiakova and N. Scott, *MAbs*, 2013, **5**, 13–21.

133 T. Maisch, *Photochem. Photobiol. Sci.*, 2015, **14**, 1518–1526.

134 A. Wozniak and M. Grinholc, *Front. Microbiol.*, 2018, **9**, 930.

135 T. Dai, Y. Y. Huang and M. R. Hamblin, *Photodiagnosis Photodyn. Ther.*, 2009, **6**, 170–188.

136 G. D. Wright, *Adv. Drug Deliv. Rev.*, 2005, **57**, 1451–1470.

137 G. P. Tegos, M. Haynes, J. J. Strouse, M. M. Khan, C. G. Bologa, T. I. Oprea and L. A.

Sklar, *Curr. Pharm. Des.*, 2011, **17**, 1291–1302.

138 C. Kourtesi, A. R. Ball, Y. Huang, S. M. Jachak, D. M. A. Vera, P. Khondkar, S. Gibbons, M. R. Hamblin and G. P. Tegos, *Open Microbiol. J.*, 2013, **7**, 34–52.

139 F. F. Sperandio, Y.-Y. Huang and M. R. Hamblin, *Recent Pat. Antiinfect. Drug Discov.*, 2013, **8**, 108–120.

140 N. S. Soukos, L. A. Ximenez-Fyvie, M. R. Hamblin, S. S. Socransky and T. Hasan, *Antimicrob. Agents Chemother.*, 1998, **42**, 2595–2601.

141 W. Vollmer, D. Blanot and M. A. De Pedro, *FEMS Microbiol. Rev.*, 2008, **32**, 149–167.

142 T. J. Silhavy, D. Kahne and S. Walker, *Cold Spring Harb. Perspect. Biol.*, 2010, **2**, a000414–a000414.

143 E. Hernández-Jiménez, R. del Campo, V. Toledano, M. T. Vallejo-Cremades, A. Muñoz, C. Largo, F. Arnalich, F. García-Rio, C. Cubillos-Zapata and E. López-Collazo, *Biochem. Biophys. Res. Commun.*, 2013, **441**, 947–952.

144 H.-C. Flemming and J. Wingender, *Nat. Rev. Microbiol.*, 2010, **8**, 623–633.

145 T. Coenye, E. Peeters and H. J. Nelis, *Res. Microbiol.*, 2007, **158**, 386–392.

146 X. Xu, Y. Zheng, Z. Zhao, X. Zhang, P. Liu and C. Li, *Medicine (Baltimore).*, 2017, **96**, e9366.

147 V. Pérez-Laguna, Y. Gilaberte, M. I. Millán-Lou, M. Agut, S. Nonell, A. Rezusta and M. R. Hamblin, *Photochem. Photobiol. Sci.*, 2019, **18**, 1020–1029.

148 J. Almeida, J. P. C. Tomé, M. G. P. M. S. Neves, A. C. Tomé, J. A. S. Cavaleiro, Â. Cunha, L. Costa, M. A. F. Faustino and A. Almeida, *Photochem. Photobiol. Sci.*, 2014, **13**, 626–633.

149 M. R. Ronqui, T. M. S. F. de Aguiar Coletti, L. M. de Freitas, E. T. Miranda and C. R.

Fontana, *J. Photochem. Photobiol. B Biol.*, 2016, **158**, 122–129.

150 V. Pérez-Laguna, I. García-Luque, S. Ballesta, L. Pérez-Artiaga, V. Lampaya-Pérez, S. Samper, P. Soria-Lozano, A. Rezusta and Y. Gilaberte, *Photodiagnosis Photodyn. Ther.*, 2018, **21**, 211–216.

151 F. Barra, E. Roscetto, A. Soriano, A. Vollaro, I. Postiglione, G. Pierantoni, G. Palumbo and M. Catania, *Int. J. Mol. Sci.*, 2015, **16**, 20417–20430.

152 K. Sun, H. Yang, X. Huang, N. Gong, Q. Qin, W. Lu and X. Lei, *Photodiagnosis Photodyn. Ther.*, 2017, **19**, 274–277.

153 T. Dai, B. B. Fuchs, J. J. Coleman, R. A. Prates, C. Astrakas, T. G. St Denis, M. S. Ribeiro, E. Mylonakis, M. R. Hamblin and G. P. Tegos, *Front. Microbiol.*, 2012, **3**, 1–16.

154 R. F. Donnelly, P. a McCarron and M. M. Tunney, *Microbiol. Res.*, 2008, **163**, 1–12.

155 S. K. Sharma, P. Mroz, T. Dai, Y.-Y. Huang, T. G. St. Denis and M. R. Hamblin, *Isr. J. Chem.*, 2012, **52**, 691–705.

156 V. Rapozzi and G. Jori, in *Resistance to Photodynamic Therapy in Cancer*, eds. V. Rapozzi and G. Jori, Springer International Publishing, 2015, pp. 3–26.

157 B. Chen, B. W. Pogue, J. M. Luna, R. L. Hardman, P. J. Hoopes and T. Hasan, *Clin. Cancer Res.*, 2006, **12**, 917–923.

158 K. Plaetzer, B. Krammer, J. Berlanda, F. Berr and T. Kiesslich, *Lasers Med. Sci.*, 2009, **24**, 259–268.

159 R. C. Gilson, R. Tang, K. S. Gautam, D. Grabowska and S. Achilefu, *Bioconjug. Chem.*, 2019, **30**, 1451–1458.

160 K. Plaetzer, T. Kiesslich, C. B. Oberdanner and B. Krammer, *Curr. Pharm. Des.*, 2005, **11**,

1151–1165.

161 B. Ortel, C. R. Shea and P. Calzavara-Pinton, *Front. Biosci.*, 2009, **Volume**, 4157.

162 E. Buytaert, M. Dewaele and P. Agostinis, *Biochim. Biophys. Acta*, 2007, **1776**, 86–107.

163 K. Berg, P. K. Selbo, L. Prasmickaite, T. E. Tjelle, K. Sandvig, J. Moan, G. Gaudernack, O. Fodstad, S. Kjølsrud, H. Anholt, G. H. Rodal, S. K. Rodal and A. Høgset, *Cancer Res.*, 1999, **59**, 1180–3.

164 S. Schipmann, M. Müther, L. Stögbauer, S. Zimmer, B. Brokinkel, M. Holling, O. Grauer, E. Suero Molina, N. Warneke and W. Stummer, *J. Neurosurg.*, 2020, 1–11.

165 P. G. Seybold and M. Gouterman, *J. Mol. Spectrosc.*, 1969, **31**, 1–13.

166 R. Schmidt, C. Tanielian, R. Dunsbach, C. Wolff and C. Womb, *J. Photochem. Photobiol. A Chem.*, 1994, **79**, 11–17.

167 S. Nonell, M. González and F. R. Trull, *Afinidad*, 1993, **44**, 445–450.

168 T. Hayashi, K. Okazaki, N. Urakawa, H. Shimakoshi, J. L. Sessler, E. Vogel and Y. Hisaeda, *Organometallics*, 2001, **20**, 3074–3078.

169 R. D. Costa, J. Malig, W. Brenner, N. Jux and D. M. Guldi, *Adv. Mater.*, 2013, **25**, 2600–2605.

170 W. Brenner, J. Malig, R. D. Costa, D. M. Guldi and N. Jux, *Adv. Mater.*, 2013, **25**, 2314–2318.

171 S. Feihl, R. D. Costa, W. Brenner, J. T. Margraf, R. Casillas, O. Langmar, A. Browa, T. E. Shubina, T. Clark, N. Jux and D. M. Guldi, *Chem. Commun.*, 2014, **50**, 11339–11342.

172 E. Vogel, M. Köcher, H. Schmickler and J. Lex, *Angew. Chemie Int. Ed.*, 1986, **25**, 257–259.

173 D. Sánchez-García and J. L. Sessler, *Chem. Soc. Rev.*, 2008, **37**, 215–232.

174 J. Waluk, *Chem. Rev.*, 2017, **117**, 2447–2480.

175 P. F. Aramendia, R. W. Redmond, S. E. Braslavsky, K. Schaffner, E. Vogel and S. Nonell, *Photochem. Photobiol.*, 1986, **44**, 555–559.

176 E. Vogel, *Pure Appl. Chem.*, 1996, **68**, 1355–1360.

177 J. Stockert, M. Canete, A. Juarranz, A. Villanueva, R. Horobin, J. Borrell, J. Teixido and S. Nonell, *Curr. Med. Chem.*, 2007, **14**, 997–1026.

178 C. Richert, J. M. Wessels, M. Mueller, M. Kisters, T. Benninghaus and A. E. Goetz, *J. Med. Chem.*, 1994, **37**, 2797–2807.

179 M. Wachowska, A. Muchowicz, M. Firczuk, M. Gabrysiak, M. Winiarska, M. Wańczyk, K. Bojarczuk and J. Golab, *Molecules*, 2011, **16**, 4140–4164.

180 N. Rubio, F. Prat, N. Bou, J. I. Borrell, J. Teixido, A. Villanueva, A. Juarranz, M. Canete, J. C. Stockert and S. Nonell, *New J. Chem.*, 2005, **29**, 378–384.

181 R. M. Szeimies, S. Karrer, C. Abels, P. Steinbach, S. Fickweiler, H. Messmann, W. Bäumler and M. Landthaler, *J. Photochem Photobiol. B Biol.*, 1996, **34**, 67–72.

182 O. Planas, T. Gallavardin and S. Nonell, in *Handbook of Porphyrin Science*, eds. R. Guilard, K. M. Smith and K. M. Kadish, World Scientific Publishers, Volume 41., 2016, pp. 299–349.

183 N. Masiera, A. Bojarska, I. Gawryszewska, E. Sadowy, W. Hryniewicz and J. Waluk, *J. Photochem. Photobiol. B Biol.*, 2017, **174**, 84–89.

184 F. M. Lauro, P. Pretto, L. Covolo, G. Jori and G. Bertoloni, *Photochem. Photobiol. Sci.*, 2002, **1**, 468–470.

185 L. Polo, A. Segalla, G. Bertoloni, G. Jori, K. Schaffner and E. Reddi, *J. Photochem. Photobiol. B Biol.*, 2000, **59**, 152–158.

186 A. Aicher, K. Miller, E. Reich and R. Hautmann, *Urol. Res.*, 1994, **22**, 25–32.

187 X. Ragàs, D. Sánchez-García, R. Ruiz-González, T. Dai, M. Agut, M. R. Hamblin and S. Nonell, *J. Med. Chem.*, 2010, **53**, 7796–7803.

188 R. Ruiz-González, M. Agut, E. Reddi and S. Nonell, *Int. J. Mol. Sci.*, 2015, **16**, 27072–27086.

189 O. Planas, T. Gallavardin and S. Nonell, *Chem. Commun.*, 2015, **51**, 5586–5589.

190 O. Planas, D. Fernández-Llaneza, I. Nieves, R. Ruiz-Gonzalez, E. Lemp, A. L. Zanocco and S. Nonell, *Phys. Chem. Chem. Phys.*, 2017, **19**, 25537–25543.

191 R. Dosselli, R. Ruiz-González, F. Moret, V. Agnolon, C. Compagnin, M. Mognato, V. Sella, M. Agut, S. Nonell, M. Gobbo and E. Reddi, *J. Med. Chem.*, 2014, **57**, 1403–1415.

192 F. Le Guern, T.-S. Ouk, C. Ouk, R. Vanderesse, Y. Champavier, E. Pinault and V. Sol, *ACS Med. Chem. Lett.*, 2018, **9**, 11–16.

193 R. Cahan, N. Swissa, G. Gellerman and Y. Nitzan, *Photochem. Photobiol.*, 2010, **86**, 418–425.

194 L. Huang, M. Wang, Y.-Y. Huang, A. El-Hussein, L. M. Wolf, L. Y. Chiang and M. R. Hamblin, *Photochem. Photobiol. Sci.*, 2018, **17**, 638–651.

195 R. Dorati, A. DeTrizio, M. Spalla, R. Migliavacca, L. Pagani, S. Pisani, E. Chiesa, B. Conti, T. Modena and I. Genta, *Nanomaterials*, 2018, **8**, 37.

196 U. Woiwode, A. Sievers-Engler and M. Lämmerhofer, *J. Pharm. Biomed. Anal.*, 2016, **121**, 307–315.

197 S. Carryn, H. Chanteux, C. Seral, M.-P. Mingeot-Leclercq, F. Van Bambeke and P. M. Tulkens, *Infect. Dis. Clin. North Am.*, 2003, **17**, 615–634.

198 B. H. Ali, M. Al Za'abi, G. Blunden and A. Nemmar, *Basic Clin. Pharmacol. Toxicol.*, 2011, **109**, 225–232.

199 C. García-de-la-Mària, J. M. Pericas, A. del Río, X. Castañeda, X. Vila-Farrés, Y. Armero, P. A. Espinal, C. Cervera, D. Soy, C. Falces, S. Ninot, M. Almela, C. A. Mestres, J. M. Gatell, J. Vila, A. Moreno, F. Marco and J. M. Miró, *Antimicrob. Agents Chemother.*, 2013, **57**, 2319–2325.

200 J. Xie, A. E. Talaska and J. Schacht, *Hear. Res.*, 2011, **281**, 28–37.

201 X. Zhang, L. de Boer, L. Heiliegers, S. Man-Bovenkerk, P. K. Selbo, J. W. Drijfhout, A. Høgset and S. A. J. Zaat, *J. Control. Release*, 2018, **283**, 214–222.

202 J. Davies and G. D. Wright, *Trends Microbiol.*, 1997, **5**, 234–240.

203 R. S. Hayward, J. Harding, R. Molloy, L. Land, K. Longcroft-Neal, D. Moore and J. D. C. Ross, *Br. J. Clin. Pharmacol.*, 2018, **84**, 223–238.

204 M. R. Hamblin, *Curr. Opin. Microbiol.*, 2016, **33**, 67–73.

205 M. F. Ross, G. F. Kelso, F. H. Blaikie, A. M. James, H. M. Cocheme, A. Filipovska, T. D. Ros, T. R. Hurd, R. A. J. Smith and M. P. Murphy, *Biokhimiya*, 2005, **70**, 273–283.

206 R. A. J. Smith, C. M. Porteous, A. M. Gane and M. P. Murphy, *Proc. Natl. Acad. Sci.*, 2003, **100**, 5407–5412.

207 H. Wang, T. Zhang, X. Ge, J. Chen, Y. Zhao and J. Fu, *Life Sci.*, 2020, **244**, 117322.

208 T. A. Prime, M. Forkink, A. Logan, P. G. Finichiu, J. McLachlan, P. B. Li Pun, W. J. H. Koopman, L. Larsen, M. J. Latter, R. A. J. Smith and M. P. Murphy, *Free Radic. Biol. Med.*,

2012, **53**, 544–553.

209 B. C. Dickinson and C. J. Chang, *J. Am. Chem. Soc.*, 2008, **130**, 9638–9639.

210 J. Morgan and A. R. Oseroff, *Adv. Drug Deliv. Rev.*, 2001, **49**, 71–86.

211 D. Kessel and Y. Luo, *Cell Death Differ.*, 1999, **6**, 28–35.

212 W. Lei, J. Xie, Y. Hou, G. Jiang, H. Zhang, P. Wang, X. Wang and B. Zhang, *J. Photochem. Photobiol. B Biol.*, 2010, **98**, 167–171.

213 C. Yue, Y. Yang, C. Zhang, G. Alfranca, S. Cheng, L. Ma, Y. Liu, X. Zhi, J. Ni, W. Jiang, J. Song, J. M. de la Fuente and D. Cui, *Theranostics*, 2016, **6**, 2352–2366.

214 Z. Hu, Y. Sim, O. L. Kon, W. H. Ng, A. J. M. Ribeiro, M. J. Ramos, P. A. Fernandes, R. Ganguly, B. Xing, F. García and E. K. L. Yeow, *Bioconjug. Chem.*, 2017, **28**, 590–599.

215 I. Nieves, C. Hally, C. Viappiani, M. Agut and S. Nonell, *Bioorg. Chem.*, 2020, **97**, 103661.

216 M. Maiuri, M. Garavelli and G. Cerullo, *J. Am. Chem. Soc.*, 2020, **142**, 3–15.

217 M. Russo, V. Petropoulos, E. Molotokaite, G. Cerullo, A. P. Casazza, M. Maiuri and S. Santabarbara, *Photosynth. Res.*, 2020, **144**, 221–233.

218 L. J. G. W. van Wilderen, C. N. Lincoln and J. J. van Thor, *PLoS One*, 2011, **6**, e17373.

219 P. K. Smith, R. I. Krohn, G. T. Hermanson, A. K. Mallia, F. H. Gartner, M. D. Provenzano, E. K. Fujimoto, N. M. Goeke, B. J. Olson and D. C. Klenk, *Anal. Biochem.*, 1985, **150**, 76–85.

220 T. Mosmann, *J. Immunol. Methods*, 1983, **65**, 55–63.

221 P. Bianchini, C. Peres, M. Oneto, S. Galiani, G. Vicidomini and A. Diaspro, *Cell Tissue Res.*, 2015, **360**, 143–150.

222 K. I. Willig, R. R. Kellner, R. Medda, B. Hein, S. Jakobs and S. W. Hell, *Nat. Methods*, 2006, **3**, 721–723.

223 A. Nakano, *Cell Struct. Funct.*, 2002, **27**, 349–355.

224 R. D. Hall and C. F. Chignell, *Photochem. Photobiol.*, 1987, **45**, 459–464.

225 X.-J. Jiang, S.-L. Yeung, P.-C. Lo, W.-P. Fong and D. K. P. Ng, *J. Med. Chem.*, 2011, **54**, 320–330.

226 D. Lin, Y. Wang, Q. Zhang, J. Zhou, L. Zhou and S. Wei, *J. Photochem. Photobiol. A Chem.*, 2016, **315**, 107–120.

227 F. Prat, C. Martí, S. Nonell, X. Zhang, C. S. Foote, R. González Moreno, J. L. Bourdelande and J. Font, *Phys. Chem. Chem. Phys.*, 2001, **3**, 1638–1643.

228 J. M. Monteiro, P. B. Fernandes, F. Vaz, A. R. Pereira, A. C. Tavares, M. T. Ferreira, P. M. Pereira, H. Veiga, E. Kuru, M. S. VanNieuwenhze, Y. V. Brun, S. R. Filipe and M. G. Pinho, *Nat. Commun.*, 2015, **6**, 8055.

229 O. Pierucci, *J. Bacteriol.*, 1978, **135**, 559–574.

230 L. Jakobsen, D. Sandvang, V. F. Jensen, A. M. Seyfarth, N. Frimodt-møller and A. M. Hammerum, *Clin. Microbiol. Infect.*, 2007, **13**, 830–832.

231 D. A. Caminos, M. B. Spesia and E. N. Durantini, *Photochem. Photobiol. Sci.*, 2006, **5**, 56–65.

232 D. a Caminos, M. B. Spesia, P. Pons and E. N. Durantini, *Photochem. Photobiol. Sci.*, 2008, **7**, 1071–8.

233 A. Guo, F. Wang, W. Lin, X. Xu, T. Tang, Y. Shen and S. Guo, *Int. J. Biol. Macromol.*, 2014, **67**, 163–171.

234 L. S. Khailova, P. A. Nazarov, N. V Sumbatyan, G. A. Korshunova, T. I. Rokitskaya, V. I. Dedukhova, Y. N. Antonenko and V. P. Skulachev, *Biochem.*, 2015, **80**, 1589–1597.

235 K. Kirakci, J. Zelenka, M. Rumlová, J. Cvačka, T. Ruml and K. Lang, *Biomater. Sci.*, 2019, **7**, 1386–1392.

236 L. Stoica, B. A. Stoica, A. Ciobica, M. Zlei, D. Timofte, N. Filip, D. Olinici and C. E. Cotrutz, *Rom. Biotechnol. Lett.*, 2018, **23**, 13862–13869.

237 E. Abbe, *Arch. für Mikroskopische Anat.*, 1873, **9**, 413–468.

238 B. Huang, H. Babcock and X. Zhuang, *Cell*, 2010, **143**, 1047–1058.

239 T. A. Klar, S. Jakobs, M. Dyba, A. Egner and S. W. Hell, *Proc. Natl. Acad. Sci.*, 2000, **97**, 8206–8210.

240 R. Kasper, B. Harke, C. Forthmann, P. Tinnefeld, S. W. Hell and M. Sauer, *Small*, 2010, **6**, 1379–1384.

241 J. Hanne, H. J. Falk, F. Görlitz, P. Hoyer, J. Engelhardt, S. J. Sahl and S. W. Hell, *Nat. Commun.*, 2015, **6**, 7127.

242 S. Ye, J. Guo, J. Song and J. Qu, *Appl. Phys. Lett.*, 2020, **116**, 041101.

243 K. Kolmakov, C. A. Wurm, R. Hennig, E. Rapp, S. Jakobs, V. N. Belov and S. W. Hell, *Chem. - A Eur. J.*, 2012, **18**, 12986–12998.

244 P. López-Chicón, M. P. Paz-Cristobal, A. Rezusta, C. Aspiroz, M. Royo-Cañas, E. Andres-Ciriano, Y. Gilaberte, M. Agut and S. Nonell, *Photochem. Photobiol. Sci.*, 2012, **11**, 1099–1107.

245 G. Carvalho, M. Felipe and M. Costa, *J. Microbiol.*, 2009, **47**, 619–623.

246 P. G. Calzavara-Pinton, M. Venturini, R. Capezzera, R. Sala and C. Zane, *Photodermatol.*

Photoimmunol. Photomed., 2004, **20**, 144–147.

247 M. Lam, P. C. Jou, A. A. Lattif, Y. Lee, C. L. Malbasa, P. K. Mukherjee, N. L. Oleinick, M. A. Ghannoum, K. D. Cooper and E. D. Baron, *Photochem. Photobiol.*, 2011, **87**, 904–909.

248 R. F. Donnelly, P. A. McCarron and M. M. Tunney, *Microbiol. Res.*, 2008, **163**, 1–12.

249 D. Pezzuoli, M. Cozzolino, C. Montali, L. Brancaleon, P. Bianchini, M. Zantedeschi, S. Bonardi, C. Viappiani and S. Abbruzzetti, *Food Control*, 2018, **94**, 254–262.

250 R. Ruiz-González, P. Acedo, D. Sánchez-García, S. Nonell, M. Cañete, J. C. Stockert and A. Villanueva, *Eur. J. Med. Chem.*, 2013, **63**, 401–414.

251 M. García-Díaz, D. Sánchez-García, J. Soriano, M. L. Sagristà, M. Mora, Á. Villanueva, J. C. Stockert, M. Cañete and S. Nonell, *Med. Chem. Commun.*, 2011, **2**, 616.

252 J. Soriano, M. García-Díaz, M. Mora, M. L. Sagrista, S. Nonell, A. Villanueva, J. C. Stockert and M. Canete, *Biochim. Biophys. Acta*, 2013, **1830**, 4611–4620.

253 M. Schröder and R. J. Kaufman, *Mutat. Res. Mol. Mech. Mutagen.*, 2005, **569**, 29–63.

254 D. Kessel and J. J. Reiners Jr, *Photochem. Photobiol.*, 2007, **83**, 1024–1028.

255 D. Kessel, M. Conley, M. G. H. Vicente and J. J. Reiners, *Photochem. Photobiol.*, 2005, **81**, 569–572.

256 L. Ludvíková, P. Friš, D. Heger, P. Šebej, J. Wirz and P. Klán, *Phys. Chem. Chem. Phys.*, 2016, **18**, 16266–16273.

257 X. Wen, X. Zhang, G. Szewczyk, A. El-Hussein, Y.-Y. Huang, T. Sarna and M. R. Hamblin, *Antimicrob. Agents Chemother.*, 2017, **61**, e00467-17.

258 V. Pérez-Laguna, I. García-Luque, S. Ballesta, L. Pérez-Artiaga, V. Lampaya-Pérez, S. Samper, P. Soria-Lozano, A. Rezusta and Y. Gilaberte, *Photodiagnosis Photodyn. Ther.*,

2018, **21**, 211–216.

259 G. M. Decad and H. Nikaido, *J. Bacteriol.*, 1976, **128**, 325–36.

260 B. Rodriguez-Amigo, Ramon Llull, 2018.

261 Z. Saddiqe, I. Naeem and A. Maimoona, *J. Ethnopharmacol.*, 2010, **131**, 511–521.

262 A. Nahrstedt and V. Butterweck, *Pharmacopsychiatry*, 1997, **30**, 129–134.

263 A. L. Vandenbogaerde, A. Kamuhabwa, E. Delaey, B. E. Himpens, W. J. Merlevede and P. A. de Witte, *J. Photochem. Photobiol. B Biol.*, 1998, **45**, 87–94.

264 S. S. Chatterjee, S. K. Bhattacharya, M. Wonnemann, A. Singer and W. E. Müller, *Life Sci.*, 1998, **63**, 499–510.

265 C. M. Schempp, K. Pelz, A. Wittmer, E. Schöpf and J. C. Simon, *Lancet*, 1999, **353**, 2129.

266 J. M. Greeson, B. Sanford and D. A. Monti, *Psychopharmacology (Berl).*, 2001, **153**, 402–414.

267 H. Brockmann, M. N. Haschad, K. Maier and F. Pohl, *Naturwissenschaften*, 1939, **27**, 550.

268 N. Durán and P. Song, *Photochem. Photobiol.*, 1986, **43**, 677–680.

269 A. Darmanyan, L. Burel, D. Eloy and P. Jardon, *J. Chim. Phys.*, 1994, **91**, 1774–1785.

270 A. Karioti and A. R. Bilia, *Int. J. Mol. Sci.*, 2010, **11**, 562–594.

271 L.-F. Huang, Z.-H. Wang and S.-L. Chen, *Chin. J. Nat. Med.*, 2014, **12**, 81–88.

272 C. M. N. Yow, H. M. Tang, E. S. M. Chu and Z. Huang, *Photochem. Photobiol.*, 2012, **88**, 626–632.

273 J. Comas-Barceló, B. Rodríguez-Amigo, S. Abbruzzetti, P. del Rey-Puech, M. Agut, S. Nonell and C. Viappiani, *RSC Adv.*, 2013, **3**, 17874–17879.

274 P. Delcanale, C. Hally, S. Nonell, S. Bonardi, C. Viappiani and S. Abbruzzetti, *Photochem. Photobiol. Sci.*, 2020, **19**, 324–331.

275 E. Buytaert, G. Callewaert, N. Hendrickx, L. Scorrano, D. Hartmann, L. Missiaen, J. R. Vandenheede, I. Heirman, J. Grooten and P. Agostinis, *FASEB J.*, 2006, **20**, 756–758.

276 P. Bianchini, M. Cozzolino, M. Oneto, L. Pesce, F. Pennacchietti, M. Tognolini, C. Giorgio, S. Nonell, L. Cavanna, P. Delcanale, S. Abbruzzetti, A. Diaspro and C. Viappiani, *Biomacromolecules*, 2019, **20**, 2024–2033.

277 T. Kiesslich, B. Krammer and K. Plaetzer, *Curr. Med. Chem.*, 2006, **13**, 2189–2204.

278 A. Kubin, F. Wierrani, U. Burner, G. Alth and W. Grunberger, *Curr. Pharm. Des.*, 2005, **11**, 233–253.

279 J. M. Jacobson, L. Feinman, L. Liebes, N. Ostrow, V. Koslowski, A. Tobia, B. E. Cabana, D.-H. Lee, J. Spritzler and A. M. Prince, *Antimicrob. Agents Chemother.*, 2001, **45**, 517–524.

280 B. Hager, W. S. L. Strauss and H. Falk, *Photochem. Photobiol.*, 2009, **85**, 1201–1206.

281 N. Nafee, A. Youssef, H. El-Gowelli, H. Asem and S. Kandil, *Int. J. Pharm.*, 2013, **454**, 249–258.

282 A. Losi, *Photochem. Photobiol.*, 1997, **65**, 791–801.

283 N. Plenagl, L. Duse, B. S. Seitz, N. Goergen, S. R. Pinnapireddy, J. Jedelska, J. Brüßler and U. Bakowsky, *Drug Deliv.*, 2019, **26**, 23–33.

284 N. Plenagl, B. S. Seitz, L. Duse, S. R. Pinnapireddy, J. Jedelska, J. Brüßler and U. Bakowsky, *Int. J. Pharm.*, 2019, **570**, 118666.

285 P. Miškovský, D. Jancura, S. Sánchez-Cortés, E. Kočišová and L. Chinsky§, *J. Am. Chem. Soc*, 1998, **120**, 6374–6379.

286 V. Engelhardt, B. Krammer and K. Plaetzer, *Photochem. Photobiol. Sci.*, 2010, **9**, 365.

287 H. C. Williams, R. P. Dellavalle and S. Garner, *Lancet*, 2012, **379**, 361–372.

288 M. Fanelli, E. Kupperman, E. Lautenbach, P. H. Edelstein and D. J. Margolis, *Arch. Dermatol.*, 2011, **147**, 917–921.

289 2015 Disease and Injury Incidence and Prevalence Collaborators GBD, *Lancet*, 2016, **388**, 1545–1602.

290 A. L. Cogen, V. Nizet and R. L. Gallo, *Br. J. Dermatol.*, 2008, **158**, 442–455.

291 H. Jones, D. Blanc and W. J. Cunliffe, *Lancet*, 1980, **316**, 1048–1049.

292 A. Charakida, P. E. Mouser and A. C. Chu, *Expert Opin. Drug Saf.*, 2004, **3**, 119–129.

293 H. Xu and H. Li, *Am. J. Clin. Dermatol.*, 2019, **20**, 335–344.

294 T. P. Van Boeckel, S. Gandra, A. Ashok, Q. Caudron, B. T. Grenfell, S. A. Levin and R. Laxminarayan, *Lancet Infect. Dis.*, 2014, **14**, 742–750.

295 S. R. de Annunzio, L. M. de Freitas, A. L. Blanco, M. M. da Costa, C. C. Carmona-Vargas, K. T. de Oliveira and C. R. Fontana, *J. Photochem. Photobiol. B Biol.*, 2018, **178**, 545–550.

296 Y.-Y. Wang, A.-R. Ryu, S. Jin, Y.-M. Jeon and M.-Y. Lee, *PLoS One*, 2017, **12**, e0170599.

297 W. Hongcharu, C. R. Taylor, D. Aghassi, K. Suthamjariya, R. R. Anderson and Y. Chang, *J. Invest. Dermatol.*, 2000, **115**, 183–192.

298 S. Jeong, J. Lee, B. N. Im, H. Park and K. Na, *Biomaterials*, 2017, **141**, 243–250.

299 X. Xu, Y. Zheng, Z. Zhao, X. Zhang, P. Liu and C. Li, *Med. (United States)*, 2017, **96**, 1–6.

300 S. Futterman and J. Heller, *J. Biol. Chem.*, 1972, **247**, 5168–5172.

301 G. H. Krause and E. Weis, *Annu. Rev. Plant Physiol. Plant Mol. Biol.*, 1991, **42**, 313–349.

302 A. Pfarrherr, K. Teuchner, D. Leupold and P. Hoffmann, *J. Photochem. Photobiol. B Biol.*, 1991, **9**, 35–41.

303 L. A. Schmitt, Y. Liu, P. A. Murphy, J. W. Petrich, P. M. Dixon and D. F. Birt, *J. Photochem. Photobiol. B Biol.*, 2006, **85**, 118–130.

304 K. Kairyte, S. Lapinskas, V. Gudelis and Z. Luksiene, *J. Appl. Microbiol.*, 2012, **112**, 1144–1151.

305 P. Delcanale, B. Rodriguez Amigo, J. Juárez-Jiménez, J. Luque, S. Abbruzzetti, M. Agut, S. Nonell and C. Viappiani, *J. Mater. Chem. B*, 2017, **5**, 1633–1641.

306 K. Aponiene, E. Paskeviciute, I. Reklaitis and Z. Luksiene, *J. Food Eng.*, 2015, **144**, 29–35.

307 C. Cecchini, A. Cresci, M. Coman, M. Ricciutelli, G. Sagratini, S. Vittori, D. Lucarini and F. Maggi, *Planta Med.*, 2007, **73**, 564–566.

308 J. R. Lakowicz, *Principles of Fluorescence Spectroscopy*, Springer, Maryland, USA, Third Edit., 2006.

309 H. C. Cheung, *3. Resonance Energy Transfer*, Plenum Press, New York, 1991.

310 T. L. McMeekin, M. L. Groves and N. J. Hipp, in *Amino Acids and Serum Proteins*, ed. Jacob A. Stekol, 1964, pp. 54–66.

311 R. F. Chen, *Anal. Lett.*, 1967, **1**, 35–42.

312 L. Liang and M. Subirade, *J. Phys. Chem. B*, 2010, **114**, 6707–6712.

313 E. Dufour, M. C. Marden and T. Haertlé, *FEBS Lett.*, 1990, **277**, 223–226.

314 Y. Cho, C. A. Batt and L. Sawyer, *J. Biol. Chem.*, 1994, **269**, 11102–11107.

315 R. Edge and T. Truscott, *Antioxidants*, 2018, **7**, 5.

316 H. Wu, C. Moser, H.-Z. Wang, N. Høiby and Z.-J. Song, *Int. J. Oral Sci.*, 2015, **7**, 1–7.

317 I. García, S. Ballesta, Y. Gilaberte, A. Rezusta and Á. Pascual, *Future Microbiol.*, 2015, **10**, 347–356.

318 R. Roy, M. Tiwari, G. Donelli and V. Tiwari, *Virulence*, 2018, **9**, 522–554.

319 S. R. de Annunzio, L. M. de Freitas, A. L. Blanco, M. M. da Costa, C. C. Carmona-Vargas, K. T. de Oliveira and C. R. Fontana, *J. Photochem. Photobiol. B Biol.*, 2018, **178**, 545–550.

320 Y. M. Jeon, H. S. Lee, D. Jeong, H. K. Oh, K. H. Ra and M. Y. Lee, *Life Sci.*, 2015, **124**, 56–63.

321 R. Schneider, F. Schmitt, C. Frochot, Y. Fort, N. Lourette, F. Guillemin, J. F. Muller and M. Barberi-Heyob, *Bioorg. Med. Chem.*, 2005, **13**, 2799–2808.

322 A. A. Ordonez, E. A. Weinstein, L. E. Bambarger, V. Saini, Y. S. Chang, V. P. DeMarco, M. H. Klunk, M. E. Urbanowski, K. L. Moulton, A. M. Murawski, S. Pokkali, A. S. Kalinda and S. K. Jain, *J. Nucl. Med.*, 2017, **58**, 144–150.

323 C. S. Oliveira, R. Turchiello, A. J. Kowaltowski, G. L. Indig and M. S. Baptista, *Free Radic. Biol. Med.*, 2011, **51**, 824–833.

324 European Medicines Agency, Committee on Herbal Medicinal Products, https://www.ema.europa.eu/en/committees/committee-herbal-medicinal-products-hmpc.

List of Abbreviations

$^1O_2$; $^1\Delta_g$	Singlet oxygen
$^3O_2$	Triplet oxygen
$^1S_0$	Singlet ground state
^1S_n	Singlet excited state
^3PS	Triplet photosensitizer
^3T_n*	Triplet excited state
9-ITMPo	9-isothiocyanate-2,7,12,17-tetrakis(methoxyethyl)porphycene
A	Absorbance
ALA	Aminolevulinic acid
aHyp	Lyophilized hydrophilic extract of *Hypericum perforatum*
aPDT	Antimicrobial photodynamic therapy
BCS	Biopharmaceutics Classification System
βLG	β-lactoglobulin
CCD	Charge-coupled device
Ce6	Chlorin e6
CFU	Colony forming units
DMEM	Dulbecco's modified eagle's medium" (DMEM)
EC_{50}	Drug concentration at which cell viability is reduced to 50%
EPR	Enhanced permeation effect
EPS	Extracellular polymeric substances
F	Fluorescence
FCS	Fluorescence correlation spectroscopy
FDA	Federal drug administration
FRET	Förster energy transfer
GMP	Good manufacturing practices
HBD	Hydrogen bond donating
HMP	Herbal medicinal product

HOMO	Highest occupied molecular orbital
Hyp	Hypericin
IC	Internal conversion
IRF	Instrument response function
ISC	Intersystem crossing
J	Spectral overlap integral
LED	Light-emitting diode
LUMO	Lowest unoccupied molecular orbital
MIC	Minimum inhibitory concentration
MTT	3-(4,5-dimethylthiazol-2-yl)-2,5-diphenyltetrazolium bromide
n	Refractive index
NIR	Near-infrared
NP	Nanoparticle
$O_2^{\bullet-}$	Superoxide radical anion
$OH^{\bullet}$	Hydroxyl radical
P	Phosphorescence
PBS	Phosphate Buffer Saline
Pc	Phthalocyanines
PDT	Photodynamic therapy
PET	Photoinduced electron transfer
PN	Phenalenone
PNS	Phenalenone-2-sulfonate
Porbutyl	2-N-butylaminothiazolo[4,5-c]2,7,12,17-tetrakis(methoxyethyl)porphycene
Porphonium	*2-(3-aminopropyl) triphenylphosphonium-thiazolo[4,5-c]2,7,12,17-tetrakis-(methoxyethyl) porphycene*
Portacin	*2-gentamicin-thiazolo[4,5-c]2,7,12,17-tetrakis(methoxyethyl)porphycene*
PPh_3^+	Triphenylphosphonium cation
PpIX	Protoporphyrin IX

PS	Photosensitizer
r	Hydrodynamic radius
R_0	Förster critical distance
RA	Retinoic acid
RB	Rose Bengal
RBG	Rose Bengal – Gentamicin conjugate
ROI	Reactive oxygen intermediates
rpm	Revolutions per minute
SD	Standard deviation
SE	Stimulated emission
SOP	Standard operational procedure
SPAD	Single photon avalanche diodes
STED	Stimulated emission depletion
TMPo	2,7,12,17-tetrakis(methoxyethyl)porphycene
TRES	Time resolved emission spectra
TRF	Time resolved fluorescence
TRNIR	(Time-resolved NIR emission)
TSB	Tryptic Soy Broth
βLG	b-Lactoglobulin
ΔA	Absorbance variation
ε	Molar absorptivity coefficient
τ	Lifetime
τ_Δ	Singlet oxygen lifetime
τ_T	Triplet lifetime
Φ_F	Fluorescence quantum yield
Φ_{ET}	Energy transfer quantum yield
Φ_Δ	Singlet oxygen quantum yield

List of Publications

Papers published directly related to the thesis

- **C. Hally**, B. Rodríguez-Amigo, R. Bresolí-Obach, O. Planas, J. Nos, E. Boix-Garriga, R. Ruiz-González and S. Nonell; CHAPTER 4. Photodynamic Therapy in *Theranostics and Image Guided Drug Delivery*, ed. M. Thanou, Royal Society of Chemistry, Cambridge, 2018, pp. 86–122.
- I. Nieves, **C. Hally**, C. Viappiani, M. Agut and S. Nonell; A porphycene-gentamicin conjugate for enhanced photodynamic inactivation of bacteria, *Bioorg. Chem.*, 2020, **97**, 103661.
- **C. Hally**, P. Delcanale, S. Nonell, C. Viappiani and S. Abbruzzetti; Photosensitizing proteins for antibacterial photodynamic inactivation, *Transl. Biophotonics*, 2020, **2**, tbio.201900031.
- P. Delcanale, **C. Hally**, S. Nonell, S. Bonardi, C. Viappiani and S. Abbruzzetti; Photodynamic action of *Hypericum perforatum* hydrophilic extract against *Staphylococcus aureus*, *Photochem. Photobiol. Sci.*, 2020, **19**, 324–331.

Other published papers

- M. A. Revuelta-Maza, **C. Hally**, S. Nonell, G. de la Torre and T. Torres; Crosswise Phthalocyanines with Collinear Functionalization: New Paradigmatic Derivatives for Efficient Singlet Oxygen Photosensitization, *Chempluschem*, 2019, **84**, 673–679.
- V. Novohradsky, A. Rovira, **C. Hally**, A. Galindo, G. Vigueras, A. Gandioso, M. Svitelova, R. Bresolí-Obach, H. Kostrhunova, L. Markova, J. Kasparkova, S. Nonell, J. Ruiz, V. Brabec and V. Marchán; Towards Novel Photodynamic Anticancer Agents Generating Superoxide Anion Radicals: A Cyclometalated IrIII Complex Conjugated to a Far-Red Emitting Coumarin, *Angew. Chemie - Int. Ed.*, 2019, **58**, 6311–6315.

- M. Á. Revuelta-Maza, P. González-Jiménez, **C. Hally**, M. Agut, S. Nonell, G. de la Torre and T. Torres; Fluorine-substituted tetracationic ABAB-phthalocyanines for efficient photodynamic inactivation of Gram-positive and Gram-negative bacteria, *Eur. J. Med. Chem.*, 2020, **187**, 111957.

Additional papers at different stage of publication

- B. Rodríguez-Amigo, **C. Hally**, P. Delcanale, N. Roig-Yanovsky, S. Abbruzzetti, M. Agut, C. Viappiani and S. Nonell; A double payload complex between Hypericin and Tretinoin in the β-lactoglobulin protein for potential acne treatment
- **C. Hally**, M. Jordà, Í. Nieves, P. Bianchini S. Abbruzzeti, M. Agut, C. Viappiani and S. Nonell; Understanding the mechanism of action of 2-aminothiazoloporphycene conjugates in Photodynamic applications.

Communications at congresses

- **C. Hally**, O. Planas, D. Fernandez-Llaneza, O. Gulias, T. Gallavardin, I. Nieves, R. Ruiz-Gonzalez, E. Lemp, A. L. Zanocco and S. Nonell; Fluoro- and chromogenic near-ir porphycenes as a platform for developing biological sensors and actuators, XXXVI Reunión BIENAL de la Real Sociedad Española de Química, Sitges (Spain), June 25th-29th 2017.
- **C. Hally**, O. Planas, D. Fernandez-Llaneza, O. Gulias, T. Gallavardin, I. Nieves, R. Ruiz-Gonzalez, E. Lemp, A. L. Zanocco and S. Nonell; Chromo- and fluorogenic near-ir porphycenes: platforms for developing biological sensors and actuators, 17th Congress of the European Society for Photobiology, Pisa (Italy), September 4th-8th 2017.
- **C. Hally**, I. Nieves, C. Viappiani, M. Agut and S. Nonell; Porphycene-Gentamicin Conjugates for aPDT, ESP Photobiology School 2018, Brixen (Italy), June 11th–16th 2018.
- **C. Hally**, I. Nieves, M. Cozzolino, P. Bianchini, A. Diaspro, S. Abbruzzetti, M. Agut, C. Viappiani and S. Nonell; Porgenta: a Novel Photosensitiser-Antibiotic Conjugate for aPDT, Photodynamic Therapy and Photodiagnosis Update 2018, Kochel am See (Germany), September 18th-22nd 2018.
- **C. Hally**, M. Jordà, I. Nieves, C. Viappiani, M. Agut and S. Nonell; Porphycene Targeting in Photodynamic Therapy Applications; I Jornada de Doctorands IQS, Barcelona (Spain), May 16th-17th 2019.
- **C. Hally**, M. Jordà, I. Nieves, M. E. Vázquez, C. Viappiani, M. Agut and S. Nonell; Porphycene Targeting in Photodynamic Therapy Applications; 17th Congress of the International Union of Photobiology and 18th Congress of the European Society for Photobiology, Barcelona (Spain), August 25th-30th 2019.